0D MICROCAVITY POLARITONS TRAPPING LIGHT-MATTER QUASIPARTICLES

THÈSE N^{O} 3815 (2007)

PRÉSENTÉE LE 6 JUILLET 2007

À LA FACULTÉ DES SCIENCES DE BASE

Laboratoire d'optoélectronique quantique

SECTION DE PHYSIQUE

ÉCOLE POLYTECHNIQUE FÉDÉRALE DE LAUSANNE

POUR L'OBTENTION DU GRADE DE DOCTEUR ÈS SCIENCES

PAR

Ounsi EL DAÏF

Maîtrise de physique, Université Paris VI, France

acceptée sur proposition du jury:

Prof. O. Martin, pésident du jury

Prof. B. Deveaud-Plédran, directeur de thèse

Prof. H. Brune, rapporteur

Dr Le Si Dang, rapporteur

Prof. J. Tignon, rapporteur

ÉCOLE POLYTECHNIQUE
FÉDÉRALE DE LAUSANNE

Suisse

2007

Contents

Abstract/résumé/moulakhas 8

Introduction **15**

I A new kind of structure **19**

1 Framework **21**
1.1 Elements of optical properties of semiconductors 21
1.1.1 Band structure and excitons 21
1.1.2 Excitons confined in a quantum well 23
1.2 Cavities: light confinement 24
1.2.1 Bragg mirrors 24
1.2.2 Microcavity 25
1.3 Strong coupling 27
1.3.1 Principles 27
1.3.2 Lifetimes and spectral broadening 29
1.3.3 Polariton nonlinearities 30
1.3.4 Experimental signatures of strong-coupling 30
1.3.5 The strong to weak coupling transition 32
1.4 The bosonic character of polaritons 33
1.4.1 Validity of the bosonic nature of excitons 33
1.4.2 Bose-Einstein condensation of polaritons 34
1.5 Confinement of 2D polaritons 35
1.5.1 Why? 35
1.5.2 A state of the art of polariton confinement 35
1.5.3 And now... how? 36
1.5.4 Orders of magnitude 37
1.5.5 39

2 Conception and fabrication of the sample **41**
2.1 Preliminary 41
2.1.1 General idea 41
2.1.2 Materials used 42

2.1.3 Characteristics of local growth methods 43
2.1.4 The structure chosen 44
2.1.5 Mesas 45
2.1.6 In situ cleaning and regrowth 47
2.1.7 Simulation 47
2.2 Growth of a microcavity with embedded mesas 47
2.2.1 First growth and characterization 48
2.2.2 Photolithography 50
2.2.3 Chemical etching 52
2.2.4 Final sample 54
2.3 Conclusion and improvement of the method 56
2.3.1 Step by step improvement 56
2.3.2 Conclusion: a satisfactory sample 57

II Physical studies 59

3 Zero and two dimensional strong-coupling regimes 61
3.1 Experimental considerations 61
3.2 Characterization of the 2D cavities 63
3.3 Strong-coupling regime in zero dimension 66
3.3.1 Strong-coupling in small mesas 66
3.3.2 The doublet: a lift of degeneracy 69
3.3.3 Larger mesas 70
3.3.4 Comment on the linewidths and high Q-factors 71
3.4 Conclusion: a high quality confinement of strongly coupled quasiparticles 72

4 Spectroscopy of polaritons in the real and reciprocal spaces 73
4.1 Spectroscopy 73
4.1.1 Experimental setup 73
4.1.2 Reciprocal space spectroscopy 74
4.1.3 Real space spectroscopy 78
4.1.4 Relaxation processes 79
4.1.5 Theoretical description of confined polaritons 80
4.1.6 Conclusion 83
4.2 2D images through resonant excitation 84
4.2.1 Set-up 84
4.2.2 Resonant Rayleigh scattering in 2D 85
4.2.3 Images of a 9 micron mesa 86
4.2.4 Images of a 19 micron mesa 88
4.2.5 Images of a 3 micron mesa 90
4.2.6 Interpretation 91
4.2.7 Conclusion 93

5 Studies in the nonlinear regime **95**
5.1 Motivation and general phenomenology of power studies . . . 95
5.1.1 General case . . . 95
5.1.2 Case of polaritons . . . 96
5.2 Non-resonant excitation . . . 99
5.2.1 Regimes observed . . . 99
5.2.2 Weak coupling regime . . . 104
5.2.3 A lab for seeing nonlinear effects . . . 107
5.3 Resonant excitation: parametric processes . . . 109
5.3.1 Principles of parametric processes . . . 109
5.3.2 Setup . . . 110
5.3.3 Parametric processes in the 2D cavity . . . 111
5.3.4 Parametric processes in a $9\mu m$ mesa . . . 114
5.3.5 Continuous wave pumping of a $9\mu m$ mesa . . . 116
5.3.6 Resonant excitation of a $3\mu m$ mesa at zero detuning . 118
5.3.7 Alternative points of view: signs of bistability? . . . 120
5.4 Balance and conclusions . . . 123
5.4.1 Balance of the observed phenomena . . . 123
5.4.2 Conclusion . . . 124

III Perspectives and discussions **127**

6 Applications **129**
6.1 Polariton single photon source . . . 129
6.1.1 Principle . . . 130
6.1.2 Potential advantages . . . 131
6.2 Twin photon source in the near infrared . . . 131
6.2.1 Existing devices and principle . . . 131
6.2.2 Feasibility with 0D polaritons: use of polariton parametric scattering . . . 131
6.2.3 Advantages of 0D polaritons . . . 132
6.3 Feasibility . . . 133
6.3.1 Global warming! . . . 134

7 Experimental perspectives **135**
7.1 Perspectives on this sample . . . 135
7.1.1 Time-resolved studies . . . 136
7.1.2 Complete imaging of the confined modes . . . 137
7.1.3 Further nonlinear studies . . . 137
7.2 The next generation of samples . . . 137
7.2.1 A new sample structure . . . 138
7.2.2 Improving fabrication methods . . . 139

7.3 New trap shapes: from simple confinement to condensate interference . . . 139
7.3.1 A new mask . . . 139
7.3.2 Multiple etchings: stairway to... ? . . . 141
7.3.3 Electron-beam lithography . . . 141
7.4 And now... just do it? . . . 142

8 Conclusion **143**

Epilogue: Between applied and basic research **147**

IV Appendices **151**

A Theoretical description **153**

B Clean room/Salle blanche **157**
B.1 Parameters used for photolithography . . . 157
B.2 Récapitulatif des points critiques en salle blanche . . . 158
B.3 Diffraction limit in the case of photolithography . . . 159

C Various works **161**
C.1 Diploma works on 0D polaritons . . . 161
C.2 Quantum well and microcavity samples characterization . . . 162

Bibliography **162**

CV **175**

Acknowledgments/Reconnaissance **178**

Abstract

Polaritons are half-matter half-light quasiparticles, arising, in a two-dimensional semiconductor microcavity, from the strong-coupling between an exciton (an elementary electronic excitation of a crystal) and a photon. This thesis presents the fabrication of polariton confining structures, their characterization and the study of the linear and non-linear optical properties of the confined polaritons.

Thanks to their bosonic character, to their extremely light effective mass and to the peculiar shape of their dispersion curve, polaritons were proven to accumulate in their ground state to form a Bose-Einstein condensate in a CdTe based sample, at a high temperature of the order of 20 Kelvin. No such effect was observed in GaAs materials, who offer a less disordered environment, where we developed a method to fabricate traps of any shape and size. The latter should facilitate the condensation of polaritons by lowering the density thresholds, and allow us to manipulate the condensate.

Thanks to the strong-coupling regime, it is possible to confine polaritons either through their photon or through their exciton part. We thus fabricated two-dimensional microcavities with local thickness variations, confining the cavity photon along its two free dimensions. We were able to perform this through high-quality molecular beam epitaxy (MBE) growth, accompanied by a controlled processing of the sample. We measured the anticrossing behaviors characteristic of the strong-coupling regime in zero and two dimensions. As the confining structures have sizes of the order of the micron, we could image the confined polaritons' wave functions in the real and reciprocal (momentum) spaces, and tried to understand how the transition between confined (0D) and extended (2D) polariton modes occurs. We also gave first evidences of the interaction between the two and zero-dimensional structures, and of the polariton trapping from one to the other.

We then studied the nonlinear optical properties of this new object, performing two different kinds of experiments:

1. a study of the response of the system to a non-resonant excitation, in order to probe the formation of a condensed phase. Collective electronic excitations were created, at energies far higher than the modes which are of interest for us. We observed the effect of high densities in the system and evidenced Coulomb interaction. We then observed the cross-over from strong to weak-coupling regime, and the onset of lasing in the weakly coupled system.

2. a study of the response of the system to a resonant excitation in order to probe parametric effects between the discrete states. In this con-

figuration a number of polaritons are intentionally created in a given state. We observed various nonlinear behaviors as a function of the created population, which may be interpreted as effects of Coulomb interaction, or indications of bistable behaviors in the system. We were nevertheless not able to discriminate.

We give some potential applications in the field of single or correlated photon emission. Although industrial applications may not be in the short-term agenda, it should be possible to take advantages of this original type of structures for research and development applications. We finally give some experimental perspectives, which may help deepen the observations shown and the interpretations proposed here, and should allow to work towards the fabrication of new samples, where BEC of polaritons is observed and controlled, as well as parametric oscillations between various confined states.

Keywords: polaritons; strong-coupling; microcavities; semiconductor quantum dots; excitons; photoluminescence; nonlinear optics; semiconductor lasers.

Résumé

Polaritons de microcavité à 0D
Piégeage de quasi-particules matière lumière

Les polaritons sont des particules mixtes matière lumière, résultant, dans une microcavité semi-conductrice à deux dimensions, du couplage fort entre un exciton (l'excitation électronique élémentaire d'un cristal) et un photon. Cette thèse présente la fabrication et la caractérisation de structures confinant les polaritons, ainsi que l'étude des propriétés optiques linéaires et non linéaires des polaritons confinés.

La condensation de Bose Einstein de polaritons –accumulation macroscopique de population dans l'état fondamental du système– a été observée dans une microcavité basée sur du CdTe. Cette condensation a eu lieu à une température élevée, avoisinant les 20 degrés Kelvin. Elle a été possible grâce à la nature bosonique des polaritons ainsi qu'à leur petite masse effective, et enfin à la forme particulière de leur courbe de dispersion. Les matériaux basés sur le GaAs offrent quant à eux une structure moins désordonnée, dans laquelle nous avons développé une méthode de fabrication de pièges de n'importe quelle taille ou forme. Ces derniers devraient favoriser la condensation des polaritons (non-observées encore dans ces matériaux) en baissant les seuils en densité, et nous permettre de manipuler l'éventuel condensat.

Grâce au couplage fort, il est possible de confiner les polaritons à travers l'une de leurs composantes: le photon ou l'exciton. Nous avons donc fabriqué des micro-cavités bidimensionnelles dans lesquelles nous avons localement introduit une légère variation d'épaisseur, permettant de confiner le photon du mode de cavité le long de ses deux dimensions libres. Nous avons réalisé cette structure par épitaxie par jet moléculaire (MBE) de haute qualité, accompagnée d'un procédé de modification de l'échantillon. Nous avons mesuré la courbe d'anticroisement caractérisant le couplage fort pour les différentes structures à zéro et à deux dimensions présentes sur l'échantillon. Comme les pièges ont des tailles de l'ordre du micron, nous avons pu réaliser optiquement des images de la fonction d'onde des polaritons dans les espaces réel et réciproque (l'espace des impulsions). Nous avons essayé de comprendre comment la transition entre un système à 0D et un système à 2D se fait. Nous avons de plus mis en évidence des interactions entre les polaritons 2D et 0D, ainsi que le mécanisme de piégeage des uns vers les autres.

Nous avons ensuite étudié les propriétés optiques non linéaires de ce nouvel objet, à travers deux types d'expériences :

1. une étude de la réponse du système à une excitation non résonante, pour permettre l'éventuelle formation d'une phase condensée. Nous avons créé des excitations électroniques en grand nombre à des énergies très élevées par rapport aux énergies des modes qui nous intéressent.

Nous avons pu observer des effets dus aux hautes densités atteintes dans le système, nous avons observé l'effet des interactions coulombiennes. Nous avons enfin observé le passage du couplage fort vers le couplage faible, et le démarrage des oscillations laser (de type VCSEL) dans le système en couplage faible.

2. une étude de la réponse du système à une excitation résonante, pour sonder les effets paramétriques entre les états discrets. Dans cette situation des polaritons sont créés intentionnellement dans un état. Nous avons observé plusieurs comportements non linéaires de l'émission en fonction de la population créée, qui peuvent être interprétés comme des effets des interactions coulombiennes, ou comme des signes de comportement bistable du système, sans réussir à distinguer l'interprétation la plus pertinente.

Nous avons proposé des applications potentielles, basées sur la structure développée dans ce travail, pour l'émission de photons uniques ou corrélés. Même si ces applications ne sont pas encore réalistes en termes industriels, il serait possible d'utiliser ce type de structures pour la recherche appliquée. Nous proposons enfin des perspectives expérimentales qui pourraient aider à approfondir nos observations et les interprétations que nous en avons proposées, et devraient permettre d'avancer dans la fabrication de nouveaux échantillons, dans lesquels la condensation de Bose-Einstein des polaritons pourra être observée et maîtrisée, et dans lesquels des oscillations paramétriques entre des modes confinés pourraient avoir lieu.

Mots-clés : polaritons; couplage fort; microcavités; boîtes quantiques semiconductrices; excitons; photoluminescence; optique non linéaire; lasers à semiconducteurs.

من حالة ثنائية البعد إلى الحالة الملتقطة.

فيما بعد فقد قمنا بدراسة الخواص الضوئية اللاخطية لذلك المركب الجديد بناءً على نوعين مختلفين من التجارب:

١– دراسة لمدى إستجابة النظام للإثارة اللاتجاوبية و ذلك بهدف سبر تشكل الطور المتكاثف. شكّلنا إثارة إلكترونية متجمعة عند طاقات عالية جداً و هي غير متوافقة مع الطاقات التي تهمّنا. بناءً على هذه التجربة فلقد لاحظنا تأثير الكثافات العالية في الجملة و الذب يثبت التفاعل المتبادل الكولومبي. من ثمّ لاحظنا إنتقال الجملة من حالة الترابط القوي إلى حالة الترابط الضعيف من جهة و بروزها كمادة فعالة لليزر في حالة الترابط الضعيف من جهةٍ أخرى.

٢– دراسة لمدى إستجابة الجملة للإثارة التجاوبية و ذلك لسبر الأحداث البارامترية بين السويات المنفصلة بفضل الإلتقاط. تنشأ تحريضياً في هذه الحالة الإختبارية عدد من البولاريتونات في سوية معيّنة. لاحظنا عدد من التصرّفات اللاخطية كتابع للإسكان المتكون للبولاريتونات، و يمكن إن يعود هذا الأمر إمّا إلى التأثير الكولومبي المتبادل أو إلى ثنائية الحالة في الجملة (حالتي الترابط القوي و الضعيف). و حتى الآن لا يمكن التمييز بين الحالتين.

تمّ برهان و وصف الخواص و الظواهر المرافقة إضافةً إلى إعطاء بعض التطبيقات: فالتطبيقات الصناعية منها ليست في القريب المنظور، أمّا التطبيقات المحتملة فتتضمّن إصدار الفوتونات الأحادية و المترابطة التي يمكن إستخدامها في البحث العلمي و التطبيقي. خلاصةً لهذا البحث فقد قدّمنا بعض المنظورات التي ممكن أن تقود إلى فهم أعمق للملاحظات التي بنيناها سابقاً و للإشارات و التفسيرات التي اقترحناها في هذا البحث. هذه النتائج ستفتح هجال عملٍ هيتقبلي متعلّق بتحضير عينات جديدة يظهر فيها تكاثف بوز– أينشتاين و الإهتزاز البارامتري بين سويات ملتقطة.

الكلمات الأساسية: بولاريتونات، ترابط قوي، فجوة ميكروية، أنصاف نواقل دو البعد صفر، أكسيتون، اصدار، البصريات اللاخطّية، لبزرات أنصاف النواقل.

ملخَّص

بولاريتونات فجوية ذو بعد صفر
إلتقاط شبه جزيئات أنصاف مادة و أنصاف ضوء

البولاريتونات هي أشباه جزيئات و توصف بأنّها ذات طبيعة مزدوجة (أنصاف مادة و أنصاف ضوء) و هي تظهر من الترابط القوي بين الأكسيتون (ثنائية إلكترون ثقب) و الفوتون و ذلك في فجوة ميكروية ثنائية الأبعاد و من أنصاف النواقل. هذا البحث هبني على دراستي. الأولى تقدم إنتاج بنية محدِّدة للبولاريتونات بالإضافة إلى دراسة خواصها. أمّا الثانية فدراسة للخواص الخطية واللاخطية للبولاريتونات.

إن التوصيف البوزوني و الكتلة الفعّالة الخفيفة بالإضافة إلى الشّكل المميّز لتابع التشتت في هذا النوع من المواد برهت على أنها العامل في التراكم في السوية الأساسية. و هذا التي تشكل تكاثف بوز– أينشتاين في عينات الكادميوم – تلّوريوم CdTe عند درجات الحرارة العالية (٢٠ كلفن).

تقدم مادة الغاليوم – زرنيخ GaAs(التي لم تشهد ذلك التكاثف) مواد ذات ترتيب أكبر في محيطها. و بناءً على هذا الأمر فقد قمنا بتطوير طريقة جديدة لتصنيع لواقط أبرزت فعاليتها مهما شكلها أو قياسها. هذه اللواقط ينبغي أن تسهّل تكاثف البولاريتونات عبر تخفيض كثافة حاجز العتبة سامحةً لنا التحكم بهذا التكاثف.

إن منطقة الترابط القوى تمكّن حصر البولاريتونات في جزئيها الفوتوني أو الأكسيتوني. لإلتقاط الفوتون الفجوي ضمن مساره ذو البعد الثنائي، قمنا بتصنيع فجوة ميكروية ثنائية الأبعاد و ذات سماكة متغيرة ببعض المواقع المحددة. إستطعنا تشكيل هذه الفجوة ذات الجودة العالية عبر نمو للبّورات حسب طريقة ال(MBE) و ذلك بترافق مع القدرة على التحكم بهندسة العينة المصنعة. إضافةً إلى ذلك فقد قمنا بدراسة خواص اللاتصالب في الفضاء الحقيقي كما في فضاء الإندفاع و هما يميّزان منطقة الترابط القوي في العينة و ذلك في الحالتين: حالة ثنائية البعد و حالة البعد صفر ، في اللواقط.

إن الكتلة الفعالة الخفيفة للبولاريتونات تكفي لإعطاء البنية المحدِّدة أبعاداً مساوية للميكرومتر. الأمر الذي منحنا إمكانية تصوير التوابع الموجية للبولاريتونات المحصورة، و ذلك ضمن الفضائين الحقيقي و الإندفاعي. و قد إقترحنا أيضاً كيفية حدوث الإنتقال من ثنائية الأبعاد إلى البعد صفر. في نفس الإطار و لأول مرة تمكنّا من تقديم برهان يدل على التفاعل المتبادل بين الجزيئات الثنائية الأبعاد و ذوات البعد الصفر، إذ إن فعل الإلتقاط يتم

Introduction

Most of the major advances in semiconductor physics and technology over the last thirty years originated from quantum confinement of elementary excitations along one, two, or three spatial dimensions [Hess et al., 1994, Bimberg et al., 1999] and from the improvement of their coupling to the electromagnetic field. Indeed confinement in semiconductor structures allows the study of various fundamental effects, ranging from the Purcell effect [Purcell, 1946] to full quantum confinement. Such confinement is also used for applications in many fields, ranging from optoelectronics to quantum information.

The various studies carried out in the past decades were focused on one hand on matter, through the confinement of excitonic resonance in quantum wells, quantum wires and quantum dots, and on the other hand on the electromagnetic field's environment, modified by optical confinement in different types of cavities. Additionally, since the mid-nineties, low dimensional devices have been designed in the strong coupling regime, yielding the observation of polaritons –eigenstates of semiconductor microcavities in strong coupling regime [Weisbuch et al., 1992]. Confinement can enhance interactions, and can modify the real and imaginary parts of the resonances' energies, or can allow new interaction processes.

In this context, quantum dots represent the model system since they allow quasi-zero-dimensional confinement of electronic states and display a discrete spectrum of energy levels. Quantum dots are usually generated by a process of spontaneous formation, resulting in a broad distribution of sizes and shapes [Bimberg et al., 1999]. This in turn limits the control over the energy-level structure and makes single-dot applications a challenging task. In this framework, 0D strong-coupling involving single or a very few number of particles is of high interest for the study of cavity quantum electrodynamic effects in semiconductors.

Research on solid state systems has also been motivated, during the last 50 years, by the ability to achieve Bose-Einstein condensation (BEC) at high temperature. This effect involves a huge number of particles, that massively accumulate into a single quantum state below a critical temperature, thus displaying macroscopic quantum properties. Bose-Einstein condensation of microcavity polaritons was recently demonstrated in a CdTe based microcav-

ity [Kasprzak et al., 2006]. These quasi-particles have the great advantage over excitons or electrons to exhibit a very light effective mass. BEC was favored by a confinement of the polaritons within small volumes [Kasprzak et al., 2006] in local defects of the microcavity (unintended in this case) an aspect confirmed by theoretical works (see in particular [Sarchi and Savona, 2006]).

0D Polaritons confinement can be achieved either through their excitonic or photonic component. Recently, evidence for 0D polaritons has been given with single quantum dots in micropillars [Reithmaier et al., 2004], photonic nanocavities [Yoshie et al., 2004, Hennessy et al., 2007], or microdisks [Peter et al., 2005] and for a large number of excitations in micropillar structures [Bloch et al., 1998, Obert et al., 2004, Dasbach et al., 2001]. Here we consider a novel system under the strong coupling regime, where 0D confinement is achieved through the photonic part of polaritons in high Q cavities. Our original structure contains mesas in the spacer layer of a semiconductor microcavity, allowing confinement of the cavity photon whilst keeping the strong coupling regime, creating thus confined polaritons. We performed spatial and spectral mapping of the polariton modes that allowed us to directly observe their squared wave function. We also performed studies under the nonlinear regime, exciting, through their photon component, a high number of polaritons interacting through their excitonic component.

We will first present a general outline of this work and then pass rather rapidly from the general to the direct context of polariton confinement. We will see at the end of chapter 1 how we decided to proceed in order to confine polaritons.

In chapter 2 we will see this choice of procedure is not straightforward, and we will elaborate on the tools necessary to conceive and build high-quality microcavity structures with patterned mesas. We will follow the whole process of the fabrication of the sample on which we focused in this work.

We will then characterize the structure we were able to build. In chapter 3 we will ensure that the strong-coupling regime is present in the sample. Then in chapter 4, we will perform a spectroscopic study of the wave functions of the polaritons (resulting from the strong-coupling) in the real and reciprocal (momentum) spaces. We will see that this can also be done surprisingly efficiently without spectroscopic means.

After characterizing the sample, we will study its nonlinear properties. Chapter 5 consists of two different parts: the first one shows the response of the system to a non-resonant excitation, where collective electronic excitations were created at energies far higher than the modes which are of interest to us. The second part of the chapter shows the response of the system to a resonant excitation, where a number of polaritons are intentionally created

in a desired state.

We will present some potential applications in chapter 6, and some experimental perspectives on the sample studied herein or on new samples, in chapter 7.

We will then conclude in chapter 8, and, as concluding does not mean ending, we will add some remarks on this research in an epilogue, not to be considered as part of this thesis work.

Finally, the last part (numbered part IV) of this manuscript will consist of several appendices. The first one deals with the theoretical description of our system, The others will not necessarily be of high interest to the reader, but will be of high interest to my friends and successors, since they include many useful details about the various tests and parameters used during the building and characterization processes.

Part I

A new kind of structure

Chapter 1

Framework

We will give, in this first chapter, some important tools necessary to understand the experiments presented in this work[1]. We will also make a brief overview of the state of the art in strongly coupled semiconductor microcavities.

In the last part (1.5) of the chapter, we will more specifically introduce the context of this work, which aim is to confine polaritons along the three dimensions of space. We will develop what has been done by various groups, and we will discuss some preliminary issues, necessary to start the following chapter about the conception and fabrication of the sample.

1.1 Elements of optical properties of semiconductors

1.1.1 Band structure and excitons

The state of an atom is usually given by its electronic configuration. In a crystal, a macroscopic number of atoms is periodically stacked. In an ideal case, the eigenstates of such a system are given by the electronic configurations of the crystal. These electronic states are characterized by a band structure in the $(E, \vec{k})$ space, were E is the bands energy and $\vec{k}$ the wave vector of the electrons. Between the various bands, some energy ranges (gaps) are forbidden to the electrons.

In most semiconductors, the valence band is completely filled with electrons and split in several subbands with different angular momentum. When the maxima of the conduction and valence band are at the same k-vector, one speaks of a direct gap, when they show different k-vectors, one speaks

[1] Section 1.1 to 1.4 of this introductory chapter are based on the theoretical description of polaritons performed by Vincenzo Savona [Savona et al., 1999], on the thesis of Jean-Philippe Karr [Karr, 2001], Stefan Kundermann [Kundermann, 2006], and Maxime Richard [Richard, 2004].

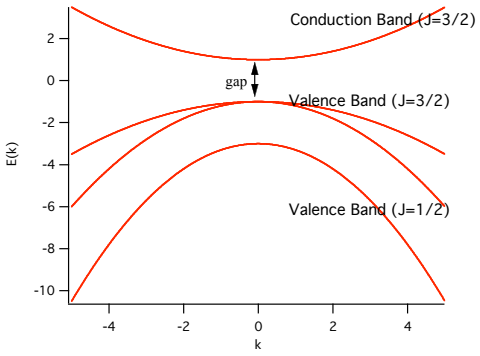

Figure 1.1: Band structure of a III-V semiconductor with a direct gap.

of an indirect gap. Without any excitation the valence band is filled with electrons and the conduction band empty. When one simply mentions the gap, it is a reference to the energy gap between these two bands.

The dispersion curves $E(k)$ can be approximated by parabola around $k = 0$, one can then identify the corresponding electrons to free particles and associate to each curve an effective mass m^* defined in the following way:

$$E(k) \;=\; E(k=0) + \frac{\hbar^2 k^2}{2m^*} \tag{1.1}$$

When an electron is excited from the valence band to the conduction band, it leaves behind a vacancy which is called a hole. Electrons and holes occupying the conduction or valence bands are attributed effective mass m^*corresponding to the curvature of their dispersion curve. They are called, as a function of their spin, heavy holes (spin $\pm 3/2$) or light holes spin ($\pm 1/2$).

Excitons

The optical properties of the crystal depend on the energy of the gap, E_{gap}. The crystal can be optically excited by an electromagnetic wave, it will absorb photons with energies higher than E_{gap}. In this process a photon excites an electron which passes from the valence band to the conduction band. A electron-hole pair is then created.

But the absorption spectrum of a semiconductor crystal shows also a sharp peak at energies lower than the gap. This peak is due to the creation of an electron-hole pair bound by Coulomb interaction, called the exciton. The energy of this excitonic resonance is then given by:

$$E_X(K) \;=\; E_{gap} - E_b + \frac{\hbar^2 K^2}{2m_X} \tag{1.2}$$

Where E_b is the binding energy of the exciton, $\hbar K$ is its momentum and m_X its effective mass, given by $\frac{1}{m_X} = \frac{1}{m_e^*} + \frac{1}{m_h^*}$. As there are two types of holes, there are two types of excitons: the heavy and the light exciton, with different energies[2] and masses.

The exciton system is similar in a way to the hydrogen atom. The hamiltonian is identical and the various exciton levels can also be labeled $1s$, $2s$, $2p$ etc.

1.1.2 Excitons confined in a quantum well

By stacking semiconductor materials with different gap energies one can confine excitons along one, two or three dimensions of space, creating quantum wells (planar structures), quantum wires (1D structure), or quantum dots (0D structures, sometimes referred as quantum boxes). As we worked on 2D structures, we will focus on the confinement of excitons along one spatial dimension, thus confinement *towards* two dimensions.

A quantum well is a 2D layer of a given semiconductor material stacked between two semiconductor materials with larger bandgaps, as shown on Fig.1.2, thus creating an energy well. The confinement energy of the excitons is, in a first approximation, given by the following expression of a particle in a 1D potential well with infinite barriers:

$$E_{conf} = \frac{\hbar^2 \pi^2}{2m^* L^2} \tag{1.3}$$

where L is the width of the quantum well along the confinement direction, we will choose this direction as the z direction of a usual cartesian frame.

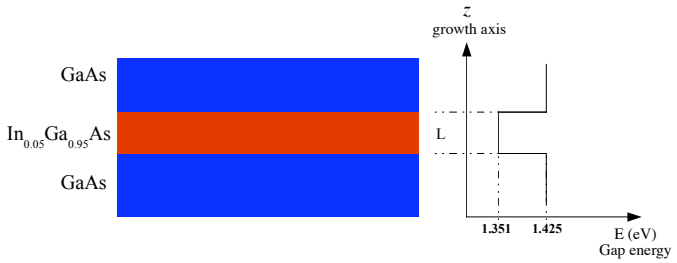

Figure 1.2: Energy profile of an InGaAs in GaAs Quantum Well at room temperature, from [Nahory et al., 1978] cited in [Palmer, 2001].

As the mass of the various heavy and light excitons (and the excitons with various angular momentum) vary, the quantum well shows an energy splitting between these exciton.

[2] Although energies are often degenerate at $k = 0$, in particular in bulk GaAs.

One can apply this description to the material used in this study. As we will see, our sample includes a quantum well consisting of an Indium gallium arsenide with 5% of indium ($In_{0.05}Ga_{0.95}As$) layer of $L = 8nm$ width, stacked between bulk Gallium Arsenide (GaAs), whose band structure shows a higher energy gap than the one of InGaAs, see Fig.1.2.

1.2 Cavities: light confinement

The second element of the system we intend to study is an optical microcavity. The microcavity is a Fabry-Pérot cavity entirely fabricated in solid state, including the spacer between the two mirrors. The mirrors are distributed Bragg reflectors (or Bragg mirrors), they have several important advantages: a very high reflectivity (on a certain range of wavelengths), the fact that they can be grown as the quantum well and in the same molecular beam epitaxy (MBE) chamber, and the fact that, as they are interferential mirrors, they do not heat under high powers as metallic mirrors. The cavity is designed in order to show a resonance at the energy of the quantum well exciton energy.

1.2.1 Bragg mirrors

Bragg mirrors can be seen as a one-dimensional photonic crystal. Photonic crystals are structures with a periodic refractive index, and this periodicity, as in the case of electronic crystals (the semiconductor we saw above), yields the appearance of photonic gaps usually called stopband. The index periodicity can be compared to the potential periodicity in electronic crystals. The calculation which shows the appearance of this gap is really similar to the one performed in a usual crystal, and yields the appearance of energy gaps, using the Bloch theorem. The book of Joannopoulos [J.D.Joannopoulos et al., 1995] shows clearly the analogy and the calculations.

In order to obtain the index periodic structure, pairs of layers of two different natures are stacked. In our case they consist of ≈ 40 alternative layers of AlAs and GaAs (so 20 pairs), having a refractive index of 3.526 and 2.926 at $\approx 10K$ and at a wavelength around $835nm$, as calculated with equations given in ref. [Adachi, 1990], the stopband is proportional to the indices' ratio and has here a width of around $100nm$ in wavelength. The central wavelength λ_0 of the stopband is related to the optical thickness of the mirrors through the relation: $\lambda_0/4 = n_i e_i$, with $i = GaAs$ or $AlAs$, and e_i the physical thickness of each layer.

In order to probe this photonic gap and the photonic modes allowed in Bragg mirror, one can simply perform a reflectivity experiment. Indeed the photonic gap yields a very high reflectivity. One can see an example of this stopband calculated through transfer matrix based simulations on Fig.1.3, the values taken correspond to the values we will concretely use later: 22.5

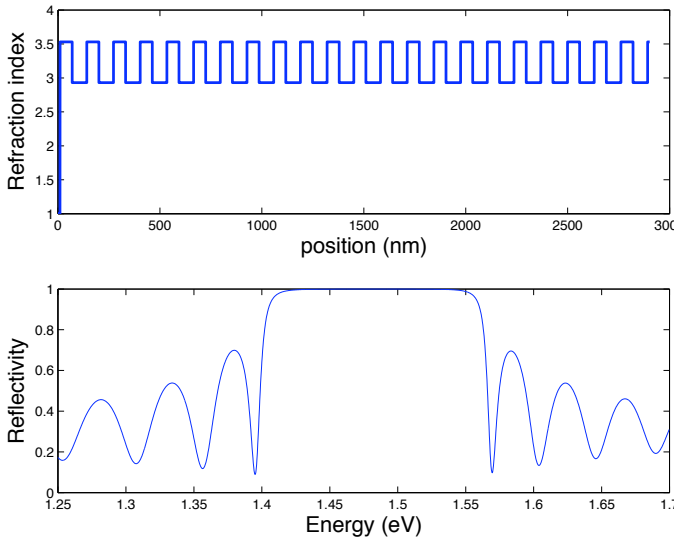

Figure 1.3: Upper figure: refractive index profile. The starting layer on the left is air, and the last layer on the right is the substrate. Lower figure: Reflectivity spectrum.

pairs of 59.4 nm GaAs and 71.6 nm AlAs. We will focus further on these calculations in the next chapter.

1.2.2 Microcavity

Two Bragg mirrors are stacked to form an optical cavity around a GaAs layer of thickness l, called the cavity spacer. As the spacer index is lower than the index of the first mirror layer (AlAs), the cavity modes at the interface between the cavity spacer and the first mirror layer show an antinode. The resonance wavelengths of such a cavity are given by $n_{GaAs}l = l_{opt} = N\ \frac{\lambda_N}{2}$ with N a positive integer and l_{opt} the effective optical thickness of the cavity.

We chose to study what we will from now on call a λ-cavity, because we will focus on the $N = 2$ cavity mode, which is given by $l_{opt} = \lambda_2 = \lambda$. This mode is chosen to be resonant with the exciton's wavelength: $\lambda_{N=2} = \lambda_X = \lambda$.

The Bragg mirrors are designed in such a way that this same λ is the central wavelength of their stopband. λ is a resonance wavelength of the cavity and the electromagnetic field is thus admitted inside the cavity with this wavelength. The reflectivity spectrum shows thus a dip, as one can see on Fig.1.4. Again this reflectivity spectrum was simulated using the parameters of the sample which we will study in this work, as we will se in the next chapter.

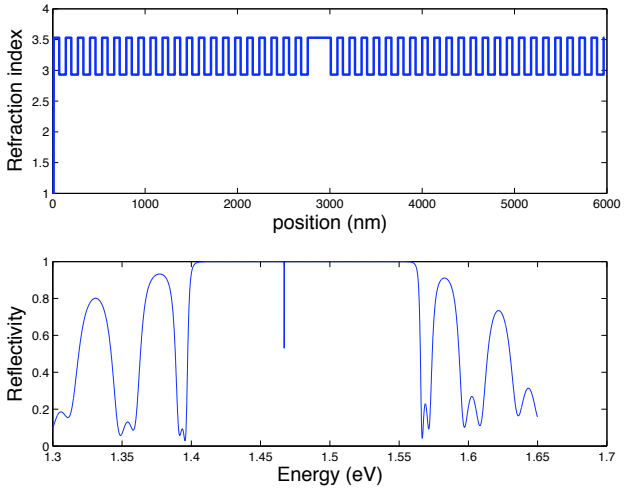

Figure 1.4: Refractive index profile (upper figure) and reflectivity spectrum (lower figure) of a λ-cavity.

Dispersion of the cavity photon

There is a dependence of the cavity resonance on the angle of incidence of the field with respect to normal incidence. The cavity imposes a quantization

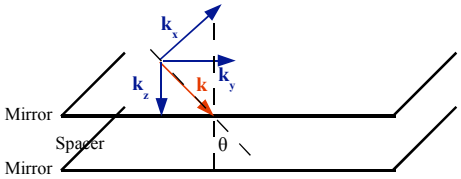

Figure 1.5: Sketch of the cavity, the incident wave vector and its components on z and the plane of the cavity. θ is the angle of incidence.

of the wave vector in the growth direction, which we chose to be z, so let us write $\vec{k}$ in terms of its component k_z along z and $\vec{k}_{||} = k_x\vec{x} + k_y\vec{y}$ (see Fig.1.5) in the plane parallel to the layers (x, y): $\vec{k} = \vec{k_{||}} + \vec{k_z}$. Thus one can write:

$$E = \frac{hc}{n_{GaAs}\lambda} = \hbar ck/n_{GaAs} = \hbar c(\sqrt{k_z^2 + k_{||}^2})/n_{GaAs} \tag{1.4}$$

one can deduce a dispersion relation

$$E(k_{||}) = \sqrt{E_z^2 + \frac{\hbar^2 c^2 k_{||}^2}{n_{GaAs}^2}} \tag{1.5}$$

This equation is parabolic-like around $k_{||} = 0$, thus one can again, as for

the exciton, attribute an effective mass to the cavity photon, deduced from the curvature of equation 1.5 at $k_{||} = 0$:

$$m_{phot} = \frac{n_{GaAs} h}{\lambda c} \tag{1.6}$$

Where λ is, as mentioned before, the cavity $N = 2$ resonance wavelength at normal incidence. For a resonance wavelength of $800nm$, equation 1.6 yields a mass of $m_{phot} = 1.4\ 10^{-36} kg$. The photon dispersion curvature around $k_{||} = 0$ is thus 10^4 times bigger than the exciton's curvature. This gives a mass of the order of 10^{-5} the free electron's mass, or 10^{-4} the exciton's mass.

Quality factor and Finesse

A cavity is an optical resonator. Resonators are characterized through two values measuring the time during which energy is stored compared to the loss rate. The quality factor is defined as follows: [Saleh and Teich, 1991]

$$Q = \frac{2\pi \text{ (stored energy)}}{\text{energy loss per cycle}} = \frac{\nu_0}{\delta\nu} \tag{1.7}$$

where ν_0 is the resonance considered and $\delta\nu$ is its spectral linewidth.

As one can see the quality factor depends on the considered mode (which determines the energy stored in the resonator). The finesse is defined as a function of the free spectral range ν_F and can be linked to the quality factor as follows:

$$\mathcal{F} = \frac{\nu_F}{\nu_0} Q \tag{1.8}$$

The best quality factors in optical cavities can reach 10^8 in dielectric microspheres [Mie, 1908, Braginsky et al., 1989], where strong coupling with a single nanocrystal has recently been observed by LeThomas et al. [2006].

In semiconductor microcavities as presented here, the best quality factors reach $20-30000$ [Stanley et al., 1994, Daïf et al., 2006b, Sanvitto et al., 2005].

1.3 Strong coupling

1.3.1 Principles

It is known since the pioneering work of Purcell [Purcell, 1946], that a 2-level atom placed at the antinode of a standing electromagnetic wave in a Fabry-Pérot cavity, sees its emission probability enhanced. If the coupling between the atom and the electromagnetic wave is sufficient, meaning that the energy exchange is faster than the coherence decay of each, the eigenmodes of the system are a superposition of the atomic excited state and the cavity mode (or cavity photon), this system is called the dressed atom.

The situation is similar for a quantum well embedded in a microcavity. When the coupling between the exciton and the cavity photon is sufficiently strong, one observes new eigenmodes in the system called polaritons. We will rapidly see how these modes can be written.

The hamiltonian of the coupled exciton photon system reads as follows:

$$H_0 = \sum_{k_{||}} E_c(k_{||}) a^\dagger_{k_{||}} a_{k_{||}} + \sum_{k_{||}} E_X(k_{||}) b^\dagger_{k_{||}} b_{k_{||}} \quad + \quad \sum_{k_{||}} \hbar\Omega_R (a^\dagger_{k_{||}} b_{k_{||}} + b^\dagger_{k_{||}} a_{k_{||}}) \tag{1.9}$$

where $a^\dagger_{k_{||}}$, $a_{k_{||}}$ and $b^\dagger_{k_{||}}$, $b_{k_{||}}$ are respectively the creation and annihilation operators of photons and excitons with an in-plane vector $\vec{k_{||}}$, and $\hbar\Omega_R$ is the coupling energy. It depends on the overlap between the exciton's and photon's wave functions, given by the design of the cavity.

The energies of the eigenstates of the hamiltonian 1.9 are:

$$E_\pm(k_{||}) = \frac{E_c(k_{||}) + E_X(k_{||})}{2} \pm \frac{1}{2}\sqrt{(\delta_{k_{||}})^2 + 4|\hbar\Omega_R|^2} \tag{1.10}$$

where

$$\delta_{k_{||}} = E_c(k_{||}) - E_X(k_{||}) \tag{1.11}$$

is the detuning between the cavity mode energy and the quantum well exciton energy. This quantity will often be used in the coming pages. When simply mentioning *the detuning*, we will from now on mean its value at $k_{||} = 0$: $\delta_{k_{||}=0}$.

In the absence of coupling ($\hbar\Omega_R = 0$), the eigenstates of this system are simply the uncoupled photon and exciton. Otherwise, the system is in a "strong coupling regime" and a splitting between $E_X(k = 0)$ and $E_c(k = 0)$ occurs, the latter are not anymore the eigenstates of the system, the energies available to the system are E_+ and E_-. The new eigenstates of the system are the upper and lower polaritons. Fig.1.6 shows the polaritons' dispersion curves, compared to the uncoupled exciton and photon dispersion curves.

The polaritons' operators are written as follows in the original photon-exciton basis:

$$\begin{pmatrix} p_k \\ q_k \end{pmatrix} = \begin{pmatrix} X_k & C_k \\ -C_k & X_k \end{pmatrix} \begin{pmatrix} b_k \\ a_k \end{pmatrix}$$

where $p^\dagger_k$, p_k and $q^\dagger_k$, q_k are the creation and annihilation operators for the lower and upper polariton, respectively, and X_k and C_k are the Hopfield coefficients, introduced by Hopfield in 1958 [Hopfield, 1945-1946], they are equal to:

$$X_{k_{||}} = \frac{1}{\sqrt{1 + (\frac{\hbar\Omega_R}{E_-(k_{||}) - E_c(k_{||})})^2}}, \quad C_{k_{||}} = \frac{1}{\sqrt{1 + (\frac{E_-(k_{||}) - E_c(k_{||})}{\hbar\Omega_R})^2}} \tag{1.12}$$

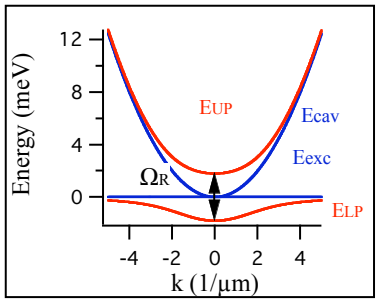

Figure 1.6: Example of dispersion of polaritons: the upper polariton (UP) dispersion follows the equation of $E_+(k_{||})$ and the lower polariton (LP) dispersion curve follows $E_-(k_{||})$. The dispersion curves of the uncoupled exciton and photon are also drawn.

Finally the diagonalized hamiltonian obviously writes in the polariton basis:

$$H_0 = \sum_k E_- \; p_k^\dagger p_k + \sum_k E_+ \; q_k^\dagger q_k \tag{1.13}$$

Analogy with classical coupled oscillators

One can make an analogy between this coupled system and the coupling between two classical oscillators. A weak coupling regime means concretely that the energy exchange between the two coupled oscillators is slower than the decay of each oscillator alone [Savona et al., 1999].

1.3.2 Lifetimes and spectral broadening

We did not consider in the description of semiconductor materials' optical properties, and later on of polaritons, spectral linewidths of the various mentioned states (electrons, holes, excitons, photons, polaritons). We described an ideal system. Nevertheless, real systems show losses and thus spectral linewidths [Pau et al., 1995]. We will mention rapidly the main sources of broadening, in order to support a good understanding of our experimental observations and interpretations.

Homogeneous broadening It is the polaritons' decay rates[3], which are a simple linear combination of the exciton and photon decay rates through:

$$\gamma_-(k) = X_k^2\gamma_X(k) + C_k^2\gamma_c(k) \; and \; \gamma_+(k) = C_k^2\gamma_X(k) + X_k^2\gamma_c(k) \tag{1.14}$$

[3]Introduced by hand as an imaginary part of the energies E_c and E_X of eq. 1.9. They include all sources of decoherence.

Inhomogeneous broadening It is due to both the quantum well and the cavity disorder. The quantum well shows a static disorder [Zimmermann, 1995, Savona, 2007] due to impurities or inhomogeneities present in the growth process. The cavity mode is broadened due to roughness of the interfaces between the layers of the Bragg mirrors [Christmann et al., 2006].

1.3.3 Polariton nonlinearities

We have considered in the description of the system in section 1.3 only linear (first order) terms, this is valid at low densities, at higher densities, several nonlinear phenomena can occur, the most relevant one in the frame of this work is the excitonic Coulomb interaction, which can yield the scattering of two excitons and can be written as follows: [Ciuti et al., 2003]

$$H_{X-X} = \frac{1}{2} \sum_{k,k',q} V_{X-X} b^{\dagger}_{k+q} b^{\dagger}_{k'-q} b_k b_{k'} \tag{1.15}$$

This term, if it becomes dominant, yields nonlinear effects, which we will rapidly mention here, we will come back on these effects in more detail in chapter 5 (nonlinear studies).

- Parametric luminescence [Ciuti et al., 2001], where collisions are the main population mean of given states $\mathbf{k'} - \mathbf{q}$ and $\mathbf{k} + \mathbf{q}$, its population shows a nonlinear dependence on the initial population of states $\mathbf{k}$, $\mathbf{k'}$.
- Parametric oscillations, analog to the optical parametric oscillator [Savvidis et al., 2000, Stevenson et al., 2000, Ciuti et al., 2000], which can lead to giant parametric amplification [Saba et al., 2001] and allow coherent control [Kundermann et al., 2003].
- A broadening of the exciton's linewidth, yielding a broadening of the polaritons linewidths through equation 1.14.
- A blueshift of the exciton's resonance, and thus of the polariton resonance, depending lineraly on the excitation intensity [Ciuti et al., 2001].

1.3.4 Experimental signatures of strong-coupling

In order to characterize experimentally the strong coupling regime, one needs to observe the splitting between the two upper and lower polaritons at resonance between the exciton and the cavity photon. Several experiments are possible, based on reflection or transmission of an incident electromagnetic beam, in order to probe the optical density of states, or based on photoluminescence experiments. We will develop these methods in chapter 3.

In all the methods, spectra are taken on various positions of the cavity, and in case of strong coupling, two modes can be seen around the resonance energy instead of one degenerate. Nevertheless, this single observation could be attributed to many phenomena different than strong-coupling, as the observation of light-hole exciton for example. The certainty of the strong-coupling regime can be brought only by an anticrossing behavior. Two kinds of behaviors can be observed (See Fig.1.7 for illustration):

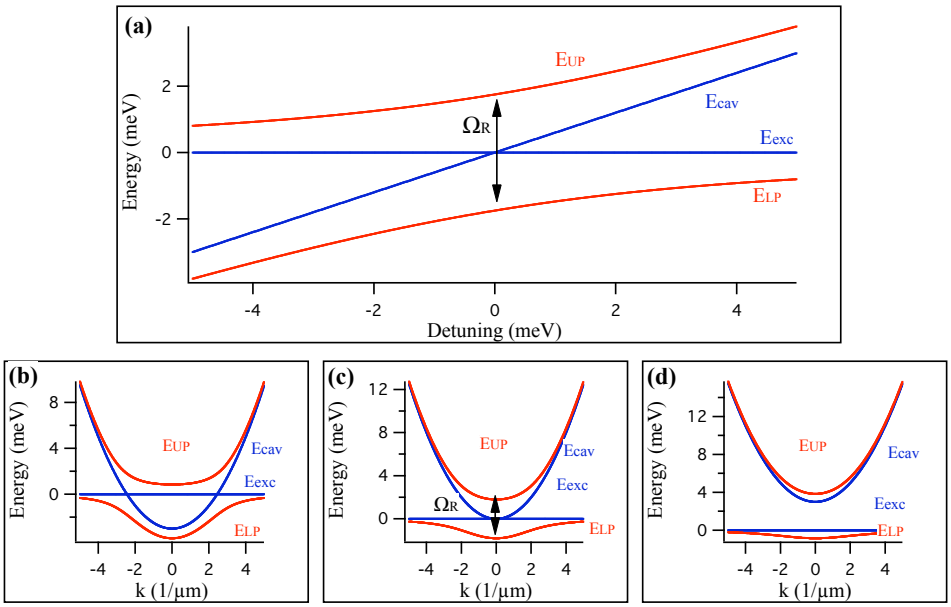

Figure 1.7: (a) Real space (at $k_{||} = 0$) anticrossing curve. Dispersion curves (b) $\delta_{k=0} = -3meV$ (c) $\delta_{k=0} = 0meV$ and (d) $\delta_{k=0} = +3meV$. Curves computed from eqs.1.2,1.4 and 1.10 with a Rabi splitting of $3.5meV$, considering the exciton energy as the origin.

Anticrossing through cavity mode tuning By suitable fabrication of the sample, one can introduce a linear variation of the cavity mode energy along the sample's radius. This allows to tune the detuning $\delta_{\mathbf{k}_{||}=\mathbf{0}}$ between the cavity and exciton energy. If, scanning between $\delta << 0$ and $\delta >> 0$, one observes an anticrossing behavior of the resonances energies as illustrated on Fig.1.7(a), it is a signature of strong-coupling. This method was used for the first experimental demonstration of strong-coupling in a semiconductor microcavity by Weisbuch et al. [1992].

Reciprocal-space anticrossing As we will see in chapter 4, it is possible to access the dispersion curve of the system through Fourier-space imaging, thanks to its 2D character. At negative detuning $\delta_{k=0} < 0$, if

one observes an anticrossing behavior at a certain value of $k > 0$ and at the symmetrical value $-k$, see Fig.1.7(b), it is an anticrossing characteristic of strong-coupling. A non-parabolic dispersion for the lower polariton dispersion curve (Figs.1.7(b)-(d)) is another characteristic feature of strong-coupling. This method was first experimentally used for a semiconductor microcavity in strong-coupling in 1994 by Houdré et al..

We will base our work on these two methods. We will use the first method to demonstrate strong-coupling in our sample in chapter 3, and illustrate it using the second method in chapter 4. Two other methods, that we will not use, are also possible:

Temperature tuning It is possible to tune the exciton's energy through temperature tuning. This method is usually used when it is not possible to vary the cavity mode's energy, for the demonstration of strong-coupling of a single quantum dot with a cavity. This method was used for example in refs. [Peter et al., 2005, Reithmaier et al., 2004, Yoshie et al., 2004].

Time-resolved studies It is finally possible to demonstrate strong-coupling by directly observing in the time domain the energy exchange (the Rabi oscillations) between the two polariton modes, this method was for example used in ref. [Norris et al., 1994].

1.3.5 The strong to weak coupling transition

The system shows strong-coupling for sufficient coupling strength Ω_R. When writing the total hamiltonian, including coupling terms[4], the coupling strength is replaced at resonance by the quantity

$$\Omega'_R = \sqrt{\Omega_R^2 - (\gamma_c(k) - \gamma_X(k))^2}$$

which depends on the coupling strength and on the linewidths of the coupled oscillators [Savona et al., 1999]. This quantity is the vacuum Rabi splitting. It is the energy difference between the two polariton modes at resonance between the exciton and cavity photon.

Due to the finite lifetime[5] of the cavity photon and of the exciton, a condition *sine qua non* for strong-coupling is that the energy exchange should be faster than the decay rates, this can be written as follows:

$$\Omega_R > \gamma_X,\ \gamma c \tag{1.16}$$

[4] e.g. to phonons

[5] In the exciton's case, one should say coherence time, as it is shorter than the lifetime, but it is the cavity photon lifetime which is the limiting parameter.

One can now give some objective criteria for the recognition of the transition[6] from strong to weak coupling regimes. Starting from a strong-coupling regime situation, the strong-coupling can be lost for two reasons:

If γ_c and/or γ_X increase Concretely the most probable situation is an increase of the exciton's linewidth γ_X, due to various effects we will describe in section 1.4.

If Ω_R decreases Ω_R is the coupling strength between the excitons and the photons. It depends on the exciton's oscillator strength ($\Omega_R \propto \sqrt{\frac{f}{S}}$). The strong-coupling regime can be therefore lost by saturation of the excitonic oscillator strength, in other terms by loss of the bosonic character of excitons, and in even simpler terms, by loss of the excitons in favor of electron-hole pairs. This happens at high densities, as shown by equation 1.18.

Experimentally, the way to interpret this is by a double inequality a derived from 1.16:

$$\Omega'_R > \gamma_-,\ \gamma_+ \tag{1.17}$$

When the splitting between the polaritonic resonances is smaller than the linewidth of each of the two modes, it is in practice nearly impossible to distinguish them anymore.

1.4 The bosonic character of polaritons

1.4.1 Validity of the bosonic nature of excitons

Excitons are bosons composed of fermions as can be an atom, with a big difference regarding the binding energy. The latter is $13.6eV$ for the hydrogen atom and of the order of several meV for the excitons in III-V semiconductors, so much lower. This means that excitons are fragile bosons!

As an exciton state is spread over a high number of electronic states in a crystal. Pauli's exclusion principle does not forbid a big occupancy of an exciton state, as long as the system is at low density. At high densities, the occupation of the electronic states increases, Pauli's exclusion principle applies and makes it more and more difficult to create new excitons.

This can be summed up by writing the commutator of the exciton's creation and annihilation operators [Haug and Koch, 1990] (which should be exactly equal to one for a perfect boson):

$$[b, b^\dagger] \sim 1 - O(na_B^2) \tag{1.18}$$

[6]The use of the word *transition* should not lead the reader to understand *phase transition*, as there is no order parameter build-up in this case, the transition is progressive.

where a_B is the exciton's Bohr radius. The critical density over which the exciton can not be considered as a boson anymore is thus $\sim 1/a_B^2$. In the case of an $In_{0.05}Ga_{0.95}As$ in GaAs quantum well, the Bohr radius is approximately $a_B \simeq 12nm$ [Grassi Alessi et al., 2000]. This yields a critical density $n_0 \sim 7.10^{11} cm^{-2}$, consistent with experimental values of about $\sim 10^{11} cm^{-2}$.

This is a cause of loss of strong-coupling, as it leads to both features described in section 1.3.5.

1.4.2 Bose-Einstein condensation of polaritons

The aim of the structure we are introducing in this work is to favor a Bose-Einstein condensation (BEC) of polaritons. Let us therefore have a short look at the properties of a polariton BEC phase.

Bosons can show a spectacular transition to a peculiar condensed phase: Bose-Einstein condensation. This condensation sees a macroscopic number of bosons accumulate in the ground state of a system, a lot has been written since its prediction by Bose and Einstein [Bose, 1924, Einstein, 1924] till its discovery in 1995 in ultracold atomic gases. In these systems temperatures of the order of the nK need to be reached. In this sense, polaritons, as long as they can be considered as bosons (in the low density limit) are of great interest as they have a very small effective mass in comparison to the exciton (thanks to their photonic component), which theoretically should allow them to show a temperature of condensation higher than $0.1K$ [Kavokin et al., 2003].

The open character of the polariton system, due to their extremely short lifetime, questions however the thermodynamic equilibrium necessary to reach condensation. It was demonstrated that despite this openness, it is possible to observe a thermodynamic equilibrium under certain density conditions [Kasprzak et al., 2006], in the same reference, Kasprzak et al. unambiguously observe Bose-Einstein condensation. Three key points were observed and allowed them to infer BEC :

Accumulation of population in the ground level of the system supported by an evaluation of its occupancy number, found to be macroscopic ($>> 1$).

Long-range order The mean correlation length jumped from $\sim 3\mu m$ (the de Broglie wavelength) to $\sim 13\mu m$.

Thermodynamic equilibrium The distribution of population along states having higher energies than the ground state was found to be a Boltzmann distribution.

1.5 Confinement of 2D polaritons

Spatial trapping of polaritons, the main subject of this work, should favor BEC. We will now see in more detail the motivation of this trapping, and what is the method chosen to achieve it.

1.5.1 Why?

In order to obtain a condensed phase in semiconductors, the peculiar trap shape of the lower microcavity polariton dispersion curve has motivated several relaxation experiments towards the bottom of this "trap" [Richard, 2004, Richard et al., 2005]. Nevertheless, when this work started, no polariton condensation was unambiguously demonstrated yet. And it appeared that, along with the "trapping" along the dispersion curve, spatial confinement of polaritons, yielding the apparition of discrete polariton states, was needed. Indeed confinement increases the density of polaritons per state, without increasing the global density of excitons per cm^2. This should help reaching the condensation threshold of more than one polariton per state, while avoiding the loss of the strong coupling regime and of the bosonic character of polaritons.

Bose-Einstein condensation has now been observed in a cadmium telluride microcavity sample (II-VI semiconductor) [Kasprzak et al., 2006]. It appears that spatial confinement on the micron scale, due to an important photonic disorder present in this kind of materials [Richard, 2004], along with the peculiar dispersion curve, was a key element that allowed condensation of polaritons.

Thanks to the light effective mass of polaritons, a lateral confinement on the micron scale is sufficient to achieve quantization of the polariton states – a quite unique situation in a semiconductor artificial structure that makes fabrication, positioning and optical addressing much easier than for other nanostructured systems.

1.5.2 A state of the art of polariton confinement

Attempts to produce spatially confined polariton states, in the past, have been made by etching micropillars of a few μm in diameter from an initially planar microcavity [Bloch et al., 1998],[Dasbach et al., 2001],[Gutbrod et al., 1998]. These structures have in general proved to be able of producing lateral confinement of polariton modes. However, they tend to display strong coupling only in the limit of very small diameter [Bloch et al., 1998], typically in the 1-2 μm range. Sometimes the spectral signature of the upper polariton – needed as a proof of the formation of polaritons as normal modes of the linear exciton-photon coupling – is absent, as in ref. [Dasbach et al., 2001]. In this reference the linewidth of the confined lower polariton is rather high.

These two features are probably due to the fact that the confined mode, at such small mesa diameter sizes, are coupled to the free 3D continuum through the lateral walls of the pillar. Indeed the lateral wall of the mesa is directly in contact with air, and shows disorder, allowing the electromagnetic waves to scatter.

Gerard et al. studied the confinement energies of pillar microcavities in 1996. Later on, in the same group, Lalanne et al. [2004] have studied the quality factor of pillar microcavities depending on their diameter [Lalanne et al., 2004], and have shown that a lower diameter limit exists, below which the Q-factor decreases very rapidly, again because of the interface roughness, that favors the coupling with the 3D continuum of electromagnetic modes. In their case it is at around $0.5\mu m$ but this limit depends on the material and interface quality of the studied sample.

Added to the basic confinement, several nonlinear phenomena were observed in such pillar microcavities in strong-coupling regime. Parametric oscillations in 1D microcavities was observed in a unique kind of linear sample by Dasbach et al. [2005]. Parametric oscillations and luminescence were reported in refs. [Dasbach et al., 2001, Bajoni et al., 2007].

For sake of exhaustivity, let us mention another way of confining polaritons, through the electronic excitations' confinement in quantum dot structures, placed in micro or nanoresonators. These systems are not candidates for BEC, as only one polariton is created, but are of great interest for cavity quantum electrodynamics experiments. This was achieved by three groups [Peter et al., 2005, Reithmaier et al., 2004, Yoshie et al., 2004] a couple of years ago. The main problem of this technique is the difficulty to place easily the quantum dot at an antinode of the cavity field. This was solved by Badolato et al. in 2005, who reported the observation of Purcell enhancement of the quantum dot emission through a suitable placement. This led them recently to the observation of strong-coupling regime between a single quantum dot and a photonic crystal nanocavity [Hennessy et al., 2007].

1.5.3 And now... how?

The idea developed at the LOEQ for the lateral confinement of polariton is inspired from the state of the art presented above, in the sense that the polaritons are to be confined through their photonic component. It is however different in the sense that the whole cavity is not etched. The idea is simply to create locally, on the spacer layer of a usual 2D sample, a thicker cavity, along several microns. This creates, locally, a slightly thicker cavity, see Fig.1.8. As equation 1.4 shows, $E_c(x) \propto \frac{1}{l(x)}$, thus the thicker cavity lowers the cavity photon energy, and finally, if the strong coupling is preserved, the polariton energy.

We will simply call these local thickness variations *mesas*, these mesas act as traps for the cavity photons, and thus for the polaritons.

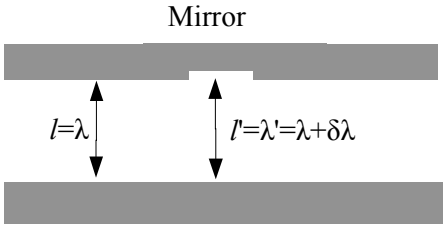

Figure 1.8: Principle of cavity photon confinement: local variation of the cavity thickness.

This method shows *a priori* several advantages, which will mostly be confirmed by the measurements presented in the next chapters.

Tunable trap depth The depth of the trap with respect to the surrounding 2D cavity is tunable, as it is directly related to the physical depth of the mesa. We will see that it is sufficient to produce a mesa height of the order of the nanometer.

No lateral losses The lateral interface is reduced to the minimum, as the mesas show height of the order of the nm, and there are no accessible states out of the mesa at the suitable energies. Compared to the micropillar walls which height is $\propto \mu m$, this reduces lateral losses, which are an important limitation to strong coupling [Obert et al., 2004].

Multidimensionality On the example shown on Fig.1.8, it is clear that the 2D and 0D structures coexist, one can thus imagine interaction between the corresponding polaritons. There is also in principle the possibility of having 1D structures, coupled to neighboring structures of any in-plane shape.

No size limitation As the surrounding environment is the 2D structure, there is no possibility of coupling with a continuum of external modes, and thus the lower size limitation shown in ref. [Lalanne et al., 2004] does not apply.

1.5.4 Orders of magnitude

In order to have a rough idea of the depth of our trap, we need to recall the fact that we want the strong coupling regime to be present both in the mesas and around, and we want to be near resonance, in order to be able to observe the degeneracy lifting. Which means that we would like the confining potential V to be smaller than or of the order of the Rabi splitting

$V \lesssim \Omega_R$, 3.6meV in our case, equivalent to a cavity thickness variation of $\approx 3nm$.

In order to have a rough idea of the width to give to our trap, we calculate orders of magnitudes, simply considering the polariton as 2D particles of mass m, confined in a cylindrical well. Leyronas and Combescot published a very useful paper [Leyronas and Combescot, 2001] giving analytical expressions for the bound states of quantum wells, wires and dotes. We applied the case of cylindrical wire confinement to our situation.

They sum up the problem through a dimensionless parameter ν defined as follows:

$$V = \frac{\hbar^2 \nu^2}{2mR^2} \tag{1.19}$$

where V is the energy depth of the confining potential, m the mass of the confined particles and R the radius of the cylinder.

To every given confinement depth V and width (radius R), one can attribute a ν through equation 1.19. Leyronas and Combescot give then an analytical expression of a parameter α, which labels the confined levels, allowing to calculate their number and energies through the following equation: $E = \frac{\hbar^2 \alpha^2}{2mR^2}$. As we are using this model to obtain a first idea, it is enough here to show the graphic results on figure 1.9.

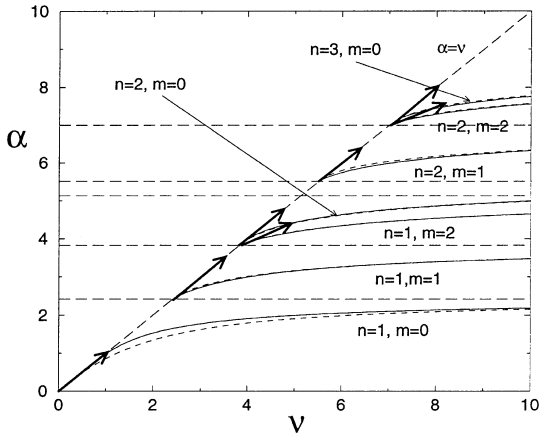

Figure 1.9: Energy and number of confined levels (labeled by α) as a function of the confining potential (labeled by ν). Figure taken from [Leyronas and Combescot, 2001].

Numerical application

We will take indicative values in order to have a rough idea of the number and energies of the confined states, taking into account that in the sample which we are presenting in this work the Rabi splitting is $\Omega = 3.6meV$.

- If $V = 1meV$
  - if $R = 1\mu m$ one confined level of energy $0.1meV$ with respect to the trap's bottom energy.
  - if $R = 10\mu m$ four confined levels of energies of the order of $\approx 0.1meV$.
- If $V = 10meV$
  - if $R = 1\mu m$ four or five confined levels of energies ranging between $\approx 1 - 10meV$.
  - if $R = 10\mu m$ several tens of confined levels of energies starting from $\approx 1meV$.

We tried several couples of (V, R), and compared to the results given by an even simpler model: a 1D infinite well, where the energies are given by $E_n = \frac{n^2\pi^2\hbar^2}{2mR^2}$, $n \in \mathbb{N}$. The latter gives similar results, with a factor of ≈ 5 of difference on the energies. We finally chose to have in mind a potential $V \simeq 5meV$ with $3 < R < 20\mu m$ while fabricating the sample.

1.5.5

We will use, to talk about the confining structures we are studying, several equivalent terms. Physically, as in a cavity the energy of the modes is inverse proportional to the cavity length, a confining structure is thicker, and is thus a mesa above the surface. These mesas, although they are thicker cavities, show lower energies, and, as we will try to show, trap the states we are studying, they can thus also simply be called traps.

Now that we have given the main tools necessary to understand our studies, let us first see how we were able to conceive and build such structures.

Chapter 2

Conception and fabrication of the sample

We will present in the following pages the method chosen to fulfill our aim, developed in the precedent chapter, of trapping polaritons through their photonic component. We will first give general elements about our sample growth and characterization apparatus, and we will then follow linearly the fabrication process which lead to the sample studied through this work.

2.1 Preliminary

Let us first see some key elements which allowed the sample fabrication to be successful.

2.1.1 General idea

The idea is to create a usual 2D-semiconductor microcavity in strong coupling regime, with local thickness variations yielded by mesas on the spacer layer. The latter would act as traps for the photon component of the polaritons[1].

As we saw in the precedent chapter, the height of these mesas is chosen of the order of the nm, in order to allow us to observe the strong-coupling regime both on and around the mesas. The mesas are expected to be populated through relaxation of the usual 2D polaritons towards confined states. Their shapes are chosen with the same objective: circular shapes are planned as the simplest trap shape, but also annular and star shapes are planned, with the idea to create corridors from the 2D zones towards the traps.

[1]The general idea was first developped by Thierry Guillet and François Morier-Genoud before my arrival, we worked together for several months and then the growth process and the further developments of the techniques were performed by François Morier-Genoud (focused on the growth part) and myself (focused on the optical part). Nothing would have been possible without this really fruitful, enlightening and joyful collaboration.

The samples are grown by Molecular Beam Epitaxy (MBE). The mesas are fabricated through selective chemical etchings of intermediate layers with carefully chosen thicknesses. The technique of selective chemical etching for GaAs and AlAs was developed for example by LePore [1980]. The thickness control is ensured through a combination between high-quality calibrated MBE growth and characterization through white light reflectivity compared to simulations. These processes will extensively be illustrated through the case of our sample in section 2.2.

As the characterizations and etchings are done in the middle of the growth process (before the growth of the upper Bragg mirror of the cavity), one needs to control regrowth techniques. Regrowth is possible on clean surfaces of GaAs.

2.1.2 Materials used

Several semiconductor materials are usually used for growing microcavity samples in strong coupling regime. In our institute, these are III-V materials based on arsenic allied with either indium, aluminum, or gallium. Our best quantum wells (in terms of luminescence intensity and linewidth) are InGaAs quantum wells, one can appreciate their extremely high quality in ref. [Deveaud et al., 2005]. They also have the advantage of allowing us to work in transmission [Houdré et al., 1994] through the substrate, as the exciton's energy is lower than the energy of GaAs absorption gap, which is shown on Fig.2.1. Generally, the rate of impurities plays also an important role in absorption, growth by molecular beam epitaxy (MBE) ensures a low impurity ($\approx 10^{14} impurities/cm^3$ [Ilegems, 1985]) concentration in our materials.

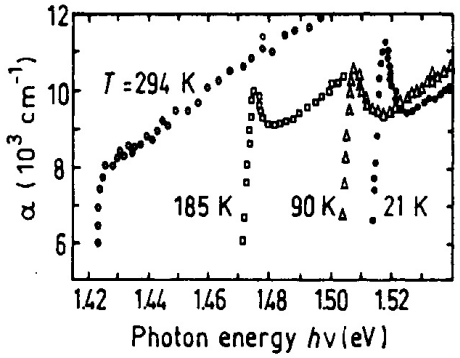

Figure 2.1: Absorption profile of bulk GaAs. [Sturge, 1962]

Experimental data for GaAs based materials are mainly taken from a review performed by the Ioffe institute [Ioffe, 199X] and from measurements performed by Bosio et al. [1988].

We chose to grow mirrors with thicknesses adapted to the exciton energy at low temperature. The mirrors were grown with $Al_xGa_{1-x}As$ alloys, which index varies at low temperatures as a function of temperature and energy. From ref. [Adachi, 1990] we write the dependence as follows:

$$\begin{aligned} n \quad & (Al_xGa_{1-x}As) = -0.6 * x \\ + \quad & \sqrt{((3.255 * (1 + 4.5 * 0.00001 * T))^2 - 6.215 * 0.133 * E^2)/(1 - 0.133 * E^2)} \end{aligned} \tag{2.1}$$

with the temperature T in Kelvin and the energy E in meV.

At room temperature empirical fitting of experimental curves given by the Ioffe institute was performed and gives (with an energy E in eV)

- If $(E > 1)$: $n(Al_xGa_{1-x}As) = 3.35 - 0.6 * x + 0.38 * (E - 1)$
- Else $n(Al_xGa_{1-x}As) = 3.35 - .6 * x$

We chose binary alloys of GaAs/AlAs in order to ensure the largest stopband. It is an important security as we will etch mesas, and thus have different cavity modes, whose resonance with the exciton should be separated by small distances along the sample's surface. Added to that, we could ensure better material and interface quality for binary alloys than for ternary ones.

2.1.3 Characteristics of local growth methods

Tuning resonances: the wedge

As mentioned available materials are gallium, indium and aluminum to be allied with arsenic. The sample holder is a $2inch-$ wafer holder, and samples are commercial GaAs substrates. The samples are grown on $5cm-$diameter circular wafers consisting of a substrate of industrial GaAs.

The flux of material which promotes the growth is not homogeneous. This yields a thickness inhomogeneity of around $20 - 30\%$ on a two inch-substrate, it can be diminished by rotating the sample. In the case presented here, we reach with this technique a thickness gradient of around $4 - 5\%$ along the sample's radius. The gradient is present on all the grown layers, although it may change a little bit with the nature of the material, from now on we will simply call this effect the wedge.

To characterize this wedge for AlAs and GaAs we grew a sample consisting of a semi-cavity, it consists of one 15 AlAs/AlGaAs pair-DBR, a spacer, with no upper mirror but the GaAs/air interface (sample labeled 1479). We then performed reflectivity experiments along the sample's wedge, and for each measurement we performed Transfer Matrix simulations[2] in order to

[2]The program used to simulate 2D AlGaAs structures, based on the transfer matrix method, was originally written by Cristiano Ciuti, we really thank him for his precious help. The program is shortly presented in section 2.1.7 in the next pages.

simulate its reflectivity. Fig.2.2 shows the thickness profile obtained along the radius. A value of 1 for $GaAs$ (respectively $AlAs$) indicates that the simulation works with the nominal thickness.

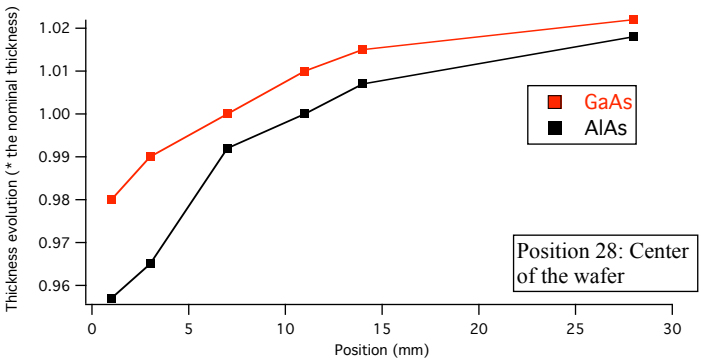

Figure 2.2: Thickness gradient for AlAs and GaAs along the sample's radius.

The thickness decreases from the center to the border. The wedge is not linear on the outer $5mm$ of the wafer, afterwards it seems linear till the center. There is a rotational symmetry around the center, it will allow us to have several different working samples with the same thickness[3].

The zone where the wedge can be considered linear shows a thickness variation of around $3-4\%$, this percentage will later allow us to vary the cavity mode energy with respect to the exciton resonance by up to $\approx 30nm$. This wedge value is similar to what was used in the first observation of a Rabi-splitting in a semiconductor microcavity by Weisbuch et al. [1992], the sample was fairly similar to the one we will be dealing with here.

The exciton is indeed nearly not affected by the wedge: the QW confinement energy depends on its thickness a as $\frac{1}{a^2}$. If one writes the exciton confinement energy as $E_{qw} = \frac{\alpha}{a^2}$, one deduces $dE_{qw} = \alpha\frac{(-2da)}{a^3}$, if a varies of 1%, $da = \frac{a}{100}$ and thus $dE_{qw} = \alpha\frac{(-2)}{100a^2} = (-2/100)E_{qw}$. The confinement energy is of the order of the meV, it has to be added to the non-confined exciton's energy given by equation 1.2 (of the order of the eV), this yields a final variation of the order of 0.01% for the quantum well exciton along the sample.

2.1.4 The structure chosen

The structure which was designed for this work is described in detail on Fig.2.3, it is a GaAs $\lambda-$cavity with an $8nm$ thickness embedded single quantum well. Namely it is composed of 22.5 pairs of GaAs/AlAs lower Bragg mirror, a spacer composed of 3 different layers : $114.5nm$ of GaAs, $8nm$

[3]The wafer is cleaved in several pieces of around $3*15mm$, which constitute each a working sample.

of InGaAs (with 4% In) and then 114.5nm of GaAs, then an upper Bragg mirror of 21 pairs of GaAs/AlAs layers comes above.

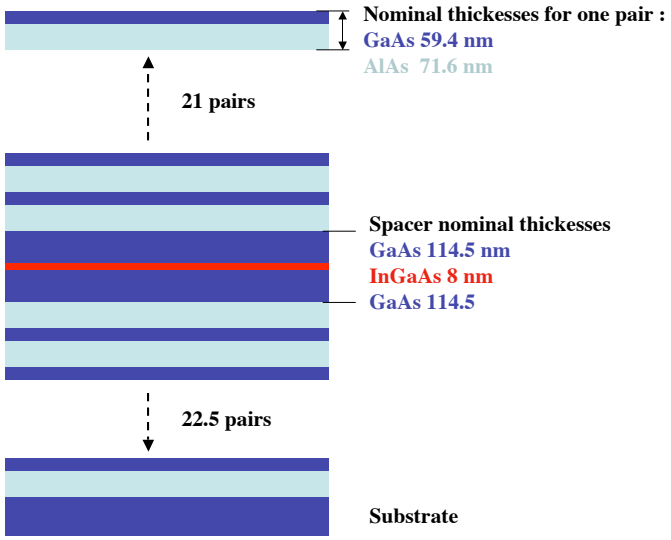

Figure 2.3: Profile of the chosen structure.

Various tests were made before reaching the suitable sample, in particular on quantum wells with various thicknesses and composition. We will see in the perspectives that these tests are still going on for further improvements of the linewidths and radiative intensities.

2.1.5 Mesas

The printing of the structure is done through a photolithography process. A mask is used to reproduce the pattern on the sample's surface previously coated with a photoresist. A first mask was designed and fabricated by Thierry Guillet and François Morier-Genoud. As described in the precedent pages the first trap shapes designed were discs, ring and star-like shapes were also drawn. All these patterns were chosen to have between 5 and 20μm in diameter (See chapter 1 for detailed explanations), and are disposed in triangles every 150μm.

Finally, in order to be able to probe the height of these mesa, and the quality of the sample, both on the mesas and around, a zone of the mask was designed with large 300μm squares where no confinement effect is expected, but where extended 2D polariton modes are expected, both on the mesas and outside. This allows us to use reflectivity techniques similar as what

was used to characterize the wedge, in order to characterize the thickness step. These four zones are sketched on Fig.2.4.

As opposed to what was planned, the discs drawn on the mask are not perfectly circular, but slightly oval-shaped. In fact all the shapes designed show small asymmetries, due to an original asymmetry which was present on the laser beam used to draw the mask itself.

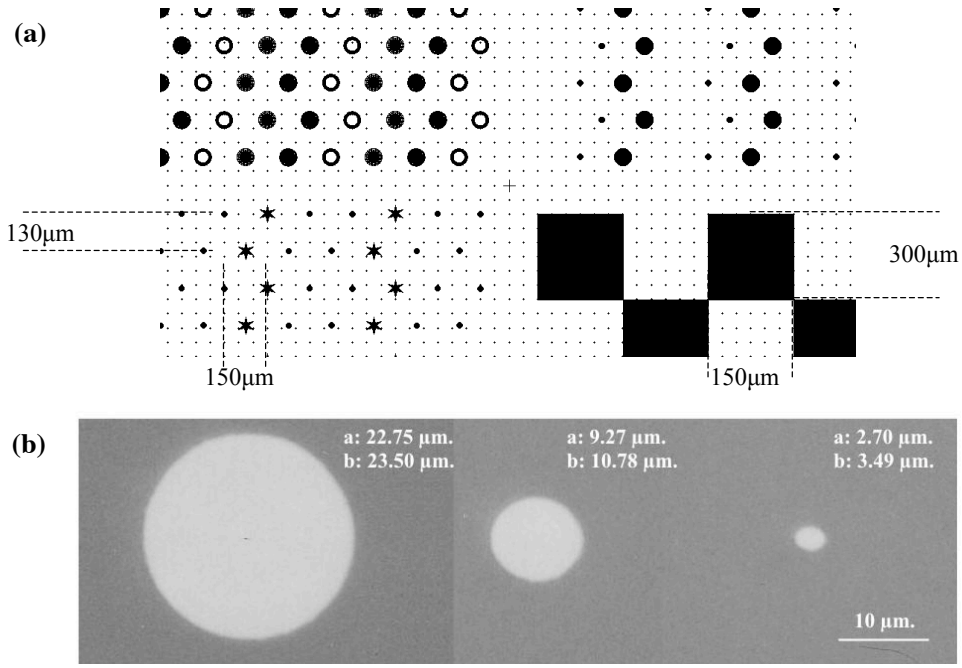

Figure 2.4: (a) Central zone of the mask. The mask is divided in three quarters, respectively filled with discs, rings, stars and large squares. (b) Photograph of the oval-shaped discs. a is the vertical diameter, b is the horizontal diameter. The originally planned diameters were 5, 10 and 20μm.

As the mesas are intended to be etched at the spacer level, this photolithography is performed on the spacer layer, before the growth of the second Bragg mirror. This needs to take the sample out of the MBE chamber to perform characterization, photolithography and etching processes, then the upper Bragg mirror is regrown on a surface which is not as clean as if it had stayed in the chamber.

2.1.6 In situ cleaning and regrowth

The MBE which was used to grow the studied sample allows[4] an *in situ* hydrogen plasma cleaning. This technique was progressively developed in the last 20 years (see for example [Petit and Houzay, 1994]). It is thus possible to clean the surface of the sample inside a chamber directly communicating with the growth chamber, hydrogen cleaning ensures a clean surface at the atomic scale. When the sample is clean, it is brought to the growth chamber under ultrahigh vacuum, without being in contact with air. An immediate start of a structure growth is made possible by the cleanness of the surface.

As we will see, this point is crucial in our case as we need to perform regrowth without being able to grow first a buffer of GaAs, as one usually does to with a commercial GaAs substrate.

2.1.7 Simulation

A program was written by Cristiano Ciuti in order to simulate the optical response of a stack of $Al_xGa_{1-x}As$ layers, using the transfer matrix method. The program takes into account several important features:

- The temperature and energy dependance of the refractive index of the layers (mentioned in section 2.1.2).
- The absorption due to GaAs at energies above its gap.

Accounting for the wedge Two variables f_{GaAs} and f_{AlAs} were used as multiplying factors to the thicknesses of AlAs and GaAs layers. These factors are automatically applied to all the layers, in case of an alloy a combination is applied depending on the proportion of Al: $f = \frac{1}{2}((1-x)f_{GaAs} + xf_{AlAs})$, x being this proportion ($0 < x < 1$).

When trying to adjust a simulation to an experimental reflectivity, the only tunable parameters are these two factors, this allowed us for example to obtain an evaluation of the wedge shown on Fig.2.2.

Having given the main elements which characterize our growth possibilities and our methods, let us go now in detail through the growth process which led to the sample on which is based this whole work.

2.2 Growth of a microcavity with embedded mesas

We will focus now on the growth of the sample, labeled 1485, on which this work is based.

[4] In fact one should say allowed, as this MBE is now out of service, yielding a new challenge for the growth of the next generation of samples: how to restart growth on a perfectly clean surface, we will deal with this issue in the perspectives.

2.2.1 First growth and characterization

Semi-cavity

The first step of the fabrication of the structure is the growth of a DBR (Distributed Bragg Reflector or Bragg Mirror) designed to show the center of its stopband at the emission energy of the Quantum Well, already described in section 2.1.2 (Materials). The DBR consists of 22.5 pairs of GaAs/AlAs $\lambda/4$ layers (with λ the central wavelength of the stopband), on a commercial GaAs substrate on which is first grown a buffer of GaAs. This DBR shows a stopband which center is chosen to be resonant, at low temperature, with the first excitonic resonance ($1s$ exciton) of a quantum well of $In_{0.04}Ga_{0.96}As$ embedded in GaAs. From now on, we will name this resonance λ, as the cavity length will be chosen according to this resonance.

The Quantum Well was previously tested separately, it has a width of $80\mathring{A}$ and shows an exciton emission at $835nm$ ($1.4848eV$) at low temperature ($\approx 10K$). The latter shows a small linewidth of $500\mu eV$. A lot of testing work was performed in order to reach this small linewidth, along with a high radiative efficiency. Some complementary information about QW emission as a function of the various parameters (Fluxes in the MBE, temperature, thickness...) are given in student's works mentioned in Appendix C.2.

Refractive index calculation at this temperature [Adachi, 1990] gives approximate values of 3.526 for GaAs and 2.926 for AlAs[5] and we deduce the optimal thickness for the mirror layers: $71.6nm$ for AlAs and $59.4nm$ for GaAs.

The cavity spacer is also chosen to be resonant with the QW exciton. As we developed in the precedent chapter, it is chosen to be a $\lambda-$cavity. The cavity thickness is $l = \lambda/n \approx 230nm$. As the InGaAs QW has a very low Indium proportion, we approximate it as GaAs in the thickness calculation. The spacer is thus made of twice $\approx 111nm$ of GaAs surrounding a 8nm-thick QW.

We will call this succession of one DBR and a cavity spacer embedding a QW *a semi-cavity.*

Etchstops

This semi-cavity is covered by a series of layers which will be used for the etching of mesas, in the presented case these layers are, from top (air) to bottom (semi-cavity):

- GaAs 20 nm
- AlAs 6 monolayers, 1.8nm

[5] We calculate the refractive index for GaAs according to equation 2.2 and then pass to AlAs by adding a linear component depending on Aluminum proportion in AlGaAs: $n(Al_xGa_{1-x}As) = n(GaAs) - 0,6x$

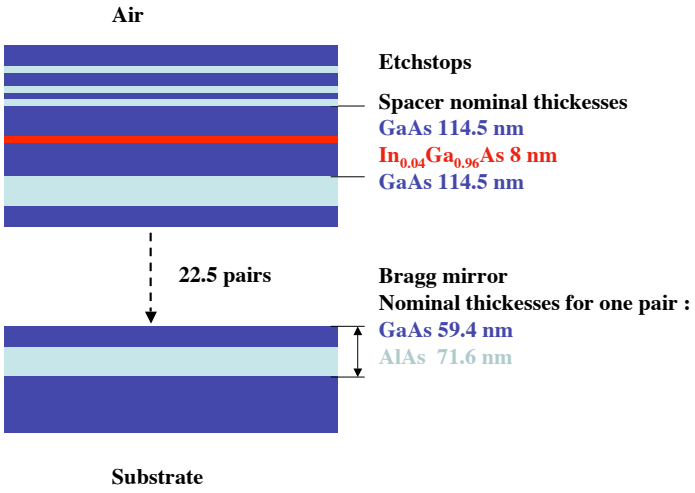

Figure 2.5: First growth: semi-cavity, etchstop layers.

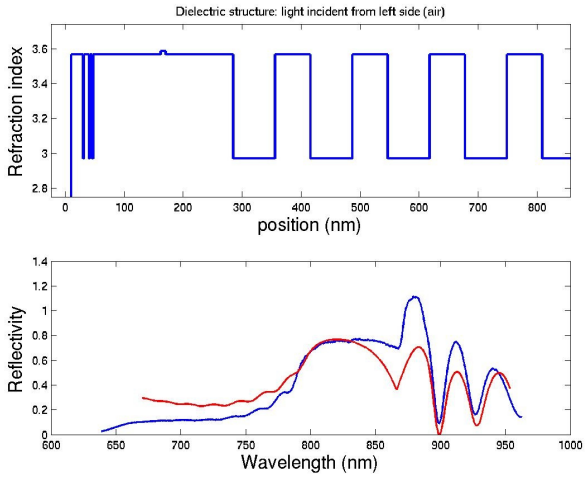

Figure 2.6: Upper figure: refractive index profile of the upper layers of the structure shown on Fig.2.5. Lower figure: Simulated (red) and experimental (blue) reflectivity spectrum (as a function of the wavelength) of the same structure. The fact that experimental data goes higher than one is due to chromaticism effects in the normalization: the mirror used to take the white light spectrum and the sample were not exactly in the same plane. And all the characterizations had to be done on small zones (diameter $< 100\mu m$), because of the patterns present on the sample's surface, which enhanced chromaticism.

- GaAs 8nm
- AlAs 6 monolayers, 1.8nm
- GaAs 4nm
- AlAs 6 monolayers, 1.8nm

These successive layers will allow mesas fabrication, as we will see it in the next step (Chemical Etching). See Fig.2.5 for this whole first structure.

Characterization

This semi-cavity is then characterized by room temperature white light reflectivity, and these reflectivities are compared to simulation done by the transfer matrix program presented in section 2.1.7, the compared curves can be seen on Fig.2.6.

These experiments allowed us to quantify the precision on the thickness during the growth, after a first calibration of the MBE, we were able to reach a precision of 1%.

As described before, the sample shows a wedge which allows to tune the cavity resonance by around 4% from the center of the wafer till its border. We place the nominal thickness on the center of the wafer, the nominal thickness gives thus the maximal thickness value.

2.2.2 Photolithography

In order to perform selective etching of the mesa structure, we first perform a photolithography of the desired pattern on the semi-cavity described above. The patterns deposed on this sample are defined by the mask described in section 2.1.5[6].

We will now see the successive steps which lead to photolithography. These steps are illustrated on Fig.2.7).

1. Deposition on the whole semi-cavity sample (2-inches wafer) of a photoresist by **spin-coating** (Fig.2.7(b)).
2. **UV exposition**. The sample covered by photoresist is exposed to UV light through the chrome mask, which yields a modification of the chemical composition of the exposed photoresist, increasing its solubility (Fig.2.7(c)).
3. **Development**. The exposed photoresist is then dissolved (Fig.2.7(d)).

[6]We have designed a new mask with new patterns, based on the results presented here, this new mask is described in details in the chapter giving future perspectives.

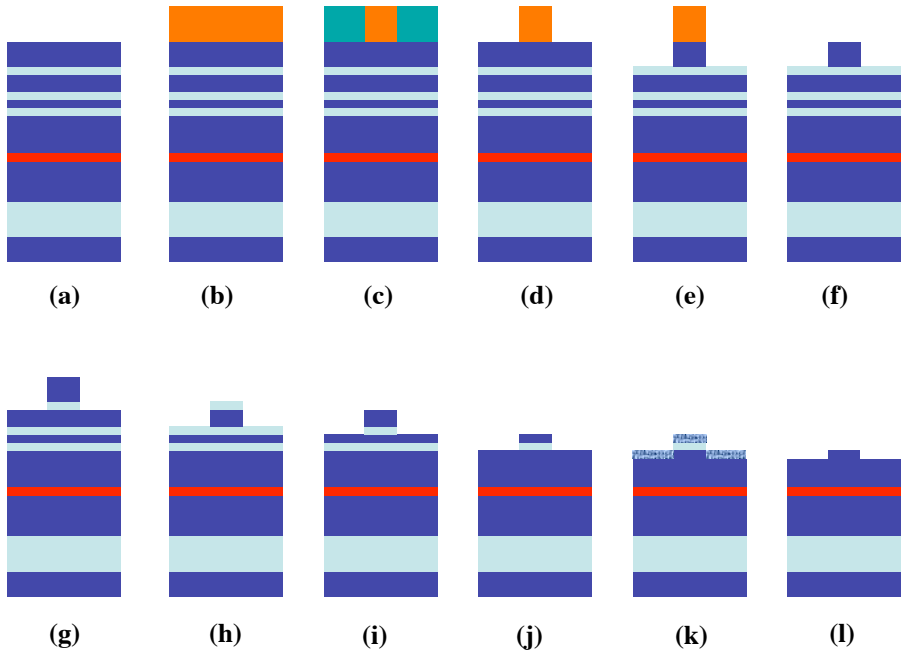

Figure 2.7: All the steps of the photolithography and chemical etching process, which lead to mesas on the 1485 sample. Fig.(a) shows the sample as described on Fig.2.5. As mentioned in the text the process could have been stopped at step (j).

Several key issues need to be taken into account in this process[7]:

Spin-coating The key issue is the thickness of resist which will be deposed. It can be controlled by the acceleration (mainly) and speed of the plate's rotation, and by the duration of the rotation. To ensure that small ($< \lambda \approx 1\mu m$) and complex patterns are afterwards well reproduced the resist layer must be as thin as possible. If it is too thick, these patterns will be modified by interference patterns due to diffraction during the exposition step. Fig.2.8(a) shows the case of a too thick photoresist on the sample's surface, after UV exposition, interference patterns appear, due to diffraction effect. Fig.2.8(b) shows a case where the photoresist thickness was suitable, and the shapes well-reproduced.

UV exposition time The exposition time should be decreased with the thinness of resist. If the exposition is too long, small patterns can disappear. It lasts usually around one or two seconds.

[7]All the numerical parameters for photolithography are given in Appendix B.

Reminding about diffraction The Fresnel number F determines if the system studied is in a situation of near-field (Fresnel diffraction, $F \geq 1$) or far-field (Fraunhoffer $F << 1$) diffraction. This number is given by $F = a^2/(\lambda R)$ where a is a characteristic length of the diffracting object, R is the distance from the object to the screen (here it is the resist thickness), and λ is the light's wavelength ($\approx 400nm$). We need to be in a situation of near-field diffraction in order to reproduced the shapes designed and not to observe interference patterns, so if $a \simeq 2\mu m$, $R \leq 8\mu m$ is needed. A profile measurement of the photoresist showed that its height was $\approx 4\mu m$ in the case of this sample.

Development time The development time is a critical parameter, it should be decreased if the exposition time was long. Over-development can erase the patterns, but under-development can yield the apparition of interference-like patterns (due to a non-homogeneous thickness of the photoresist left on the surface). It lasts usually around 3 to 4 minutes.

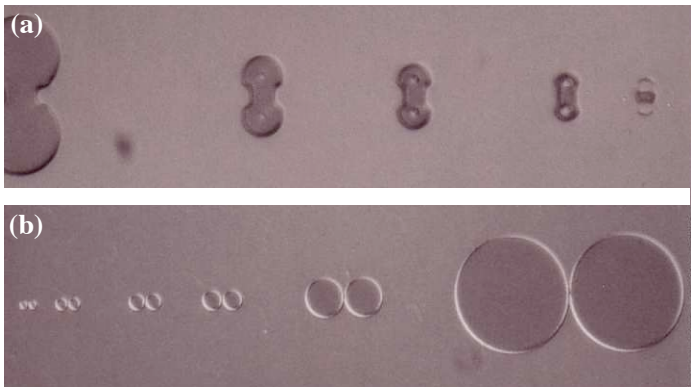

Figure 2.8: Images of the photoresist on the sample: (a) blurred by interference patterns (b) well deposed.

2.2.3 Chemical etching

Once the desired patterns are drawn with photoresist on the sample, the sample's surface looks as shown on Fig.2.7(d), the selective chemical etching process which will lead to the mesas can begin. Several successive chemical etchings are performed.

1. As the sample's upper layer (in contact with air or photoresist) is made of GaAs, the sample is first dipped in a solution with a slightly basic pH of 7.05. This etches GaAs. The solution is $H_2O_2 + NH_4^+$ (ammoniac dissolved in water) with a ratio of $100mL$ for $2mL$. This solution etches 100 monolayers of GaAs for a monolayer of AlAs (because of a

kinetic of reaction difference), it does not etch the photoresist [Logan and Reinhart, 1973, LePore, 1980]. See Fig.2.7(e).

2. The photoresist is then cleaned (Fig.2.7(f)) by usual cleaning methods (acetone and isopropanol in ultrasounds, then rinsing with clean water).

3. A second selective etching removes AlAs (and GaAs oxide due to the contact with air) by dipping the sample in solution of chlorhydric acid HCl 30% (Fig.2.7(g)).

   At this point we obtain a sample surface with mesas of $20nm$-height, above 6 monolayers of AlAs, as seen on Fig.2.7(g).

4. This mesa is far higher than what is aimed at, in fact this first step is performed as a check step, allowing to perform a first characterization of the thicknesses, of the depth of the step (and so a check of the etching times). One can perform here a white light reflectivity and compare it with simulations in order to check the absolute thicknesses and thus the height of the step. We performed reflectivity experiments at room temperature. The step is deduced from the difference between the cavity modes on and outside a mesa.

5. We then reproduce steps 1 and 3, this gives us a mesa of 8nm height (Fig.2.7(i)). One can here again characterize thicknesses through reflectivity experiments.

6. We then reproduce steps 1 and 3, this gives us a mesa of 4nm height (Fig.2.7(j)) above 1.8nm of AlAs.

7. Then, in order to obtain a mesa made entirely of GaAs, we pass the sample under an ozone (O_3, more oxidant than O_2) atmosphere during a given time in order to oxidize 4nm of GaAs (Fig.2.7(k)), and a last time in HCl to remove the AlAs and the GaAs oxide that was formed (Fig.2.7(l)).

It appears now that the last step is not necessary, indeed, as it can be seen by simulation, it is possible to work with mesas composed partly of AlAs as represented on Fig.2.7(j)), the index difference simply has to be taken into account in order to calculate the trap depth.

The comparison between experimental reflectivity and transfer matrix simulations showed a step of 6nm height, for the sample on which this description is based (labeled 1485), so a little higher than expected, maybe because the ozone step was mis-calibrated, but we do not know with certainty.[8]

[8]Our first trial showed after the first etching (point 4) a step of 36nm, far too deep, due to a too long HCl etching, or a HCl solution too concentrated. The second trial gave us the result presented here.

Choice of the height of the mesas As one can see from the chemical etching process, the definition of the height of the mesas (*ie* the depth of the traps) has to be done once for the whole sample. In order to change the depth of the trap, one has to fabricate a new sample.

On the contrary, as the substrates used for growth usually have a dimension of $5cm$, and the patterns drawn have dimensions of the order of $1-10\mu m$, it is possible to have thousands of different patterns on the same sample, the only constraint is the wedge: each pattern has to be repeated all along the wedge.

2.2.4 Final sample

Upper mirror

The spacer and lower mirror thicknesses were originally planned for a usual cavity, where one wants to obtain resonance between the exciton and the cavity photon in the middle of the sample. In our case, it is needed to have **both** resonances, *exciton-2D cavity photon*, and *exciton-mesa cavity photon*, around the middle of a working sample.

In order to achieve this in the case of this sample (N°1485), we had to regrow $10nm$ of bulk GaAs above the etched spacer. Then the upper Bragg mirror was grown above the spacer, with one pair less than the lower one in order to favor photons' emission to the side opposed to the substrate.

The first step in a growth process is to remove the GaAs oxide which is naturally formed, even after only a few minutes of exposition to air. This is usually done by heating the substrate under an arsenic flux in the MBE growth chamber. This is done at $\simeq 620°C$ and leaves a slightly rough surface. So the growth begins with a GaAs buffer. In our case we want to perform an immediate regrowth on the surface of the sample, so we need to avoid the roughness due to heating. We manage to avoid the heating by removing the oxide by hydrogen plasma cleaning. This cleaning leaves a planar surface at the atomic scale. It is done in a chamber connected to the MBE chamber, thanks to the *in situ* cleaning mentioned in section 2.1.6.

Atomic Force Microscopy

After the growth of the whole sample, observations of the final surface were performed through AFM measurements, where the high quality of the sample could be appreciated [Daïf et al., 2006b]. Fig.2.9 shows several examples of mesas on the surface of the complete structure. Amazingly enough, the $6nm$ step height of the etched mesas is kept even after the regrowth of the $2.5\mu m$ thick top Bragg mirror. The abruptnesses of the steps as a function of the crystal orientation is correlated to the mobility of the various elements during growth. The profile along [011] is much steeper ($0.5\mu m$ width) than along $[0\overline{1}1]$ ($3\mu m$ width), this is due to a slower mobility of the

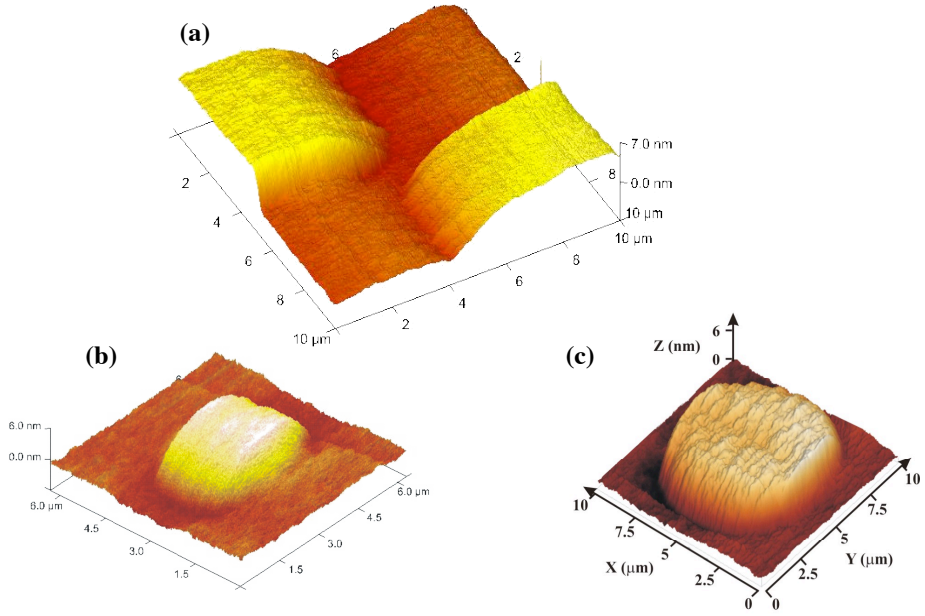

Figure 2.9: AFM images of various mesas' shapes. (a) A crossing between large squares. (b) A $3\mu m$ mesa. (c) A $9\mu m$ mesa.

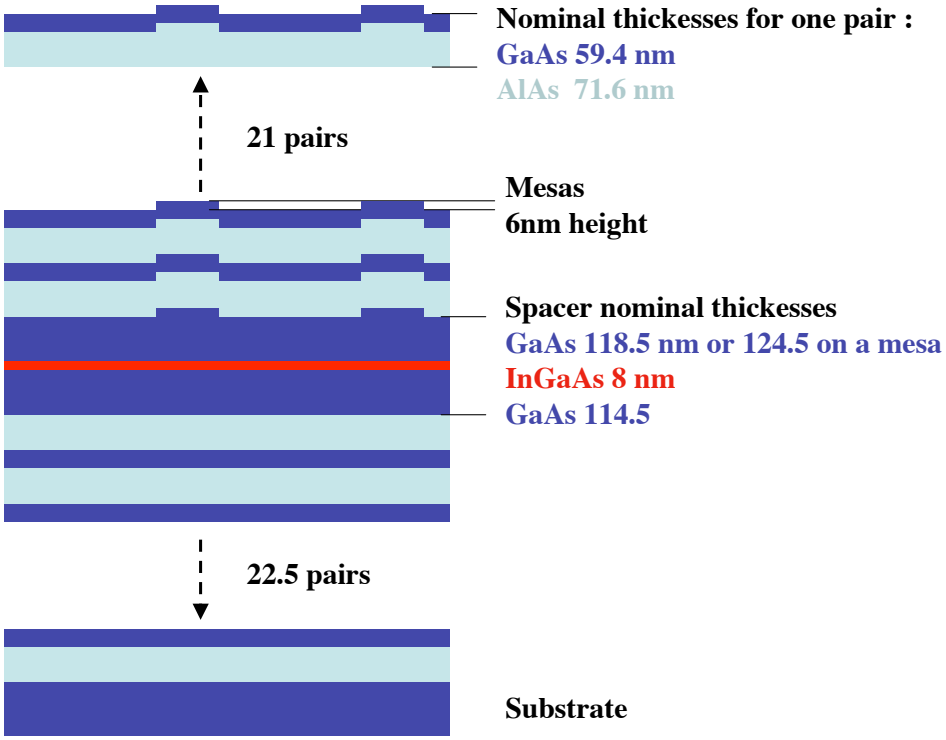

Figure 2.10: Profile of the final structure. The mesas are disposed every $150\mu m$ (section 2.1.5).

atoms. This gives rise to a surface asymmetry along the different crystalline orientations, with a smoothing of the etched faces that increases proportionally to the overgrowth thickness, it is particularly visible on Fig.2.9(b), where the mesa had a diameter of $3\mu m$ at the spacer level.

As the cavity mode field extends only over the first pairs of the mirror (closest to the spacer layer [Savona et al., 1999]), the optical properties of the mesas will be weakly affected by this effect. Similar observations have recently been reported for QDs embedded in similar mesas by ref [Lu et al., 2005], although the growth induced asymmetry seems to be much more pronounced, probably due to different growth conditions.

The step height measured by AFM corresponds to the height calculated by transfer matrix simulations. We performed the transfer matrix simulations on and around mesas, and deduced the cavity mode energy on the 2 zones, the difference between these 2 cavity modes gives the height of the step. According to the AFM measurement on the top mirror of a $6nm$ step, we compute an energy difference of $9meV$, in very good agreement with the photoluminescence experiment results, as we will see in the next chapter.

The structure of the sample finally looks as shown on Fig.2.10.

2.3 Conclusion and improvement of the method

Let us see how some particular steps of the above described method could be improved, and conclude.

2.3.1 Step by step improvement

Lithography

As we saw in section 2.2.2, the optical method used to deposit the photoresist pattern on the sample's surface is subject to diffraction. Even if one can avoid some of these effects by making the photoresist layer as thin as possible, this technique shows an intrinsic limitation because of the use of UV light, which has a wavelength of the order of $0.4\mu m$. Due to the diffraction limit, it should not be possible to draw an object having a size smaller than $\approx 2 * a$, a being the thickness of photoresist, so in the best case the smallest size reachable is $\approx 0.5\mu m$ (the detailed calculation is performed in appendix B).

If one keeps this selective etching method, one possibility to overcome the diffraction limit is the use of electron-beam lithography to deposit the patterns on the sample's surface. This method reaches a precision of the order of $1 - 10nm$, far smaller than with UV photons.

Use of AFM

One could imagine to use AFM at various steps of the growth and etching process, instead of performing reflectivity measurements and simulations, in order to check the etching process. This forces either to be able to perform AFM measurements on a whole $2in$ wafer (not possible for us), or to perform the growth on small parts (but then attention has to be paid to the cleaning of the observed surfaces).

Nevertheless, if easily available, AFM will allow a faster characterization of the step height, and will give an idea of the smoothness of the surface, of the steepness of the step...

Oxygen plasma

Instead of chemically etching the GaAs, one could pass it under oxygen plasma to oxide a given thickness, and then remove the oxide by simple usual cleaning. This alternative method is only interesting if the calibration of the oxidation time is better than the calibration of the chemical etching time.

2.3.2 Conclusion: a satisfactory sample

The method chosen to grow the sample allowed us to grow an original structure. We will see in more detail in the next chapters its optical properties. We can nevertheless already say that, from a crystallographic point of view, it was a success. The surfaces show the smoothness of usual MBE grown GaAs structures, and the structures' shapes were deposed as they were designed, and conserved along the regrowth process.

Part II

Physical studies

Chapter 3

Zero and two dimensional strong-coupling regimes

Our first aim after the realization of the sample is to characterize the coupling regime between the exciton and cavity photon modes. We will first have a look at the experimental methods we used, we will then see the results for the 2D structure and finally for the 0D structure.

3.1 Experimental considerations

In order to observe the modes of the microcavity, several kinds of measurements are possible: reflectivity, transmission or luminescence measurements will all give information.

Principles

White light reflectivity experiments consist of optically exciting the sample with a wide range of energies, covering all the energies which are of interest in the frame of our study. The excitation is performed at extremely low intensities, where no effect due to density is expected. The reflection or transmission spectra are then studied and show the optical modes of the system. In particular, the photonic component of the polariton modes are observed (as reflectivity dips or transmission peaks) in case of a microcavity showing strong coupling regime.

Another possibility, as we are in presence of a system which shows energy states involving electronic excitations, is to populate the system at energies higher than the energies of interest for us, namely the exciton and cavity mode energies. The excitation energy should be higher than the stopband's energy, in order to efficiently couple to the system. The sample is pumped by a laser beam, showing low enough intensity not to induce nonlinearities. The system relaxes then towards low energy states, and the latter (polaritons)

emit photons.

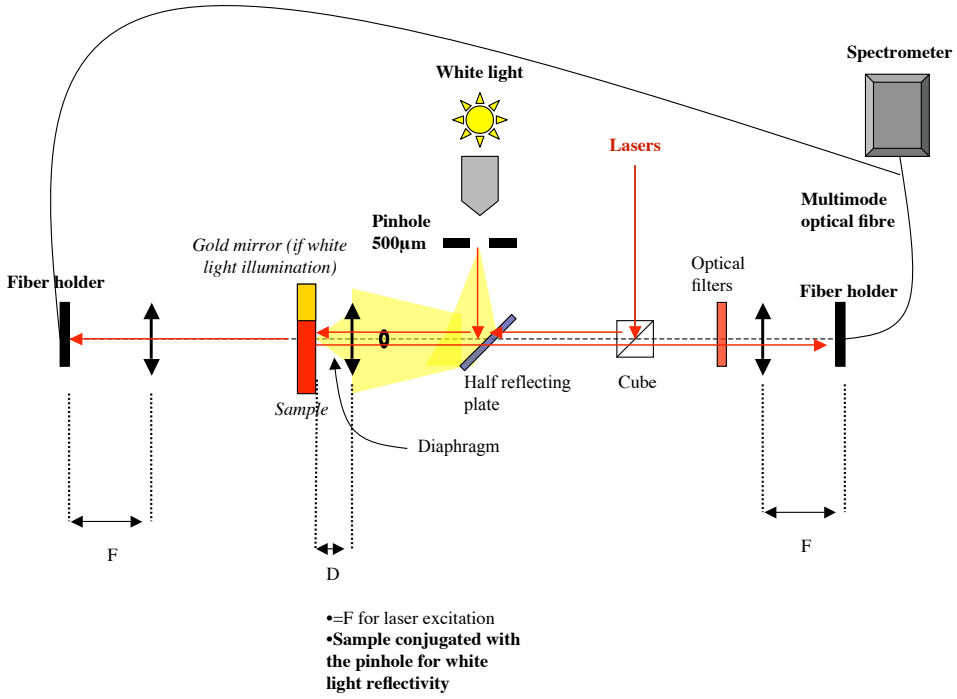

Figure 3.1: Characterization setup. The sample's plane is conjugated with the pinhole for white light reflectivity, and placed at the focal length of the lens for a laser excitation. It is mounted on a submicron resolution 3D set of translations stages, the lenses, the cube and the pinhole are mounted on $10\mu m$ resolution translation stages.

Experimental procedures

White light reflectivity The set-up used to perform such experiments is shown on Fig.3.1. The source is a commercial white filament lamp, emitting with a black body spectrum at around $1500K$. As the studied cavity shows patterns on its surface, the dimension of the shined surface must be controlled carefully. The white light is focused on a pinhole which size is chosen to be $500\mu m$ and which acts as a secondary emitter. This allows us to choose the size of the excitation spot on the sample's surface through a given choice of the position of the pinhole-lens-sample ensemble. In order to make a compromise between the patterns' sizes (the squares are $300\mu m$ wide) and the unavoidable chromatic aberration, we chose the excitation spot to have a diameter of $100\mu m$.

The lenses are achromatic lenses but given the wide range of wavelength shined, chromatic aberrations are unavoidable. Hence, the spectrum illumi-

nating the sample is not flat. In order to achieve a proper normalization, a gold mirror is placed near the sample, at an identical distance from the focusing lens. Gold reflects 100% of the light at the wavelengths of interest (between 700 and 950nm).

Photoluminescence with laser excitation The laser is a continuous wave argon laser shining at very high energy ($E = 2.34eV$ or $\lambda = 532nm$, higher than the stopband's energy), it is focused to a spot varying between 30 and 80μm on the sample's surface. It populates high energy states, namely a gas of free carriers (electrons and holes). The excitation is performed with powers high enough to create a non-negligible number of excitations, to allow them to relax and emit, but the system is always kept on purpose in a linear regime, meaning that collision phenomena between free carriers (or at lower energies between excitons or polaritons) are not present or negligible. The only relaxation means available are phonons or photons emission.

In both situations the sample is cooled to about 10K, the signal is focused on a large-core (500μm) fiber and analyzed with a 25μeV resolution spectrometer. Finally, a diaphragm is disposed in the Fourier plane of the sample[1], in order to choose the angular width to integrate.

Spot size measurements

The spot size on the surface of the sample was measured through a measurement of the laser beam waist in the sample's plane. The beam waist was measured using Knife-Edge techniques and simple calculations derived from ref. [Siegman et al., 1991]. The laser beams were always considered as gaussian beams[2], the beam waist is then given by $w = 1.5\delta$, where δ is the distance crossed by a sharp surface to hide successively 10% and 90% of the beam power. The sharp surface is the edge of the sample.

3.2 Characterization of the 2D cavities

Let us first consider the properties of the 2D microcavity and of the large mesas. This will allow us to check the effect of etching and regrowth on the coupling of photons and excitons. We measure the resonances resulting from the expected strong coupling regime, on a zone containing large square mesas of 300μm (Fig.3.2(a)). On these mesas no confinement effect is expected, but the photonic resonance is red-shifted due to the larger thickness of the cavity.

As mentioned the wedge is of about 4% in this sample and allows to tune the cavity resonance with respect to the excitonic resonance. It corresponds

[1] See chapter 4 about this point.

[2] The beam is produced gaussian by the laser, it may diverge from its gaussian profile due to large angle incidence on convergent lenses, we will neglect this phenomenon.

to an energy variation for the photonic resonance of about $50meV$ across the whole sample. In the zone of interest this variation is about $2.4meV/mm$. As we saw in the precedent chapter (section 2.1.3), the quantum well exciton is less affected by the wedge: its energy variation is below $3meV$ across the whole sample.

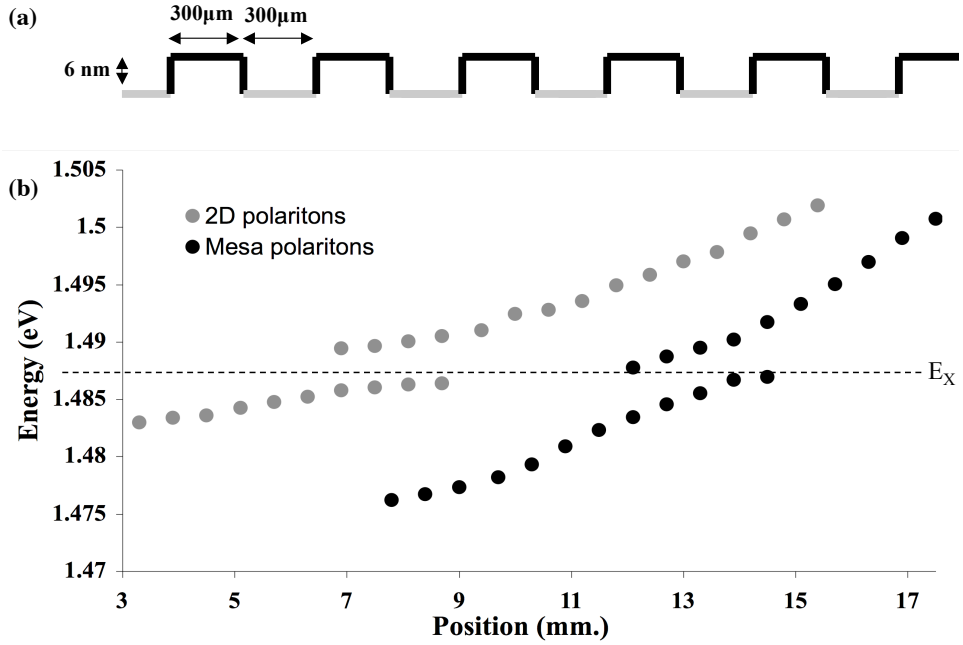

Figure 3.2: (a) Pattern and thickness profile of a zone of squares. The entire mask was shown on Fig.2.4. The whole zone contains hundreds of squared mesas. (b) Anticrossing curves obtained through reflectivity measurements along the wedge, successively on and outside squared mesas. The exciton's mean energy E_X is indicated by a dashed line.

The spectral properties are studied through the two kinds of experiments presented in the first section: photoluminescence and reflectivity. The measurements are performed every $300\mu m$, alternatively on a mesa and between two mesas. The profile of the surface is shown on Fig.3.2(a), where the mesas are drawn in black, and the zones between mesas in grey.

The spectra show dips in the reflectivity stopband. The observed modes as a function of the position (and thus detuning between the exciton and photon mode) are shown on Fig.3.2(b). Two anticrossing behaviors characteristic of a strong coupling regime can be seen. This is due to the presence of two cavity thicknesses showing two cavity modes: on the mesas and between mesas. The colors on the graph correspond to the colors on the pattern. As expected a mesa is higher physically but lower energetically.

In photoluminescence, the signal measured is a peak intensity at the

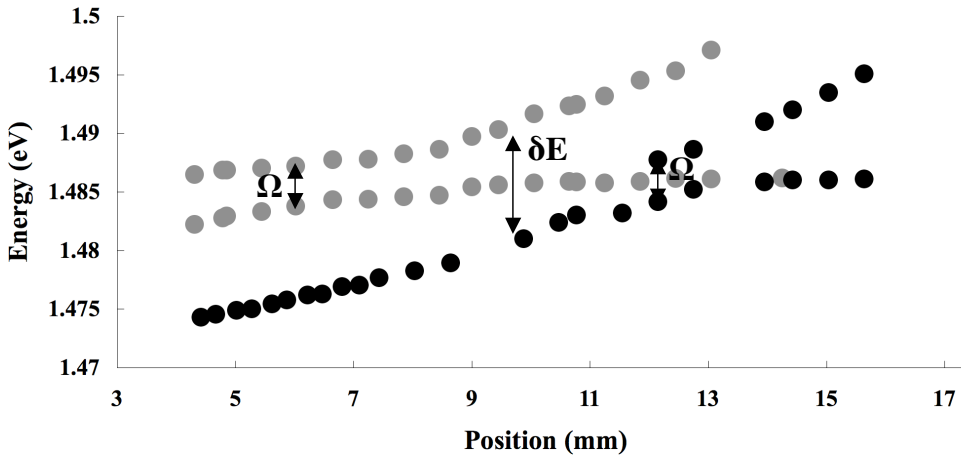

Figure 3.3: Anticrossing curves obtained through photoluminescence measurements. Arrows indicate the energy difference δE between the two cavity modes and the Rabi splitting Ω.

modes of the cavity. We plotted the measured peaks' energies as a function of position on Fig.3.3. A similar double anticrossing behavior is measured.

Quantitative properties

We extracted the quantitative properties of the cavity from the PL spectra, considering that at such low temperatures ($T \leq 10K$), the two reported methods show similar results. The microcavity shows a strong coupling regime and features a Rabi splitting energy of $3.5meV$, and a full width at half the maximum (FWHM) of $\gamma_c = 220\mu eV$ for the cavity photon mode, corresponding to a quality factor of $Q \simeq 7*10^3$, and of $\gamma_X = 500\mu eV$ for the quantum well exciton. At resonance ($\delta = 0$) the polariton linewidth is $\gamma_{LP} \simeq 350\mu eV$. These linewidths are slightly larger than reported in [Saba et al., 2000], which reports one of the best GaAs samples fabricated, and has a very similar structure. The latter shows $\gamma_c = 100\mu eV$, $\gamma_X \simeq 150\mu eV$. Their Rabi splitting is $\Omega = 3.6meV$, in agreement with our present observations.

Cavity modes

The two cavity modes -on the mesas and around the mesas- are separated by $\delta E = 9meV$. This can be measured through the difference between the peaks far from resonance with the exciton, on Fig.3.3. This value is hence the energy depth of the trap formed by the mesas. According to our transfer matrix simulations, this energy difference corresponds to a thickness difference of $6nm$ between the two cavities, in agreement with the AFM measurements on the surface of the sample, and with the reflectivity mea-

surements performed at the surface of the spacer (after the chemical etching, see chapter 2).

The cavity mode shows the same linewidth on both domains. The two anticrossings are identical, which guaranties that the etching process just shifts the cavity mode, and does not affect the quality factor.

3.3 Strong-coupling regime in zero dimension

We now focus on the effect of the confinement of the polaritons in circular mesas, through photoluminescence experiments[3]. The experimental conditions are similar to the ones described above, but the laser spot which has now a diameter of $\simeq 17\mu m$ in order to enhance the mesa to 2D-cavity intensity ratio. These results were published in reference [Daïf et al., 2006b].

The spectra shown display both the mesa confined modes and the 2D polaritons of the planar cavity outside the mesa, displaced towards higher energies. Let us note that the light emission from one single mesa is very intense, which allowed us to perform all experiments on single mesas, well below any nonlinear regime, in contrast to the case of pillar microcavities [Dasbach et al., 2001, Obert et al., 2004].

3.3.1 Strong-coupling in small mesas

The smallest circular mesas, where the confinement should be the strongest, have a diameter of $3\mu m$, we will focus in this section on photoluminescence (PL) measurements performed on these mesas.

Photon confinement In order to probe first the confinement of the cavity photons, we took spectra on mesas which cavity mode(s) is (are) expected to be far from resonance with the exciton.

Fig.3.4(a) shows the spectrum of a mesa relatively far from resonance (the bottom of the photonic trap shows an energy $6meV$ smaller than the exciton energy). The lower polariton mode of the mesa is thus quasi-photonic. It is split into several peaks. For sake of clarity, we will first only consider the ground level (G) and the first excited level (E1) (which is a doublet, we will comment this further in the next section, 3.3.2) although more modes are visible. The quantized photonic peaks have a spectral width of about $90\mu eV$, a factor of two smaller than observed on the non-confined cavity photon mode. The smallest value measured reached $70\mu eV$, indicating a quality factor of $Q \simeq 2.1 * 10^4$ for the confined photon modes (better than for the 2D photon modes, we will come back to this point in section 3.3.4). The energy of the confined ground level is $1.5meV$ above the energy of the

[3]Reflectivity experiments were carried out but given the small surface of the mesas, the signal to noise ratio was rather bad.

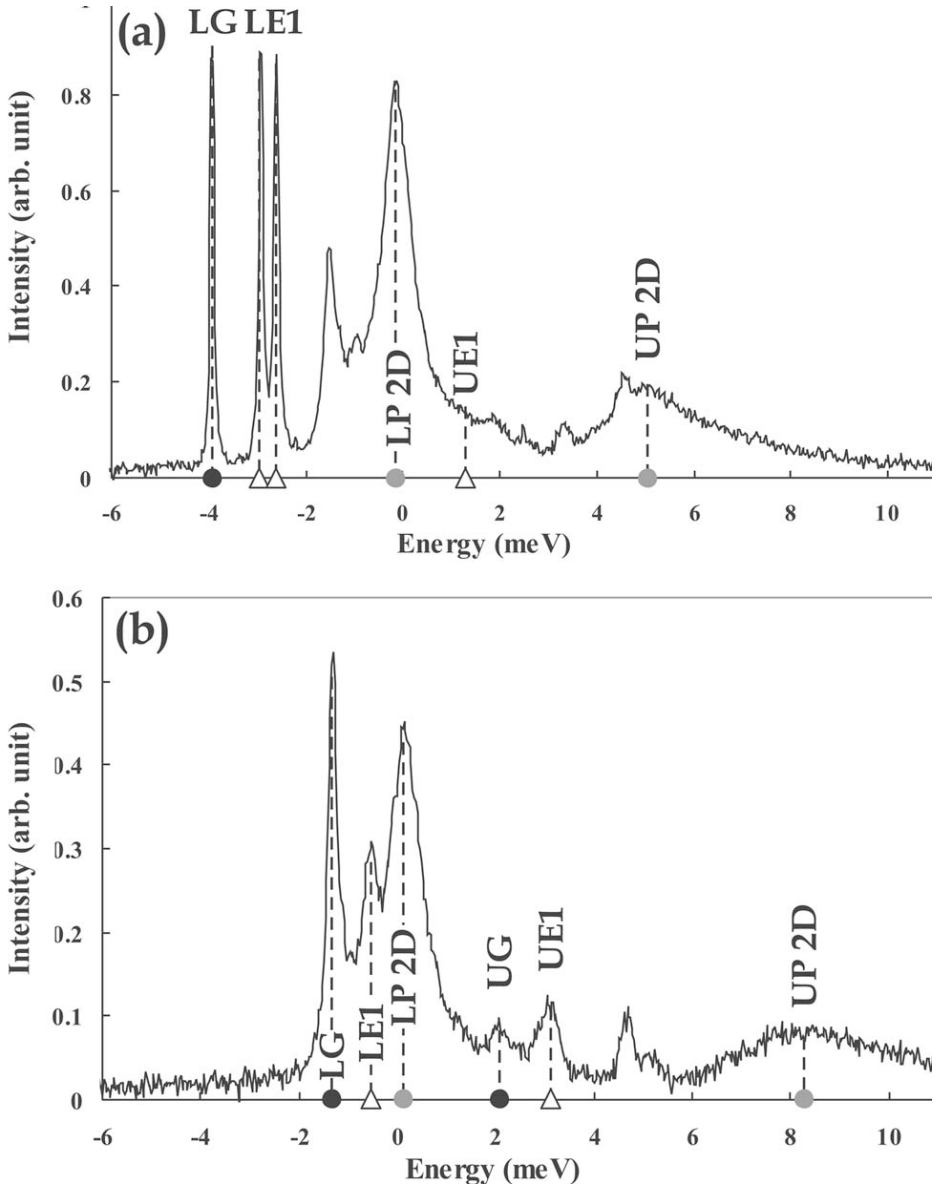

Figure 3.4: Photoluminescence spectra of a circular $3\mu m$ diameter mesa at two different positions along the wedge. The origin of the horizontal axis corresponds to the exciton energy. Grey circles: lower (2D LP) and upper (2D UP) 2D polaritons around the mesa. Dark circles: lower (LG) and upper (UG) polariton of the ground level of the mesa. Triangles: lower and upper polariton of the first excited level (E1) of the mesa (these symbols are kept all along this work). (a) The confined lower polariton states are quasi-photonic. (b) The excitonic and photonic components are comparable for the confined polariton states. Other confined levels are visible on both spectra but are not labeled.

bottom of the trap (as measured on the large mesas at the same position on the wedge).

Polariton confinement To probe the strong coupling in these mesas and the polariton nature of the confined states, we systematically measured the spectra on mesas disposed along the wedge, so with different detunings with respect to the exciton, the resulting curve is shown on Fig.3.5. On this set of measurements, we are always rather far from the position for which the exciton and 2D cavity mode are at resonance (We are at positions corresponding to $10mm < x < 15mm$ on Fig.3.2 and 3.3.). Hence, the 2D lower polariton mode stays near the exciton energy on the whole range of positions shown in Fig.3.5.

Strong coupling is very nicely demonstrated for each confined state by an anticrossing behavior. They present a Rabi splitting of around $3.35meV$, it is identical for all the confined states, and fairly similar (though a slightly smaller) than the 2D Rabi splitting of $3.5meV$. Fig.3.4(b) displays the photoluminescence spectrum very close to zero detuning in the trap, where the confined lower and upper polariton modes are resolved. Despite the relatively large linewidth of the 2D exciton, the high Q factor and the very efficient relaxation to the traps allow to observe confinement for both the lower and upper polariton states.

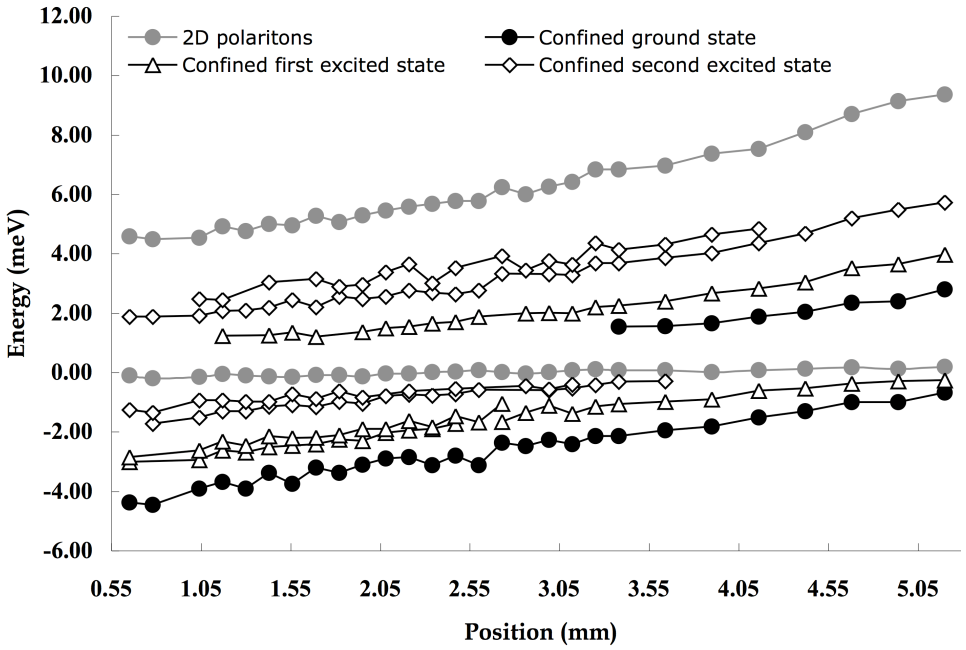

Figure 3.5: Anticrossing for all confined states. Symbols of Fig.3.4 were kept. The exciton energy was chosen as the origin. The spectra on Fig.3.4 were taken at: $x = 1.04$ (a) and $x = 4.42$ (b).

Asymmetry of the anticrossing One can see that the anticrossing curves are not symmetric with respect to the exciton energy: it was possible to see the LP peaks at energies nearer to the exciton than the UP peaks. This is probably due to the broader linewidth of the upper polariton, and to a lower emission intensity, linked to its coupling with higher energy modes, and to its more numerous relaxation channels available (lower energy states). We will see a similar effect in the next section 3.3.2.

3.3.2 The doublet: a lift of degeneracy

As one can see on Fig.3.4 and 3.5, the confined first and second excited levels appear as doublets on part of the measurements, this doublet is due to an asymmetry already present on the mask used for photolithography[4]. As we are in a 2-dimensional (x, y) system, the eigenstates $E_{x,y}$ of the traps (here the circular mesas) are linear combinations of eigenstates in each dimension x or y of the plane:

- the ground state of the mesa is simply due to the combination between the ground states in each dimension,
- the first excited state is due to a combination between the first excited state in one dimension x and the ground state in the other dimension y, or the opposite combination of the ground x state and the excited y state.

Therefore, if the two dimensions are different enough, it may lead to a splitting of the excited states due to both combinations. This splitting must nevertheless not be considered as a polarization splitting, which is also present (see for example [Sanvitto et al., 2005]) but which we did not observe: when selecting a linear polarization in detection, we did not observe any significant sift of the peak energy.

One can see on Fig.3.5 that in certain conditions, it is not anymore possible to see the splitting. Namely for the upper polariton of the confined first excited state (triangles), and at positions above $2.75mm$ for the lower polariton's first and second excited states. For all these situation the cause of the disappearance of the splitting is a spectral broadening of the modes. This broadening is due, for the lower polariton states, to their increasing excitonic component when detuning is inscreased. As the exciton has a spectral linewidth of $500\mu eV$, and the splitting is $\approx 300\mu eV$, when the mode shows an excitonic Hopfield coefficient of more than 50%, its linewidth is larger than the splitting. For the upper polariton the main reason for this broadening is on one hand the coupling with the GaAs absorption band at slightly higher energy ($\simeq 1.52eV$) and on the other hand the numerous lower energy states towards which it can relax.

[4] described in the precedent chapter, section 2.1.5.

3.3.3 Larger mesas

We performed PL measurements in the same experimental conditions on $9\mu m$ and $19\mu m$-diameter mesas. As expected from traps with larger dimensions, the confined states energies get closer to each other with increasing the trap size. It was thus not possible to follow the states' energies as for the smallest mesas, and perform anticrossing measurements. We nevertheless show two PL spectra of $9\mu m$ mesas at two different exciton-photon detunings on Fig.3.6 and 3.7. The supposed positions of some modes are shown with the same symbols used in the precedent figures.

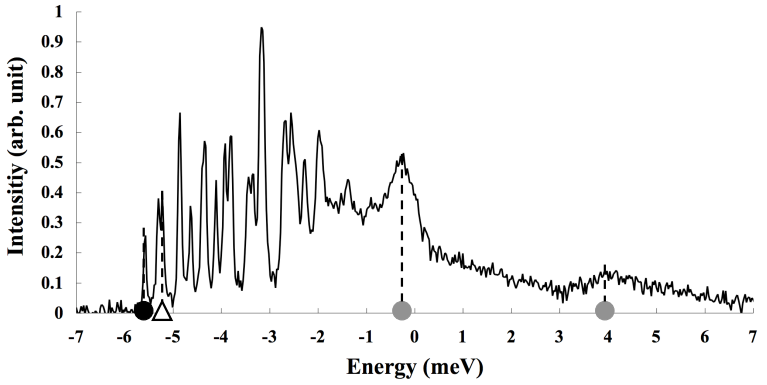

Figure 3.6: PL of a $9\mu m$ mesa at very negative detuning for the confined ground state $\delta_{0D} \simeq -5.5meV$. The energies' origin is chosen at the exciton's energy.

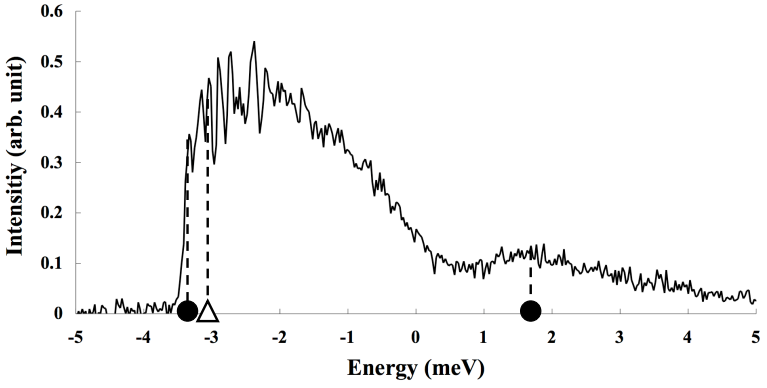

Figure 3.7: PL of a $9\mu m$ mesa at a slight negative for the confined ground state $\delta_{0D} \simeq -2meV$. The energies' origin is chosen at the exciton's energy.

One can see on Fig.3.6 the 2D polaritons, at rather high positive detuning, meaning that the upper polariton is mostly photon-like. The latter is also very large spectrally, because of the combination of several factors: its proximity with the GaAs absorption band at slightly higher energy

($\simeq 1.52eV$) and the numerous lower energy states towards which it can relax. Confined lower polariton states are on the opposite extremely sharp spectrally, with linewidths similar to what was observed for smaller mesas, around $80\mu eV$. As a high number of confined modes is present, on can observe on the same lower polariton the broadening of the peaks with increasing energy towards the exciton line.

On Fig.3.7 the ground mode of the mesa is closer to resonance with the exciton, and 2D polariton emission is on one hand dominated by the 0D LP (at the exciton energy) and on the other hand the photonic UP is at very high energy. So only the signal due to the mesa is visible, and the peaks are clearly too wide to distinguish the quantization effect of confinement. We will see this point more in details when studying images.

3.3.4 Comment on the linewidths and high Q-factors

We mentioned in section 3.3.1 the fact that the confined cavity mode's linewidth is smaller than that of the 2D, due to additional lateral confinement. One can be more precise by saying that this effect is a change in the inhomogeneous cavity mode linewidth, and that its homogeneous linewidth should not be affected by the lateral confinement.

Two broadening factors in 2D are influenced by the confinement in the mesas. These factors are in 2D:

- In case of a spatial detection with a resolution on a zone larger than $\approx 10\mu m$, inhomogeneous broadening due to disorder in the cavity [Savona, 2007].

- In case of a high spatial resolution in detection, resolution is lost in angle and thus in $\mathbf{k}-$space. As the dispersion curve is parabolic-like around normal incidence ($\vec{k}_{||} = \vec{0}$), integrating PL on a large angular scale broadens the spectral linewidth.

In the present confinemed situation:

- The mesas studied have diameters of 3 and $9\mu m$, they are thus not influenced by optical disorder. The fact that the 2D cavity feels this disorder does not affect the mesas' modes, because their energy is different from the 2D energy.

- PL signal coming from the confined modes shows no angular dependence of this energy. This means that there is no broadening of the peak due to the angular loss of resolution.

Thanks to these two points, the linewidths measurement gets free from two inhomogeneous optical broadening factors, and yields the observation of a high Q-factor. The same results were obtained on photonic dots [Sanvitto

et al., 2005, Muller et al., 2006]. These dots were grown in similar ways, through a local thickness variation on the spacer of a 2D microcavity, and an improvement in the Q-factor was observed. The best Q-factor observed reached 30000.

As the confined polaritons linewidths is dominated by the radiative lifetime, these values result in a polariton lifetime of $\simeq 10ps$ yielded by the confined photon lifetime. This is shorter than any other dephasing mechanism expected in this system at such low temperature and density.

3.4 Conclusion: a high quality confinement of strongly coupled quasiparticles

The strong-coupling regime was demonstrated in all the available structures: highly confining 0D structures and traditional 2D structures. To our knowledge, this is the first time a single sample containing polaritons of various dimensionality is realized. It is also the most non-ambiguous strong-coupling regime in 0D, with a high Rabi to linewidth ratio: $\Omega/\gamma \simeq 10$ in the 2D structures and $\simeq 20$ in the 0D structures. Several groups performed micropillar-shaped microcavities showing strong-coupling regime between a quantum well excitons and confined photons, but either with difficulties to observe a high Ω/γ ratio [Bloch et al., 1998], difficulties to observe the upper polariton [Dasbach et al., 2001], or no mode splitting characteristic of the confinement [Obert et al., 2004].

Another kind of 0D polaritons is being performed since a couple of years through another method: a confinement of electronic excitations in quantum dots [Peter et al., 2005, Reithmaier et al., 2004, Yoshie et al., 2004]. This kind of strong-coupling is different from what is described here, and the problems and perspectives are also different. The difficulties are not as much in producing a high quality structure as they are in producing a high coupling, through a suitable placing of the quantum dot inside the cavity, a problem for which a very clever solution was found by Badolato et al., see Badolato et al. [2005]. This led them to a recent observation of the strong-coupling regime between a single quantum dot and a photonic crystal nanocavity [Hennessy et al., 2007]. In these works perspectives are not on the side of collective effects, as the particle is by definition single, but towards the control of single excitations in solid state, for various application (quantum computing, communication, cryptography) or fundamental studies.

Chapter 4

Spectroscopy of polaritons in the real and reciprocal spaces

In order to fully characterize the confined polaritons, we imaged the polariton states' photoluminescence (PL). Staying at excitation densities well below any nonlinear threshold, we performed images in several configurations:

Spatially resolved spectroscopy Observation of the PL spectrum as a function of one spatial dimension of the plane of the microcavity (x or y).

Angularly resolved spectroscopy Observation of the PL spectrum as a function of one dimension of the reciprocal ($\vec{k_{||}}$) space of the microcavity (k_x or k_y).

Two dimensional imaging 2D imaging either in real or reciprocal space.

4.1 Spectroscopy

4.1.1 Experimental setup

The experimental setup used to perform these various measurements is shown on Fig.4.1. It is designed to give an image of the surface of the sample on the detector, in the real-space configuration, or of its Fourier plane, in the reciprocal space configuration, we will discuss further the notion of Fourier plane in the next paragraphs. The detectors are two CCD cameras: one imaging directly the two dimensions of the considered space (without spectral filtering), the other one is placed at the exit of a spectrometer, which selects one dimension and disperses it spectrally.

When imaging real space, the magnification is simply given by the ratio between the lens focusing on the CCD or spectrometer, and the microscope objective. As we worked with a microscope objective of NA 0.55 optimized

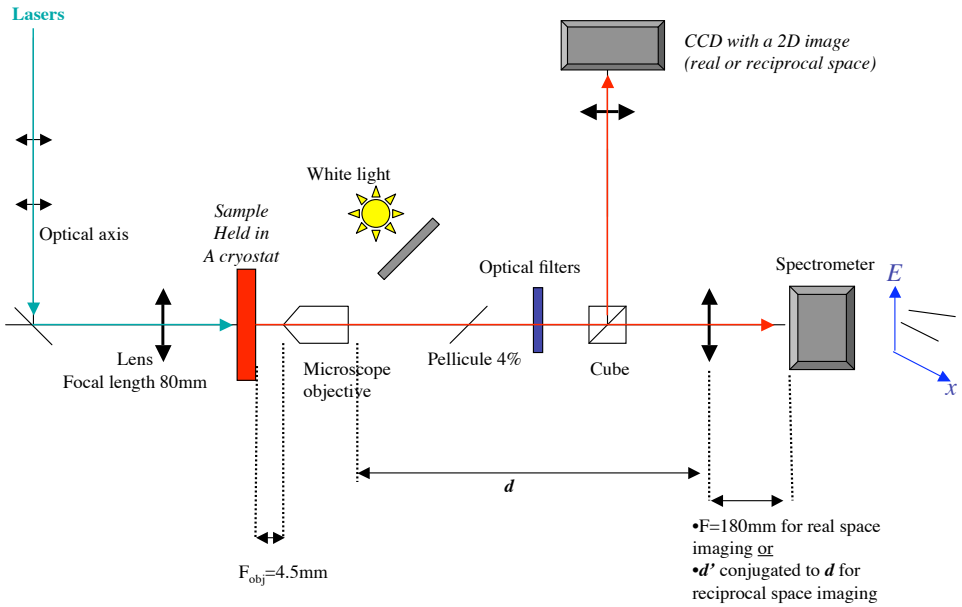

Figure 4.1: Setup for imaging using non-resonant pumping.

for a magnification of 40, we chose the lens's focal length to be $180mm$, this yields a resolution limited by the diffraction of $\frac{\lambda}{2NA} \simeq \lambda \simeq 0.8\mu m$, and a scale of one pixel on the CCD array corresponding to $0.45\mu m$ on the sample's surface.

The sample is held in a cold finger cryostat, cooled to $\approx 10K$, and pumped (except for the last series of images) non-resonantly with an argon laser, at very high energy ($E = 2.34eV$ or $\lambda = 532nm$), the excitation spot has a diameter of $\simeq 35\mu m$.

Reflection Some images shown here were taken with a slightly different set-up, where the excitation laser comes from the detection side. This imposes to get rid of laser scattering with a spectral filter or a polarizer. It does however not affect the image interpretation.

4.1.2 Reciprocal space spectroscopy

Principles

The space in which the eigenstates of the system are defined is the wave vector space. In order to see the wave function of the polaritons, it is therefore relevant to image the modes in this space. We will see in this section how to access this space, through angle resolved measurements, and measure the dispersion curve of the polaritons.

Confined polaritons do not show the same dependency of the eigenstates:

the relevant quantum numbers on which they depend are a quantization number n labeling the confined energies, and an azimuthal number m, labeling the angular dependency of the wave function (see section 4.1.5). It is nevertheless through the same kind of angle resolved measurement that we will be able to observe the eigenstates of the system.

The wave vector $\vec{k_{||}}$ of a given polariton state is accessible through its angle of emission with respect to the plane of the cavity, through the relation $|\vec{k_{||}}| = \sqrt{\epsilon_0}(\omega/c)\sin(\theta)$, where ϵ_0 is the vacuum's permittivity, ω the frequency (in radian per second) of the emitted electromagnetic wave, and θ the emission angle. The first polariton dispersions, which were measured by Houdré et al. [1994], were taken using a fiber for detection. The fiber was moved along the Fourier plane and a series of measurements were taken for a series of angles. Later, several kinds of images were taken in the reciprocal space, with spectral resolution or integrating on the whole energy range, as in refs. [Houdré et al., 2000, Richard, 2004, Baas et al., 2006b], among others. In 2004, Wolfgang Langbein gathered all these kinds of images, and took direct images of the reciprocal space in the two (k_x, k_y) dimensions and of the dispersion curve $(E(k), k_x)$ [Langbein, 2004], through Fourier plane direct imaging, spectrally resolved and spectrally integrated, with time-resolution for some of the images.

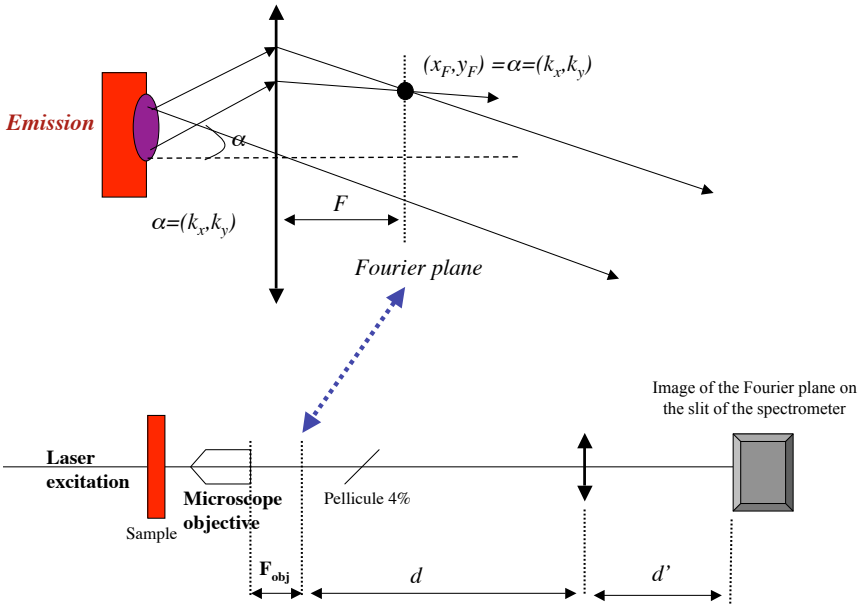

Figure 4.2: Principle of reciprocal space imaging. Upper part: the image of the surface is formed at the infinity. Lower part: d' is conjugated to d.

The principle of k-space imaging is explained on Fig.4.2. The main idea is to image a plane where each point corresponds to an angle of emission of the

cavity. Indeed, a parallel beam emitted by the sample is focused on a point of the focal plane. This leads us to make the assumption that the emission zone shows first-order phase coherence, otherwise the two mentioned beams will simply see there intensities summed. More explanation about Fourier optics for the same application can be found in the thesis of Maxime Richard [Richard, 2004] pp. 42 and following, and in references therein.

Results

Fig.4.3 shows dispersion curves for 3 mesa sizes at zero detuning for the $3\mu m$ mesa ground mode and slightly negative detunings for the $9\mu m$ and $19\mu m$ mesas. These images were taken by Reda Idrissi Kaitouni in collaboration with Maxime Richard, and published in references [Kaitouni et al., 2006] and [Baas et al., 2006a]. They were taken in an experiment where excitation and detection are situated on the same side of the sample, excitation is performed with a $3\mu m$ spot. The dispersion of the extended polaritons (barely visible in the $19\mu m$ mesa), is highlighted by dashed lines. We estimate a positive detuning of $6.4meV$ between the extended 2D cavity mode and the exciton, it is hence a good approximation to consider the 2D lower polariton at the exciton's energy. The strongest PL signal appears on the three images below and above the 2D LP mode. In particular, on Fig.4.3(a), the $3\mu m$ mesa shows few discrete lines extending over broad angular regions, with energy spacings in the meV range. Compared to the $3\mu m$ mesa, the $9\mu m$ mesa dispersion, shown on Fig.4.3(b) shows a larger number of more closely spaced spectral lines, with a smaller angular spread. Finally, the $19\mu m$ mesa dispersion, shown on Fig.4.3(c), shows a quasi-continuuous spectrum, while the angular extension is still smaller, approaching a 2D behavior.

Negative detuning Let us now see an example of dispersion we took at negative detuning on Fig.4.4, the confined lower polariton is mostly photonic in this case. The 2D signal is here more intense than the 0D signal. The contrast has been enhanced by a factor of 50 for the confined lower polariton to be visible. Relaxation is less efficient towards a photonic state.

One can see an unexpected signal at an energy of $\approx 1.50eV$, this signal is characteristic of bulk GaAs polluted with carbon [Ilegems, 1985]. As these measurements were taken in the usual transmission setup, the substrate is also excited by the laser. This peak is an indicator that the impurity concentration has exceeded $10^{16} impurities/cm^3$ ([1]), this is a reasonable number for commercial bulk GaAs. One can note the directionality of this emission, centered around $\vec{k}_{||} = \vec{0}$, with secondary preferential axes at higher angles, we could not find any reason for this feature.

[1] As opposed to the high purity concentration of $10^{14} impurities/cm^3$ reached for the GaAs grown by our MBE.

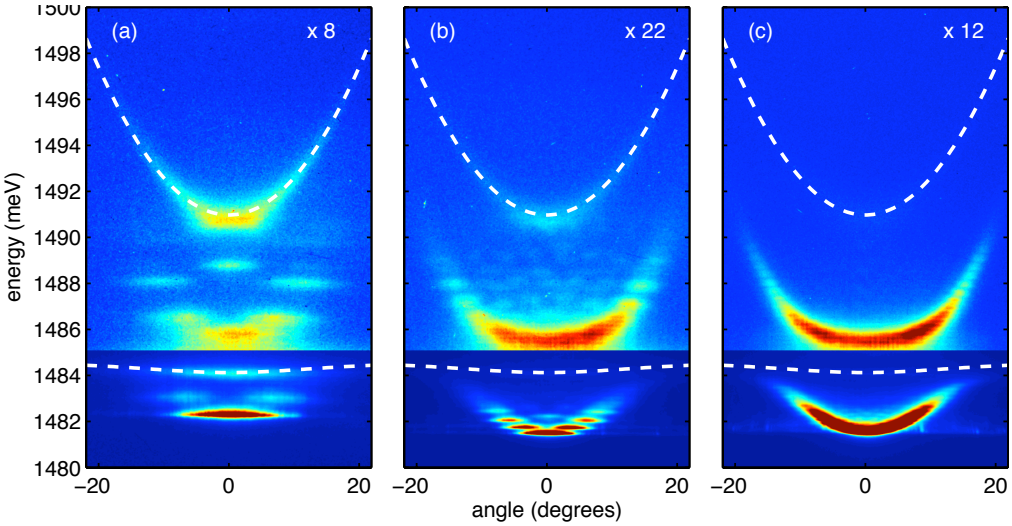

Figure 4.3: Dispersion curves: Measured PL intensity (linear color scale from blue to red) as a function of energy and emission angle for: (a) the $3\mu m$, (b) the $9\mu m$ and (c) the $19\mu m$ mesa. Dashed lines: calculated dispersions of the extended polariton modes. These three experimental dispersion curves are shown again on Fig.4.8 and compared with theory.

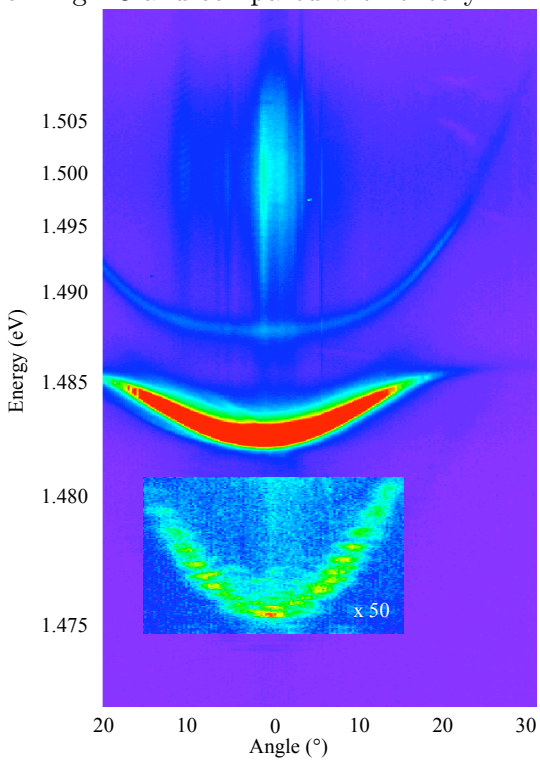

Figure 4.4: Example of dispersion curve at negative detuning, for a $9\mu m$ mesa, in a transmission experiment. The angular window is not symmetric in order to allow the observation of large angles.

4.1.3 Real space spectroscopy

In order to perform real space spectroscopy, we simply image the surface of the sample on the entrance slit of the spectrometer, instead of the reciprocal space, in order to see the density of polaritons in real space. In the case of mesas, we are in presence of a confined system where the various states are discrete in energy, thus the profile at a given energy is directly related to the presence probability of the polariton at this energy, as a function of position. Similar images were taken for photonic dots in ref. [Lohmeyer et al., 2006].

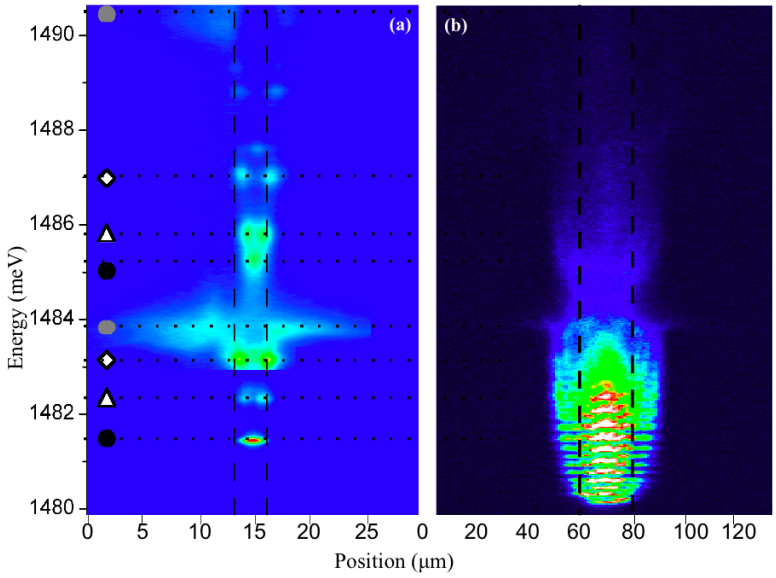

Figure 4.5: Photoluminescence intensity as a function of energy and position for $3\mu m$ (a) and $19\mu m$ (b) diameter mesas. (a) For clarity, the intensity above 1484.2 meV has been enhanced. The same symbols than in the precedent chapter are used to label the various states: grey circle for the 2D polaritons, black circle for the confined ground state, white triangle for the confined first excited state, white rhombus for the confined second excited state. (b) The contrast is identical on the whole figure.

Fig.4.5(a) shows a spatially resolved spectrum of a $30\mu m$ long stripe of the sample surface (horizontal axis) containing a $3\mu m$ diameter mesa, non-resonantly excited through a $2\mu m$ diameter laser spot. The mesa is at a position along the wedge where the ground mode is at slight negative detuning ($\delta \simeq -0.25meV$) with respect to the exciton. The stripe axis was chosen perpendicular to the wedge in order to prevent non-intrinsic sources of asymmetry. The luminescence emitted outside the mesa (delimited by the dashed vertical lines) at $1483.8meV$ and $1490.5meV$ originates from the 2D upper and lower polaritons at a positive detuning of $\delta = E_{cav} - E_{exc} \simeq 2\Omega_R$. Note that the luminescence part of these modes situated inside the

mesa exhibits much weaker intensity than outside, we will come back to this point in section 4.1.4. The states localized within the mesa can clearly be attributed to the lower and the upper 0D polariton states.

Fig.4.5(b) shows a spatially resolved spectrum of a $19\mu m$ diameter mesa under the same excitation conditions. The mesa is at a neighboring position and thus at a more negative detuning, as the confined ground mode is nearer to the bottom energy of the trap. In this case the 2D signal is barely visible, which confirms the case of Fig.4.3(c): when excited with a small spot, the 2D signal is no more visible for $19\mu m$ mesas.

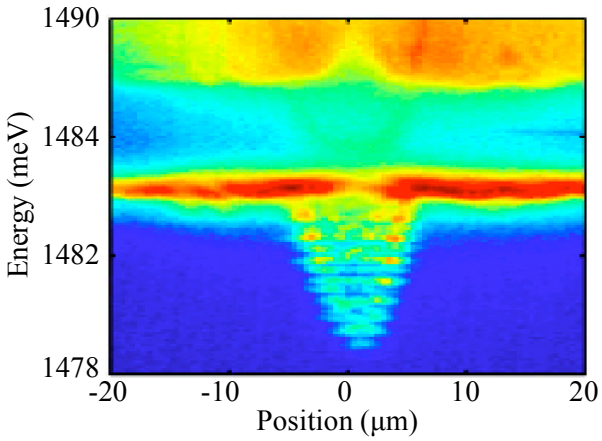

Figure 4.6: Photoluminescence intensity as a function of energy and position for a $9\mu m$ diameter mesa. Image taken in transmission.

Fig.4.6 shows the energy spatial profile of a $9\mu m$ mesa. The image was taken in transmission, one can thus see above $1488meV$ a continuum which has two origins: between 1488 and 1490 the PL is due to the upper 2D polariton, and above $\simeq 1490meV$ the signal is due to the luminescence of the polluted GaAs. These features are similar to the features observed on Fig.4.4, which were taken for the same size of mesa at a similar detuning.

4.1.4 Relaxation processes

The real-space measurements can give some indications on the polariton trapping mechanism.

In the case of Fig.4.5, the excitation spot had a diameter of $2.5\mu m$, but as excitation is done at high energy, the excited region at the polaritons' energies is larger. One can take an idea of the extension of the excited region through relaxation by the size of the 2D emission zone on Fig.4.5(a), which has more than $2\mu m$ of diameter.

In the case of Fig.4.6, the excitation spot had a Gauss diameter of $25\mu m$, thus exciting a much wider area than the mesa. As a result, PL from

the spatially-extended states is dominant. In general, however, confined upper and lower polaritons are clearly visible in the three spectra. And they show a pattern which represents the spatial dependence of the squared wave function of the polariton states. Some asymmetries can be seen, they are probably due to the fact that the mesas are not perfectly circular. We also notice the irregular intensity pattern formed by the extended lower polariton branch, which is particularly evident in the 3 and $9\mu m$ spectra. The spatial fluctuations of the PL peak energy and the varying intensity suggest the occurrence of weak spatial localization over a few tens of μm. This polariton localization is indeed expected in planar microcavities, due to the intrinsic fluctuations of the cavity thickness produced in epitaxial growth (see ref. [Savona, 2007] and references therein).

2D-0D interaction... One can see on figures 4.5(a) and 4.6 that the signal of the 2D polaritons is much weaker above the mesas. These intensity "holes" could be attributed to the efficient coupling between the 2D and 0D polariton states coexisting inside the mesa. In particular, the lower extended polariton (lower dashed line in Figs. 4.3) is almost fully exciton-like, with a vanishing photon component that results in a very long radiative lifetime. These states act as a reservoir from which polaritons relax into the confined states at lower energy. The relaxation can take place through interaction with the thermal bath of phonons [Tassone et al., 1997], with free carriers, or via mutual polariton interaction [Porras et al., 2002].

...or a change in the density of states A competing interpretation is to say that the density of 2D states decreases above the mesa. Simulations in real space tend to validate this point of view, an example is shown on Fig.4.7, but it is not possible, from these measurements, do figure out whether the decrease in PL intensity is more pronounced than the decrease in the density of states... It is not possible with the present data to say which of two processes is dominant.

4.1.5 Theoretical description of confined polaritons

In order to support the measured data, Pierre Lugan, Davide Sarchi and Vincenzo Savona developed a theoretical model of trapped polaritons, published in refs. [Kaitouni et al., 2006, Lugan et al., 2006]. The model is based on the re-writing in cylindrical coordinates of the 2D electromagnetic field, confined in circular mesas, and of the 2D free exciton wave function. We provide the interested reader with a brief summary of this theory in appendix A. In this section we simply intend to compare the results of simulations based on this theory, to our experimental curves. One should mention that a theoretical article describing the case of cylindrical micropillar cavities was published by Panzarini and Andreani [1999], where the issue was different

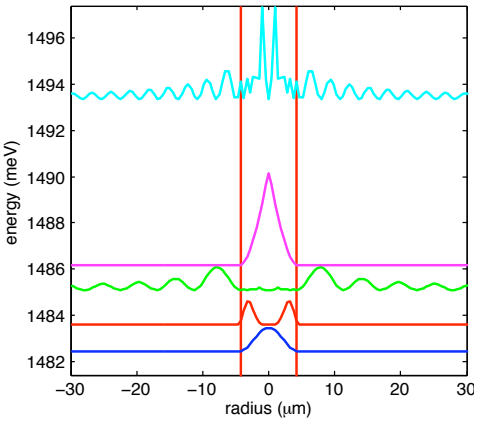

Figure 4.7: Simulated spatial profile of the photon component of confined and extended polaritons, in the case of a perfect circular mesa of $8.6\mu m$ in diameter. The modes shown are, from low to high energies: the confined LP ground mode (blue), the confined LP fourth mode (red), an extended LP mode (green), the confined UP ground mode (magenta) and an extended UP mode (clear blue).

as the leakage out of the cavity for small diameters had to be taken into account.

Parameters used in the simulation The model described allows to simulate the pattern of the measured spectra. For these simulations, circular mesas were assumed. The values of the diameter D and the detuning δ between the 2D cavity mode and the exciton, used in the simulations, were fitted to the experimental data. For the 3, 9 and $19\mu m$ mesas these values are, respectively, $D = 3.46$, 8.6, and $20.0\mu m$, and $\delta = 5.9$, 6.8, and $7.1meV$. For the remaining parameters, the nominal values of the sample were used.

Comparison Figs. 4.8 (d)-(f) display the simulated polariton spectral density for the three different mesas. Although the PL intensities in the measured spectra (Figs. 4.8 (a)-(c)) account for the population of each state, it is not the case in the simulation as population densities are not taken into account, and only the density of states are calculated. This implies that it is not relevant to compare experimental and simulated intensities. A slight discrepancy in the energies of the smallest mesa is probably due to its not perfectly circular shape. In general however, the model faithfully reproduces both the energy position and angular extension of the various spectral features.

We point out that the discrete modes in Fig.4.8(b) and (e), follow a pattern that mimicks the energy-momentum dispersion of 2-D polaritons. For

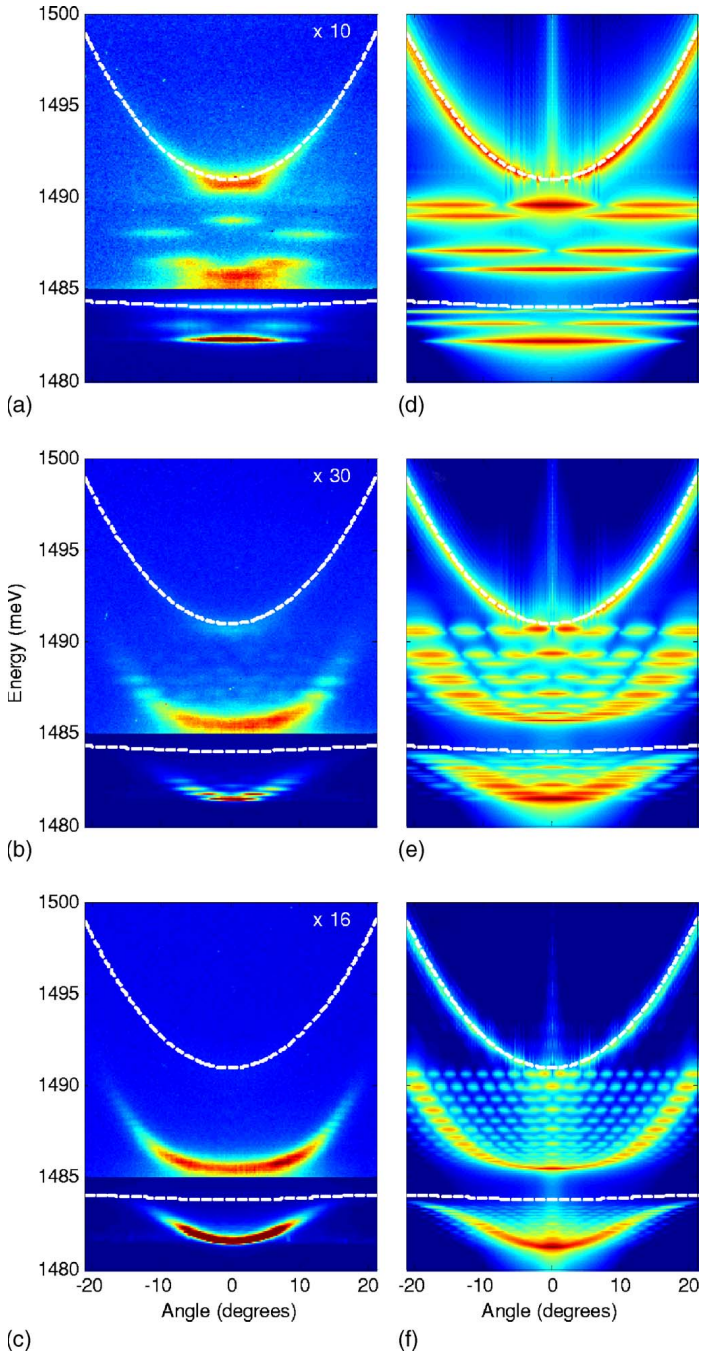

Figure 4.8: Left-hand column: Measured polariton PL intensity (taken from Fig.4.3) as a function of energy and emission angle for: (a) the $3\mu m$, (b) the $9\mu m$ and (c) the $19\mu m$ mesa. Dashed: dispersion of the extended polariton modes, computed from a coupled oscillator model. Right-hand column: Intensity plot of the simulated polariton radiative spectrum for: (d) the $3\mu m$, (e) the $9\mu m$ and (f) the $19\mu m$ mesa (color log-scale, 4 decades from blue to red). Figure taken from ref. [Kaitouni et al., 2006]. Courtesy of Vincenzo Savona.

diameters larger than 20 μm, the simulation results in a spectrum practically identical to that of 2D polaritons in a microcavity of thickness equal to that of the 2D cavity plus the mesa height.

4.1.6 Conclusion

We performed a spectroscopy of the confined and extended polaritons' wave functions profile in photoluminescence, in the relevant configurations: energy as a function of the reciprocal space and of the real space. The 0D character of the confined polaritons is confirmed by the angular width of the confined states. The real space spectroscopy allowed us to directly probe the wave function profile with optical imaging, a quite unique situation in such systems, allowed by the very low effective mass of polaritons.

4.2 2D images through resonant excitation

We saw, in the first part of this chapter, measurements of the eigenenergies of the system we are studying as a function of one dimension of its reciprocal or real spaces. This allowed us to observe the wave function profile, but did not allow us to observe in particular the potential effect of asymmetries of the mesas. This needs a 2D imaging in both spaces. We performed such images through a quite unusual method we will develop in the first section, we will then present the results[2] and finally propose some possible interpretations.

4.2.1 Set-up

We excited resonantly (in angle and energy) at extremely low pump power a given state of the system. For this purpose we performed small changes in the set-up described in the precedent section, the present set-up is shown on Fig.4.9. Imaging is performed in transmission with respect to the laser. The excitation was performed with a TiSa continuous laser, focused to a spot of $\simeq 35\mu m$ in diameter.

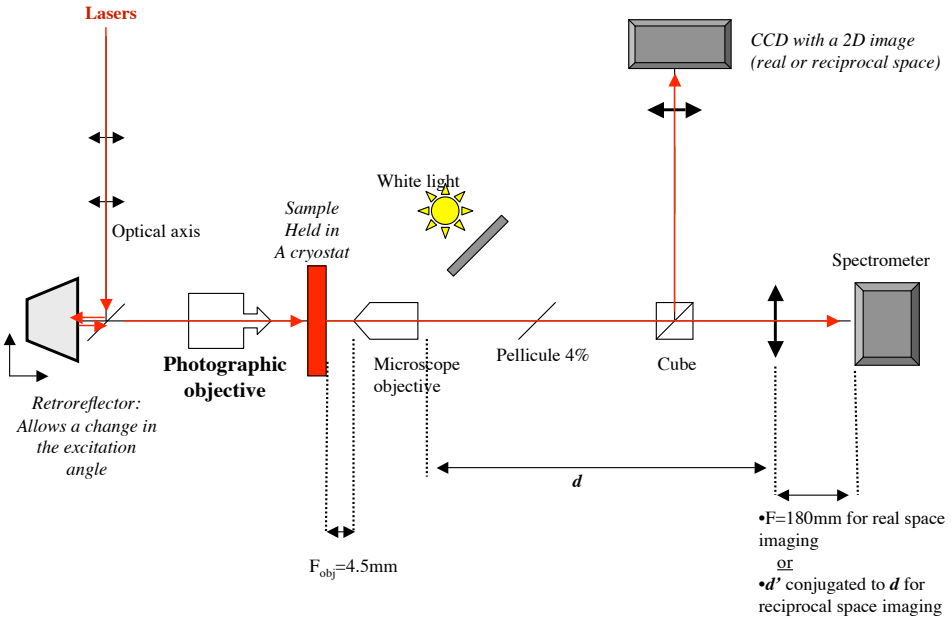

Figure 4.9: Setup for resonant excitation.

[2] *Nota bene:* as it is important that each image and its corresponding comments are seen on the same page, we will repeatedly insert page breaks till the end of this chapter.

4.2.2 Resonant Rayleigh scattering in 2D

Rayleigh scattering concept was used by Lord Rayleigh [Rayleigh, 1871] (cited in a interesting and exhaustive overview of Rayleigh's contribution to the scattering theory peformed by Twersky in 1964) to explain the reemission of light in different directions, by particles with sizes smaller than its wavelength. In a disordered 2D system as the one we are studying, one expects to observe resonant Rayleigh scattering (it was observed in quantum wells by Hegarty et al. [1982] and described by Zimmermann [1995]), due to scattering on static excitonic defects. Is it the case in the 0D systems presented? We will try to question this issue in the next pages.

Resonant Rayleigh scattering in 2D microcavities in strong-coupling regime is a consequence of elastic collisions. These collisions conserve energy and the momentum $|\vec{k}|$, meaning that the final states towards which polaritons are scattered are situated on a ring in the reciprocal $(E, \vec{k_{||}})$ space [Houdré et al., 2000]. Polaritons' coherence yields speckles on the scattered ring.

In order for the reader to have a reference, we show here below an image of resonant Rayleigh scattering taken in the reciprocal space of a 2D zone on our microcavity.

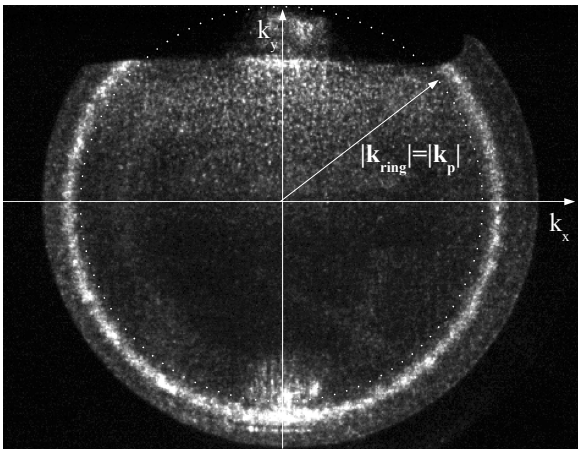

Figure 4.10: Rayleigh scattering ring taken on a 2D zone of our microcavity excited resonantly on the lower polariton branch. Polaritons are scattered at the pump's energy, with a conservation of the momentum $|\vec{k_{ring}}| = |\vec{k_{pump}}|$. The upper part of the ring is hidden is order to avoid the transmitted laser beam, which would overwhelm the scattered signal. The outer dark ring is due to the experimental set-up.

4.2.3 Images of a 9 micron mesa

In order to recall the spectrum of the $9\mu m$ mesa studied, its 2D and 0D lower polaritons spatial and angular profiles are shown on Fig.4.11, through a non-resonant pumped PL experiment.

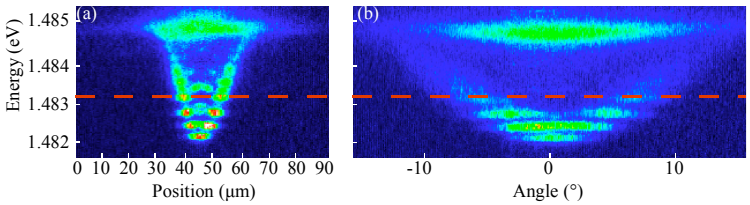

Figure 4.11: A $9\mu m$-mesa. PL images of (a) the energy as a function of one spatial dimension, (b) the energy as a function of the angle. Only the lower polaritons are shown.

A specific angle-energy couple was chosen to excite resonantly a state observed on the dispersion curve. Nevertheless, the laser is probably not perfectly mode-matched with the excited mode, as the laser electromagnetic mode can not be adapted to the polariton mode.

We pumped a $9\mu m$ mesa at $\delta_{0D} \simeq 0$ with an angle of 7° at $1.4831eV$. The measured PL intensity is mostly emitted at the pumped energy, as can be seen on Fig.4.12, where the dispersion curve of the confined lower polariton is shown when pumped resonant on the fourth confined LP state.

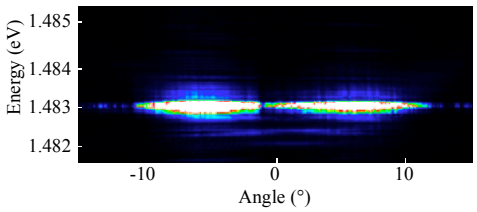

Figure 4.12: Lower polariton dispersion when pumped resonantly on the fourth confined LP state (third excited state). The pump energy is clearly seen just above $1483meV$ thanks to laser scattering. But the transmitted laser can not be seen as the reciprocal plane line imaged does not contain the incident laser beam. The latter does not hit the slit of the spectrometer.

We performed in this configuration 2D images in the real and reciprocal spaces, shown on Fig.4.13(a) and (b). One can see on both images 6 emission lobes, periodically disposed in angle, though one is less intense. These lobes are the maxima of the squared excited wave function in real and reciprocal spaces, but so far one can not discriminate whether this wave function describes an eigenstate of the system or a superposition of eigenstates, we

will discuss this further at the end of the chapter.

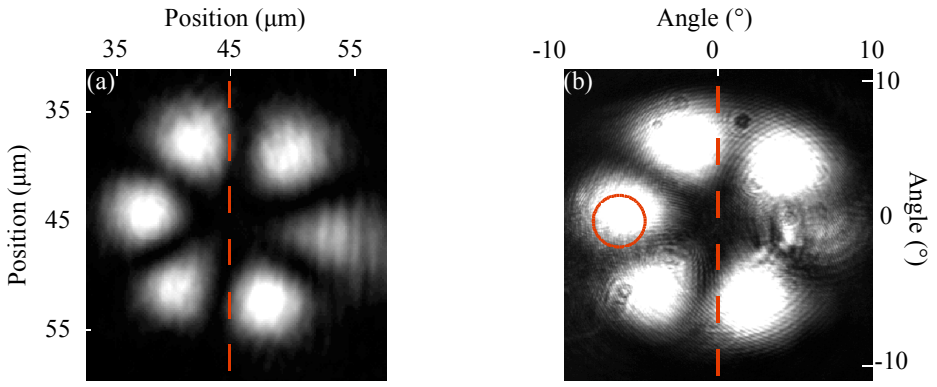

Figure 4.13: A $9\mu m$-mesas resonantly pumped with an angle of 7° at $1.4831eV$ (as shown on Fig.4.12 and indicated by the dashed red lines on Fig.4.11). (a) The 2 planar spatial dimension. (b) The 2 reciprocal space dimensions, the laser beam incident direction is shown by a red circle.

It is remarkable that the laser can not be distinguished from the PL signal. In particular on the reciprocal space images (Fig.4.13(b)), it would be impossible to guess which reciprocal space point (k_x, k_y) is excited if it was not indicated by the red circle.

4.2.4 Images of a 19 micron mesa

We pumped in similar conditions a $19\mu m$ mesa. We have already seen on the dispersion curve shown on Fig.4.3(c), that for this size the dispersion is quasi-continuous. On the mesa studied here, the polaritons dispersion is shown on Fig.4.14(b) in PL, its corresponding real space image is shown on Fig.4.14(a).

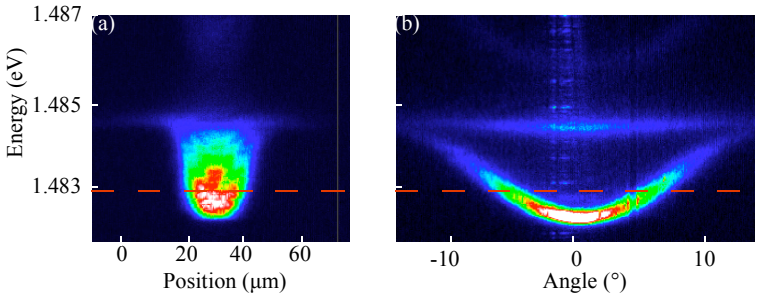

Figure 4.14: A $19\mu m$-mesa. PL images of (a) the energy as a function of one spatial dimension, (b) the energy as a function of the angle. The confined upper polariton can be seen at high energy.

As mentioned, the confined lower polariton was excited resonantly on a confined LP excited state, see Fig.4.15.

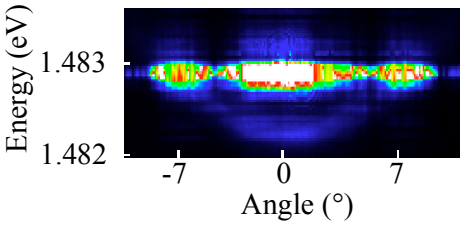

Figure 4.15: Lower polariton dispersion when pumped resonantly. The pump energy is clearly seen just below $1483meV$ thanks tom laser scattering. But as in the $9\mu m$ case, the transmitted laser can not be seen as the reciprocal plane line imaged does not contain the incident laser beam. At 7° at the pump energy, the signal intensity is 21000 (arb. units), at 0° at the bottom of the curve, it is 4000, corresponding to the population which relaxed through phonon along the dispersion curve.

We similarly performed 2D images in the real (Fig.4.16(a)) and reciprocal (Fig.4.16(b)) spaces. In real space we observe a quite irregular pattern. PL signal seems to be more intense in the middle of the mesa. This can be attributed to the inhomogeneity of the exciting spot. The latter has a diameter of $35\mu m$ and a gaussian profile. As the mesa has a diameter of

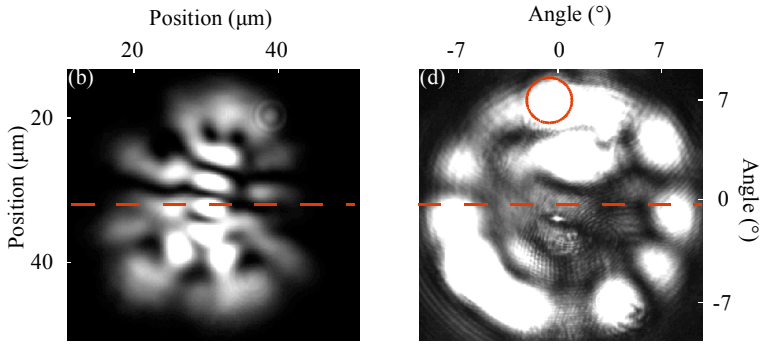

Figure 4.16: A $19\mu m$-mesas resonantly pumped with an angle of 7° at $1.4831eV$ (as shown on Fig.4.15 and indicated by the dashed red lines on Fig.4.14). (a) The 2 planar spatial dimension. (b) The 2 reciprocal space dimensions, the laser beam incident direction is shown by a red circle.

$19\mu m$, its surface can not be considered negligible compared to the spot's surface. We may therefore be exciting and observing a superposition of states showing a higher amplitude in the center of the mesa.

The 2D reciprocal space image (Fig.4.16(b)) is less regular and periodic than in the $9\mu m$ diameter mesa case. We nevertheless observe a ring with intense regular patterns which are very different from the speckles observed on Fig.4.10. One can also see a rich signal at angles smaller than the pump angle of 7°. As there is no spectral filtering, it can be attributed to lower energy signal or to lobes of the excited confined state. Fig.4.15 shows the dispersion curve with the resonant excitation. It is difficult to discriminate between the two sources which probably both contribute to the signal...

4.2.5 Images of a 3 micron mesa

We also pumped the smallest mesas in similar conditions. Its lower polariton energy profile is shown. A technical problem of the pump laser made it impossible to pump the first excited level of the mesa.

We thus pumped the ground level, as indicated by red dashed lines on Fig.4.18(a) and (b), on a figure taken under non-resonant excitation.

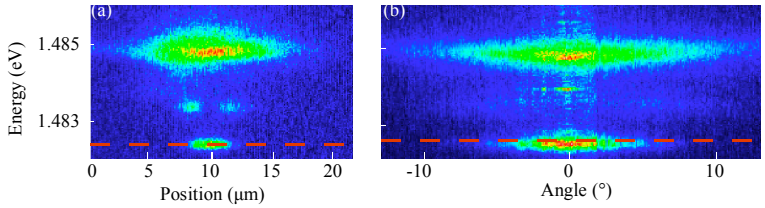

Figure 4.17: A $3\mu m$-mesa. PL images of (a) the energy as a function of one spatial dimension, (b) the energy as a function of the angle (or one reciprocal space dimension). Only the lower polaritons are shown.

As expected this level simply shows a single lobe in both real and reciprocal spaces, as shown on Fig.4.18.

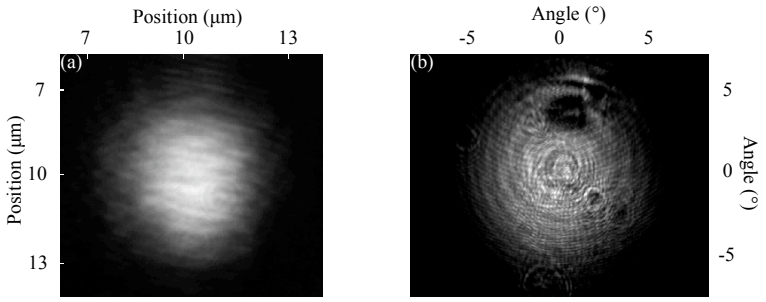

Figure 4.18: A $3\mu m$-mesas resonantly pumped with an angle of 7° at $1.4827eV$ (as shown by the dashed red lines on Fig.4.17). (a) Energy as a function of one spatial dimension, (b) Energy as a function of the angle (or one reciprocal space dimension).

Here again one can note that it is absolutely impossible to distinguish the laser beam from the mesa signal.

4.2.6 Interpretation

Let us propose now an interpretation of our observations in 0D, and a link between the 2D and 0D cases.

Rayleigh or not?

Let us first focus on the $9\mu m$ mesa. In both real and reciprocal spaces, resonant excitation of a given state allowed us to observe what seems to be a single state, *without performing any spectral filtering.*

This state has 6 lobes in both spaces, as Fig.4.13 shows, it is therefore likely to be a state showing an azimuthal number $m = 3$. For a perfect circular symmetry, the latter is degenerate into values ranging between $m_n = -3$ and $m_n = +3$. As we are not in a case of perfectly circular mesas, there is certainly a lift of degeneracy between $m_n = \pm 1$, ± 2, and ± 3, yielding energy differences larger than the laser's linewidth. These states show $|2m_n|$ lobes, thus we should be observing a state showing $m_n = \pm 3$. Each of these single quantum states probably see its lobes' positions defined by the asymmetries of system: crystalline axes, rough round interface of the mesa...

It is likely that we are exciting a linear combination of these two states, precisely the combination showing a lobe corresponding to the laser's incidence angle. The mechanism through which we see this state is thus a mode-matching mechanism, and not Rayleigh scattering. An experiment which will allow to validate this interpretation is be to turn the laser's incidence on the same solid angle.

One could however be more general in the interpretation: the excitation is performed through a laser showing a certain profile in k-space, this profile corresponds to a certain combination in the (n, m) space (see appendix A about the quantum numbers), and this combination does not necessarily includes states sharing the same quantum number n.

In order to check this possibility a theoretical calculations of the modes for perfectly circular mesas of several diameters 8, 8.6 and $9\mu m$ is shown on Fig.4.19. As we already saw in chapter 2, the mesas are not perfectly circular, but elliptic. Their energies are therefore a superposition of circular mesas' energies. On Fig.4.19, the two lines at energies E and E' are guide-to-the eye lines showing that several states (belonging to the same size or to different sizes) share very close energies. It is thus likely that a combination including several (n, m) states is excited.

Broader mesa and transition to 2D Despite the fact that its dispersion curve on Fig.4.14 is hard to differentiate from a 2D continuous dispersion, one can see that the $19\mu m$ mesa signal in reciprocal space, while excited resonantly (Fig.4.15 and 4.16), shows a profile clearly different from the 2D Rayleigh scattering shown on Fig.4.10. It seems to have 10 lobes, corre-

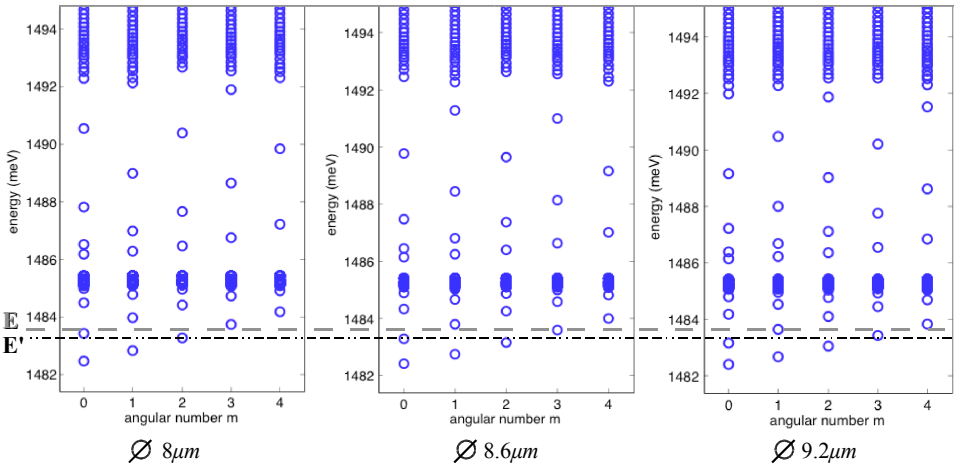

Figure 4.19: Energy of the modes in the (n, m) space. For each value of m, the states are labeled with an increasing number n with increasing energy. The fourth state in terms of growing energy for the $8.6\mu m$ mesa is indicated by the black dashed line, the state showing $m = 3$ for the same mesa is indicated by the grey dashed line.

sponding to $m_n = \pm 5$. So we are probably again exciting a combination of states showing the same energy, and this combination shows on of the lobes at the incidence angle of the laser, as in the $9\mu m$ case.

Increasing the mesa size brings more (n, m) states to be involved in the superposition of states necessary for the laser to couple into the system, the resulting superposition shows thus narrower angular lobes. Going towards the 2D limit, this superposition's result is reduced to one lobe, and this lobe's angular width is reduced when the number N of states involved increases. It defines the angular width of the transmitted laser, which is usually smaller than the incident one.

And where is the Lord? It is difficult to figure out at which confinement diameter Rayleigh scattering begins to play a role. As one can see on Fig.4.16, the emission pattern is not regular for a $19\mu m$ mesa, it is thus likely that other states were populated, with neighboring energies, through Rayleigh scattering. But this mechanism does nevertheless not seem to be dominant, as th main pattern shows clear periodical lobes.

The latter case is to be opposed with the 2D case on Fig.4.10, where Rayleigh scattering clearly dominates and populates a whole ring in k-space, made of a high number of states.

Impact of disorder: Rayleigh scattering is related to disorder, that has two sources: cavity or exciton disorder.

1. For small mesas with diameters $\lesssim 10\mu m$, confinement and quantization of the energies renders the states insensitive to photon disorder, which in addition is present on larger typical lengths ($> 10\mu m$). When increasing the size of the mesa, the dispersion gets quasi-continuous and the diameter becomes larger to the typical size ($\approx 10\mu m$) of the photonic disorder in a GaAs cavity. It is thus possible that this disorder starts to play a minor role for the $19\mu m$ diameter mesa, while it plays an important role in the broadening of the linewidths in the 2D structure.

2. On the other hand, exciton disorder shows a typical size of the order of $10-100nm$. Collisions of polaritons on these static defect (that would be Rayleigh scattering) can not play a role in this discrete system as no states towards which polariton could scatter are available. Again, when increasing the confinement size, states at similar energies than the pumped state appear, and Rayleigh scattering can play a role.

4.2.7 Conclusion

In conclusion we propose here an innovative spectroscopy technique through resonant pumping. We directly observe the wave function of a superposition of confined states and their Fourier transform. It is a quite unique situation at such scales in a quantum system, possible thanks to the exceptionally small mass of the polaritons.

We point out the question of the transition between two situations: a confined situation where a single quantum state is excited, and a situation where a continuum of states is available, and populated (excited) by Rayleigh scattering. We proposed some possible answers, further experiments through variation of the excitation conditions, may give some more clues to understand further and situate this transition.

Chapter 5

Studies in the nonlinear regime

After having studied the optical properties of the sample in the linear regime, and confirmed that we are in presence of 0D polaritons, we will come to the study of our first motivation for starting this work: condensation effects. These effects are studied through the measurement of the response of the system to an increase of the pump power, in various conditions. We will first study the non-resonant excitation case, then the resonant excitation.

5.1 Motivation and general phenomenology of power studies

Let us first introduce the general phenomenology of power studies, in order to have basic tools to understand our observations. This will allow us to have an overview of the literature on these issues.

5.1.1 General case

The issue we want to address is the possibility of seeing a spontaneously condensed polariton phase. Spontaneity is of importance and leads us to populate non-resonantly the system at high energy. The relaxation towards low energy states (polariton states) occurs then through phonon scattering processes, which do not transmit the coherence properties of the excitation laser. Another issue concerns parametric effects, which allow to observe for example amplification or correlated polariton populations, by creating a high density of population in a well-chosen state.

These phenomena rely on the excitonic nonlinearities, and thus occur under high excitation densities. In an optically pumped semiconductor, the population (the number of excitations created) is related to the power of the pump. In our case, the pump being a laser beam, the population is directly

related to the power of this laser, depending on which sate is excited (it can be a polariton state or a high energy state, creating unbound electron-hole pairs). The term *population* mean here *population of total excitations* (including free carriers, uncoupled -dark- excitons and polaritons).

So one can summarize as follows : we are performing a *study of the response of the system to a variation of the pump power*, which concretely means a *study of a given state's population* (usually the ground state) *as a function of the total population created* (or the total number of "excitations").

A clear overview of the phenomenology of the nonlinear optical properties of semiconductor systems (under a high excitation) can be found in [Klingshirn, 1995].

5.1.2 Case of polaritons

1. Non-resonant excitation

   Polaritons are composite bosons, meaning that they can show stimulation effects, while they interact. This means that several regimes (linear and nonlinear) are expected while populating non-resonantly the system at a high energy, see Fig.5.1 for an illustration. Each density regime depends on the dominant mean of relaxation.

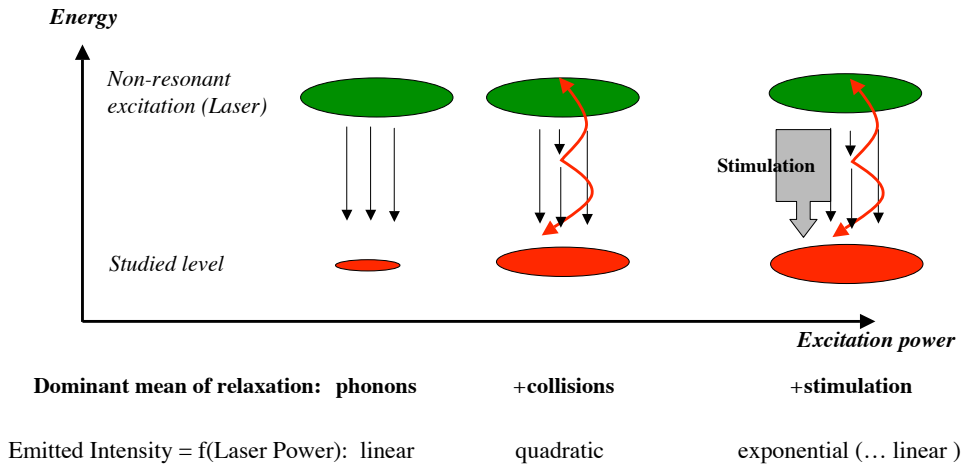

Figure 5.1: Diagram of the various regimes that can be observed while varying the density of a quasi-bosonic system, in the case of a non-resonant excitation.

Phonon relaxation In a very low density regime, the only relaxation process involves phonons, so relaxation rates do not depend on density, and the population of a given state (which energy is lower

than the pump energy) will vary linearly with the pump power. It is an incoherent process. [Tassone et al., 1997]

Effect of Coulomb interaction Coulomb interaction enters into account for excitons, yielding collisions between free carriers or high energy excitons. If collisions are the dominant mean of relaxation, the relaxation rates depend on density, and a quadratic behavior of the population as a function of the pump power is observed [Senellart et al., 2000].

Stimulation When, at a given energy level (most probably the ground level), the density of occupation exceeds 1 particle per state, the bosonic nature of the involved particles implies a stimulation of the transition by the population of the state. Meaning that this population will depend exponentially on the pump power. [Porras et al., 2002]

Saturation At very high density, when the whole available amount of population created in the system is transfered to the stimulated state(s), or to a certain number of low-energy states (the stimulation regime may have not been reached), a linear evolution of the population as a function of the pump power reappears. It is indeed impossible to have more particles in the system than what is created by the pump.

Weak coupling At high excitation densities, however not depending on the regime, the strong exciton-photon coupling may be lost [Butté et al., 2002]. This will not affect the different regimes, the phenomenology described above is similar in strong and weak coupling regimes, as it is driven by the excitons.

2. Resonant excitation

The term resonant excitation can be ambiguous, because one could imagine exciting resonantly any electronic state of the system, when using this expression, we systematically mean "resonant with a polariton state", either 2D or 0D. In this case some differences can arise with respect to the non-resonant case. The various regimes expected are drawn on Fig.5.2.

The various density regimes still depend on the dominant mean of relaxation.

Phonon relaxation At very low densities, the only relaxation process involves phonons, exactly as in the precedent case.

Effect of Coulomb interaction The fermionic component of the excitons enter into account, yielding collisions between excitons towards a signal and an idler state. As mentioned in the theoretical introduction, equation 1.15 yields a quadratic behavior of

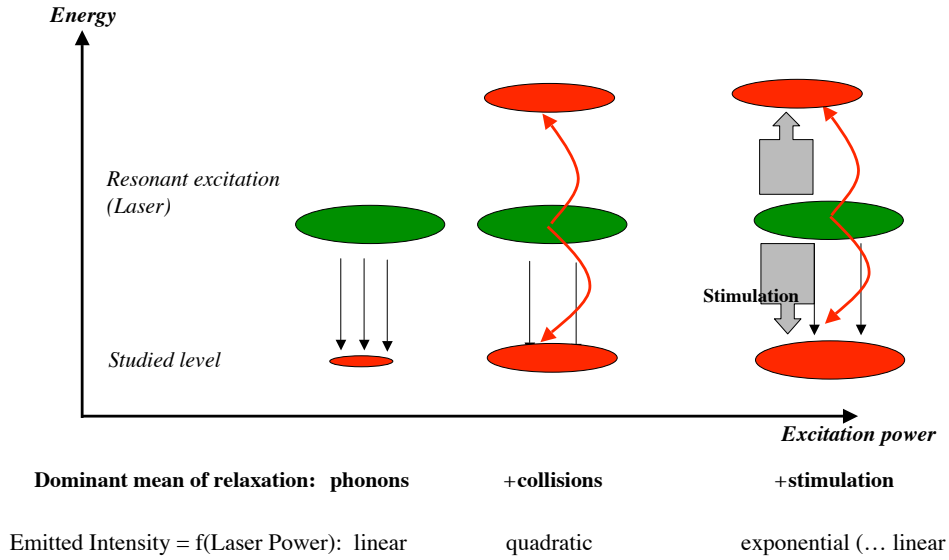

Figure 5.2: Diagram of the various regimes that can be observed while varying the density of a quasi-bosonic system. Non-resonant excitation.

the populated (signal and idler) states as a function of the initial state population, and thus of the pump power. Usually the studied state is a final state of the collision process. [Ciuti et al., 2001]

Stimulation When, in the final states of the collision process (usually the studied state and its complementary with respect to the pumped state), the density of occupation exceeds 1 particle per state, the bosonic character of the involved particles implies a stimulation of the relaxation, and thus parametric oscillations [Savvidis et al., 2000, Stevenson et al., 2000, Ciuti et al., 2000]. Meaning that this population will grow exponentially with the pump power.

Saturation At very high density, as in the non-resonant case, when the whole available amount of population created in the system is transfered to the stimulated states, a linear evolution of the population as a function of the pump power reappears. A saturation of the absorption of the populated state is also possible.

Weak coupling At high densities the strong exciton-photon coupling may be lost. As we are pumping in a polariton state, this will imply a loss of resonance between the pump and the pumped state, and may lead to optical bistability [Tredicucci et al., 1996].

5.2 Non-resonant excitation

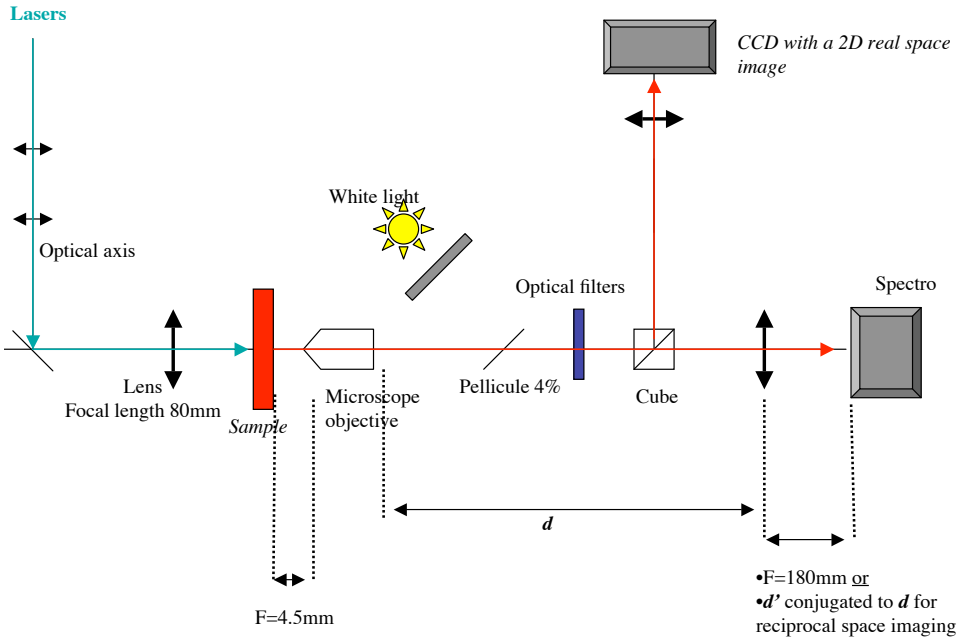

Figure 5.3: Set-up used to perform non-resonant excitation studies.

The set-up to pump non-resonantly the sample is shown on Fig.5.3, it allows to have energy dispersed images of one real or reciprocal space dimension.

The sample was excited with different excitation conditions (laser energy, spot size), and at various detunings, we found no qualitative change in the results depending on these parameters. Results in various conditions are shown.

5.2.1 Regimes observed

Let us study in details the case of the smallest mesas, where the modes are well spectrally distinguishable. We will see several excitation conditions.

a - A $3\mu m$ mesa at zero detuning

The first example is a $3\mu m$ mesa at zero detuning for the ground confined polariton state, a photoluminescence spectrum in real space is shown on Fig.5.4 (this spectrum was already shown and commented in chapter 4 Fig.4.5(a)). The mesa is excited with a continuous laser, showing a spot of $\approx 3\mu m$ at an energy of $1.6eV$ ($780nm$, hence $0.12eV$ above the exciton energy), which corresponds to the upper edge of the mirrors' stopband. PL intensity, linewidth

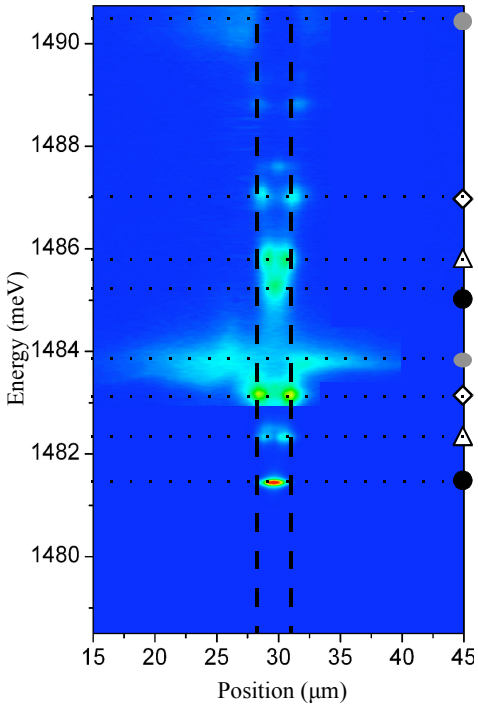

Figure 5.4: PL intensity as a function of energy and position for a $3\mu m$-diameter mesa. The same symbols than for the precedent chapters are used to label the various states: grey circle for the 2D polaritons, black circle for the confined ground state, white triangle for the confined first excited state, white rhombus for the confined second excited state.

and energy of the ground level of the confined LP are shown on Fig.5.5 as a function of the laser power.

As we have mentioned before, the photoluminescence (PL) intensity is directly related to the polariton population, through its photonic component. The first graph shown on Fig.5.5(a) is thus the angle and space-integrated PL intensity of the ground state (lowest energy level on Fig.5.4), in a Log-scale, as a function of the laser pump power. As one can see four regimes are clearly distinguishable: linear, quadratic, strongly nonlinear and linear again. These regime fairly correspond to the phenomenology introduced at the beginning of this chapter.

The question is now to determine what kind of particles we are addressing. This means figuring out where the loss of the strong-coupling regime occurs. As this cross-over from strong to weak coupling is not a phase transition, there is a wide density (or pump power) range where it is not clear whether we are dealing with polaritons or not. Indeed the progressive exciton saturation diminishes progressively the oscillator strength and thus the Rabi splitting. In order to determine the coupling regime, we have plotted

two other types of data: energy and linewidth of the studied state. Two criteria give lower and upper limits between which strong coupling is broken[1]: one is the onset of the decrease of the linewidth, the other one is the crossing between the PL peak and the uncoupled exciton line, these two extreme criteria give a pump power range between 0.75 and 4mW for the loss of strong coupling. This ensures that the superlinear regime seen after the quadratic is in a state of weak coupling, it is the expression of laser oscillations (so we are in presence of an optically pumped VCSEL - Vertical Cavity Surface Emitting Laser [Butté et al., 2002]), confirmed by the very sharp linewidth.

[1]See for more details section 1.4

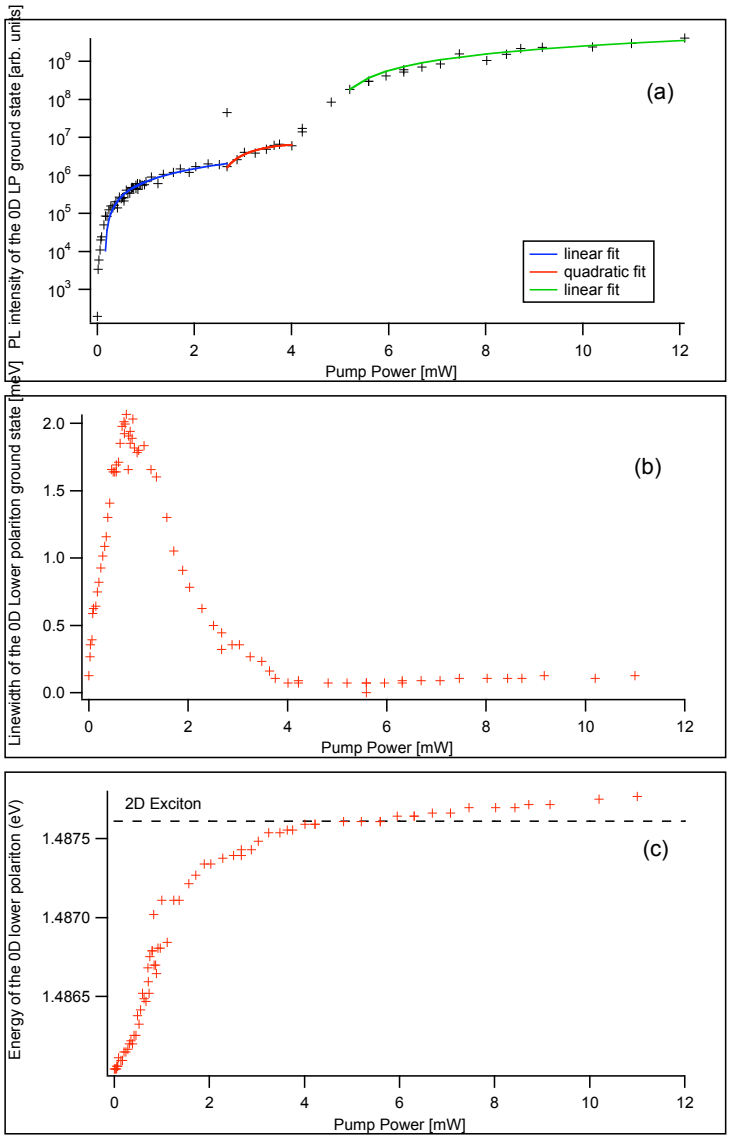

Figure 5.5: (a) Photoluminescence intensity (semi-Log scale), (b) linewidth and (c) energy of the LP ground state of a $3\mu m$ mesa at zero detuning as a function of the pump power. PL intensity was integrated angularly in order to include all the emission of a given energy, corresponding to a given state, as we are in presence of a discrete spectrum.

b - A $3\mu m$ mesa at negative detuning

We have performed the same kind of study in a different configuration: we chose a mesa where the ground photon level is at negative detuning with respect to the exciton line energy ($\delta \approx -7meV$[2]), and thus its excitonic component is negligible. One would expect relaxation to be less efficient in this configuration, and nonlinear thresholds to be higher.

The excitation is now done with a laser pumping at very high energy ($2.43meV$, it is a green Argon laser emitting at $512nm$), with a spot of about $30\mu m$ in diameter.

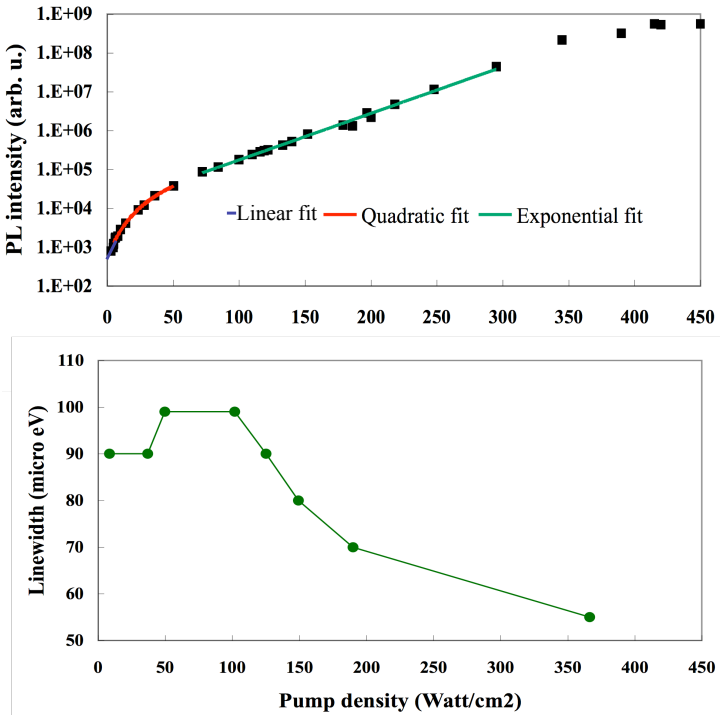

Figure 5.6: PL intensity (semi-Log scale) and Linewidth of the ground level of a $3\mu m$ mesa at negative detuning as a function of the pump power.

The behavior of the PL intensity, shown on Fig.5.6, is similar here to the behavior observed at zero detuning, with two quantitative differences:

- An exponential behavior is clearly visible (it was barely visible on Fig.5.5 between pump powers of 4.5 and $5mW$.). This behavior is due to a lasing in weak-coupling regime, we will see this further in section 5.2.2.

[2]This means that the ground lower polariton state we are studying is at an energy equal to the uncoupled photon mode at the same position, strong coupling loss can thus not be deduced from a an energy shift argument.

- The broadest linewidth reached is $100\mu eV$ (see Fig.5.6), to be compared to $2meV$ in the previous case ! This is the most visible effect of the difference in the excitonic components.

Occupation number We calculated the number of polaritons created in the studied state at the quadratic threshold through a method inspired from ref. [Senellart et al., 2000]. As we integrate angularly the whole signal, we simply measured the PL power emitted at the ground state energy at the threshold, equal to approximately $P_{detected} \approx 30nW$. This power should be multiplied by $\simeq 2$ in order to take into account the two sides of the cavity.

$$N_{ground\ state} = \frac{P_{detected}\tau_{cav}}{C^2 E} \approx 0.1 polariton$$

where N is the number of polaritons in the state, τ_{cav} is the cavity photon lifetime, C is the Hopfield coefficient, and E is the energy of the state in Joule. The uncertainty is given by $\tau_{cav} = 10ps \pm 5\%$ and C^2 can be considered equal to one (the error related to the error on the detuning which is around 5%) at such negative detuning. As one can see the uncertainty on this number is around $\approx 10\%$, but nevertheless low enough to say that $N_{ground\ state} < 1$.

Larger mesas

Identical studies were performed on larger mesas (9 and $19\mu m$ in diameter) and no qualitative difference was found.

5.2.2 Weak coupling regime

In order to check the onset of lasing in weak coupling regime on the whole sample, we performed in parallel 2 series of measurements along the sample's wedge, while pumping the mesas non-resonantly (with the same conditions than for the $3\mu m$ mesa at negative detuning), one well below the breaking of the strong coupling (in the linear regime) and one well above (in the lasing regime).

Each measurement is done exciting the system with a $30\mu m$ laser spot, far wider than the mesa, which means that both $0D$ and $2D$ signals are observable. As we chose a position where the confined ground mode is tuned around resonance with the exciton, the 2D cavity mode is positively detuned between $\delta \simeq +6meV$ and $+8meV$ with respect to the exciton mode, thus the 2D-Lower polariton is exciton-like, this allows us to always have the exciton signal on our spectrum, as a reference. At low excitation power, one sees on Fig.5.7 the usual anticrossing behavior between the 0D lower polariton and upper polariton (only the ground state is represented). At very high excitation power, only one mode can be seen, crossing the exciton line, it is the VCSEL lasing regime of the ground 0D cavity mode. One can

note that this mode does not cross the exciton line precisely at the resonance (zero detuning) position. The latter is at a position $x \simeq 10mm$, where the splitting between the 0D lower and upper polariton is the smallest. Thus, one can see that the energy of the lasing mode is slightly detuned towards low energies with respect to the uncoupled cavity mode. This may be attributed to the index refraction change at high excitation densities.

Stimulation in the weak coupling regime is characteristic of a Vertical Cavity Surface Emitting Laser (VCSEL) [Butté et al., 2002], lasing is also confirmed by the linewidths behavior on Fig.5.5(b) and Fig.5.6. This VCSEL shows some peculiarities: it is optically pumped and lasing on a single mode (given by the 0D confinement). The single mode lasing could be of interest under electrical injection [Hofmann et al., 2007], and the broad angular pattern of the ground mode indicates a behavior that recalls non-directionnal lasing recently reported [van Vugt et al., 2006].

A beautiful succession of images[3] on Fig.5.8 illustrates this progressive loss of the strong-coupling regime, and then lasing on the ground photon mode. One can note on Figs.5.8(a) and (b) the intensity "holes" in the 2D upper and lower polariton signal we mentioned in chapter 4 section 4.1.4.

On Fig.5.8(e) the 0D uncoupled modes are clearly visible and several confined states are resolved. Finally on Fig.5.8(f) one can see the lasing regime on the ground confined photon state.

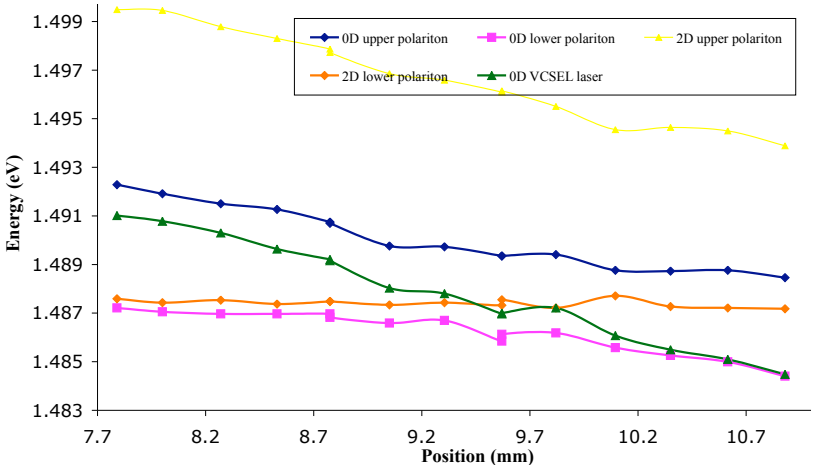

Figure 5.7: Anticrossing (at low pump power) and evolution of the VCSEL (high pump power) signal for the confined system. The 2D LP is at the exciton's energy, as the 2D cavity shows strong positive detuning for this range of positions.

[3]Nicely designed and formatted by Gaël Nardin.

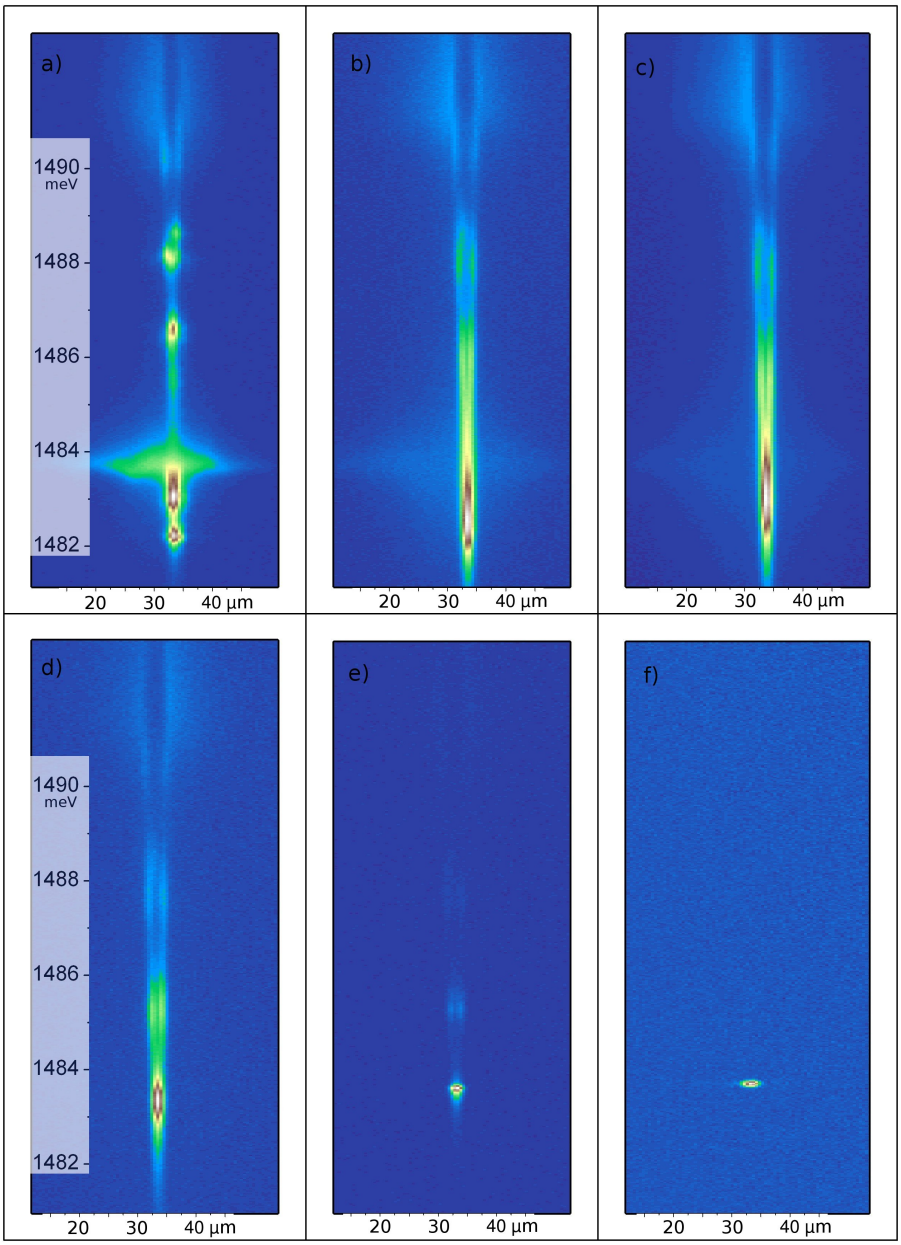

Figure 5.8: Illustration of the strong to weak coupling cross-over, followed by lasing, with spatially resolved PL spectra under non resonant excitation of a $3\mu m$ mesa, at various pump powers, corresponding to the measurements presented on Fig.5.5. (a) 0.03 mW (b) 0.49mW (c) 0.97mW (d) 2.03mW (e) 3.75 mW (f) 6.69mW pump power.

5.2.3 A lab for seeing nonlinear effects

We were able to observe successively and separately several kinds of behaviors which can occur when increasing the density of quasi-bosons. But the nature of the studied particles changed during the study! Indeed the stimulation regime observed was in a situation of weak-coupling between excitons and photons, this regime is representative of a photon condensed phase, a laser, where the active medium is the quantum well, and the cavity modes are the confined mesa modes. The strong to weak-coupling regime transition was observed through an increase of the excitation density, by excitonic saturation and interaction. It is also possible to observe it through a variation of the temperature [Gutbrod et al., 1998].

Communicating vessels

An interesting point to mention is the comparative evolution of the confined and 2D (or continuum) states. We could observe nonlinear behaviors on the excited states of the mesa, similar to what was observed on the ground state, although these behaviors appeared to be very unstable: the slightest perturbation in the experiment would drastically change the PL intensity, hence, it was not possible to draw their behavior on a large excitation power range. Moreover, in the same series of studies, we also observed nonlinear behaviors of the 2D signal when increasing the pump, also accompanied by a strong-to-weak coupling regime transition.

Following these observations several interesting features should be mentioned:

- The confined excited states show nonlinear thresholds similar to what observed for the ground level, at similar laser powers (though slightly higher). It is difficult to give precise values because of the instability of the system as soon as more than one state shows a nonlinear behavior.
- The 2D signal shows nonlinear behaviors at even higher thresholds (3-4 times higher). It shows a quadratic behavior, followed by an exponential in the weak coupling regime.
- When the 2D signal passes the transition from a quadratic to an exponential behavior, the 0D states show a change in their emission regime simultaneously, but an opposite change, from what seems to be the onset of en exponential back to a quadratic regime. Fig.5.9 shows this behavior, it occurs in the weak coupling regime.

These measurements show that the 2D and 0D states share the same reservoir: when the 2D continuum states stimulate the relaxation towards them, the reservoir does not show sufficient population to allow the relaxation stimulation towards the 0D states. The latter are then populated by

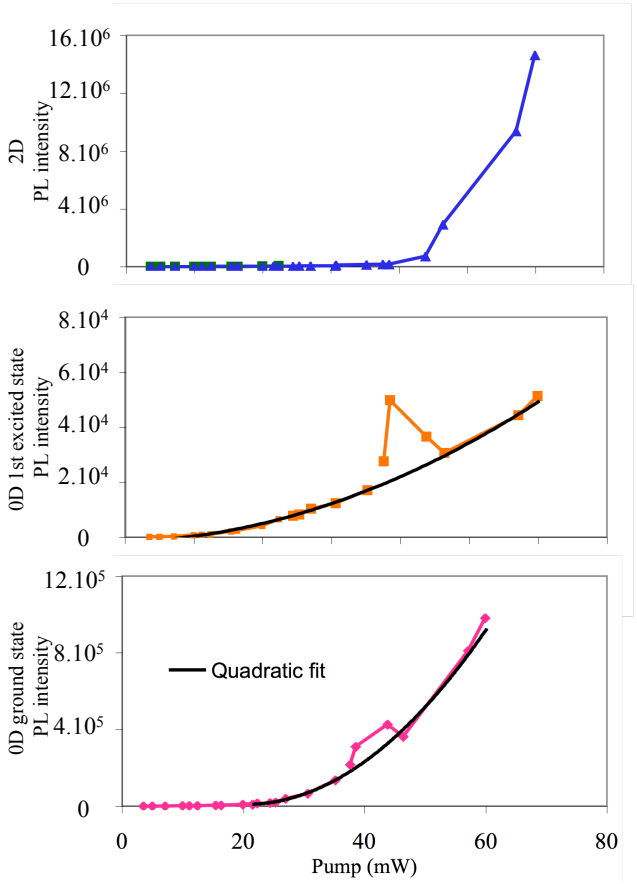

Figure 5.9: Upper graph: transition of the 2D signal towards a lasing regime. Lower two graphs: Falling of the mesa LP ground and first excited states intensity, from a starting lasing regime (exponential) back to a quadratic regime. The quadratic fit was performed on the points taken before the transition at $38mW$. All scales are linear.

a process which stays present: Coulomb scattering in the pumped state (at high energy).

In conclusion We observed a rich phenomenology of nonlinear effects. Moreover, spatial overlap of the 2D and 0D wave functions seems to be sufficient to yield interaction. It is nevertheless difficult from this kind of time-integrated measurement to obtain more information, and in particular to figure out if the 0D states populate each other. This would need time-resolved measurements of the population along one spatial axis, at given energies, in order to follow population and depopulation of the various states. This kind of measurements are being performed at the moment by Taofiq Paraïso and Gaël Nardin.

5.3 Resonant excitation: parametric processes

The non-resonant excitation of the system creates free carriers contributing to the total density of population and thus to the strong-coupling loss. Resonant excitation of the system creates only polaritons. It has lead to the observation of several phenomena of interest as giant parametric amplification [Saba et al., 2001] or coherent control of polaritons [Kundermann et al., 2003] along with the varied phenomenology we introduced at the beginning of this chapter.

Resonant excitation concretely means excitation of the system through a polariton state. In order to excite selectively a given eigenstate, one needs to be able to observe these states. As they are defined in the wave vectors' basis, it is necessary to observe the reciprocal space of the sample in order to be able to select which state to populate. As shown in chapter 4, the reciprocal space is accessible through angle resolved imaging and excitation.

5.3.1 Principles of parametric processes

We gave in section 5.1.2 the general phenomenology which can occur while exciting resonantly a polariton system. Let us see more precisely the case of the parametric oscillator. Since several years now parametric oscillations, a phenomenon similar to the optical parametric oscillator (OPO), was observed when pumping the system above a certain critical density: thanks to their excitonic content, polaritons can interact strongly, added to their peculiar dispersion shape, this allowed to observe polariton parametric scattering where two polaritons in a pump initial state $(E_p, \vec{k_p})$, scatters towards one idler $(E_i, \vec{k_i})$ and one signal $(E_s, \vec{k_s})$ states, along the LP dispersion curve. These processes should respect energy and momentum conservation: $2E_p = E_s + E_i$ and $2\vec{k_p} = \vec{k_s} + \vec{k_i}$, see Fig.5.10.

Thanks to its non-parabolic shape, it is possible to find such states on the lower dispersion branch, given that k_p is larger than the inflection point [Langbein, 2004]. For one given pump state, the allowed couples of signals and idlers are described by 8-shaped lines in the 2D reciprocal space, as was observed by Langbein [2004]. The most interesting pump state is at the so-called magic angle, for which the signal state corresponds to the bottom of the dispersion, that is the polariton ground state $(E_0, \vec{k} = \vec{0})$. This situation shows the smallest density threshold for parametric conversion [Savvidis et al., 2000, Stevenson et al., 2000, Ciuti et al., 2000], it is schematically shown on Fig.5.10.

As shown by Ciuti et al. [2001], the threshold for which parametric oscillations occur is the same than for the optical parametric oscillator (OPO). It is given by

$$\Delta_{k_p,k_{p'}} = \sqrt{\gamma_0 \gamma_{2k_p}} \tag{5.1}$$

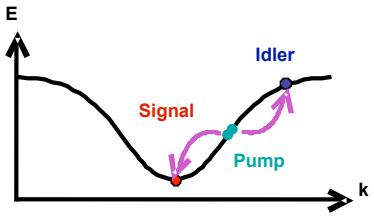

Figure 5.10: Diagram of the parametric scattering process when exciting at the magic angle.

Where $\Delta_{k_p,k_{p'}}$ is the blueshift of the pump state, when this blueshift (due to the density increase) equals the linewidth because the scattering rate equals the losses, the parametric oscillation starts. It is proportional to the density of polaritons created in this state

$$\Delta_{k_p,k_{p'}} \propto n_p \tag{5.2}$$

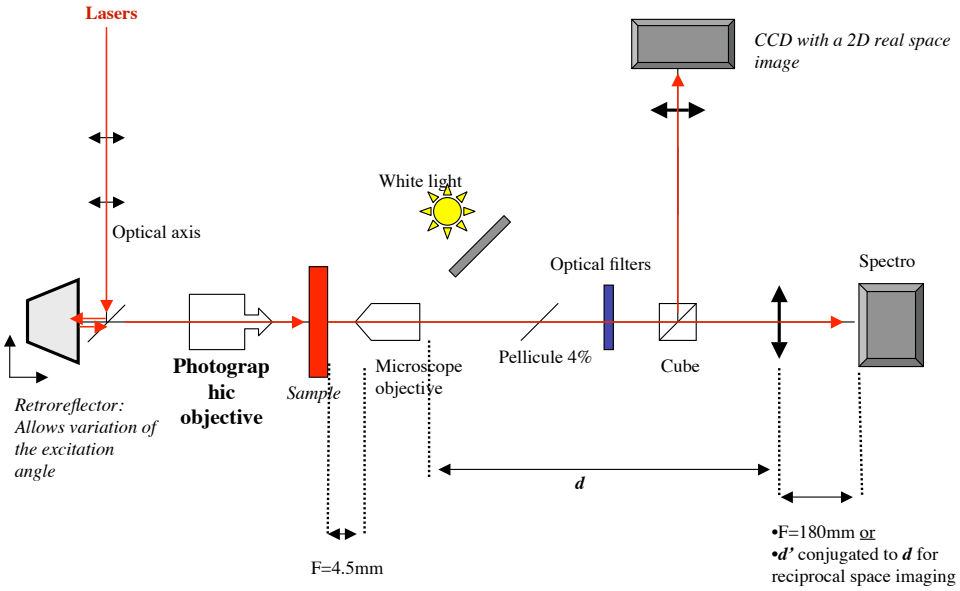

Figure 5.11: Set-up used to perform resonant excitation studies, the retro-reflector allows to change the angle of excitation both in the vertical and horizontal dimensions, parallel to the cavity plane.

5.3.2 Setup

The set-up to pump resonantly the sample is shown on Fig.5.11, it allows to have energy dispersed images of a dimension in real or reciprocal space, and

to excite the system with a given angle. This means that we are creating a population of polaritons in a (nearly) single state, determined by the laser's energy E and excitation angle.

The sample was excited with different excitation conditions (laser energy, spot size, continuous or pulsed), and at various detunings, but no qualitative change was found to occur in the results depending on these parameters.

5.3.3 Parametric processes in the 2D cavity

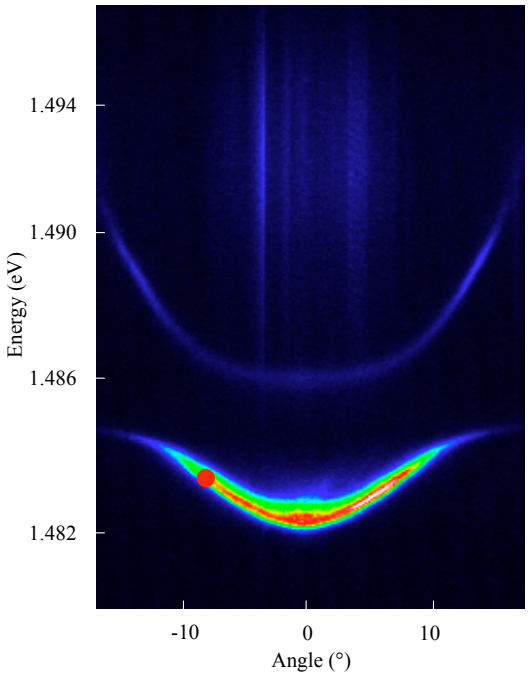

Figure 5.12: PL of the 2D polaritons in the reciprocal space: dispersion curve. The pump laser energy and angle are indicated by a red disc.

In order to have an idea of the characteristics of this sample, compared to other similar samples where parametric phenomena have been observed [Savvidis et al., 2000, Stevenson et al., 2000, Saba et al., 2001, Kundermann et al., 2003], we first performed a study of the 2D-polaritons' behavior when pumping resonantly at the so-called magic angle, as shown on Fig.5.12.

The excitation was chosen to be done with a pulsed laser, with pulse lengths of $5ps$, which means a linewidth of $1meV$, this allows us to be independent from the blueshift of the polaritons (in particular the pumped state) dispersion curve with the increase of density. The dispersion is expected to shift energetically by the linewidth of the pumped polariton state $\simeq 350\mu eV$ at the parametric oscillation threshold, small enough ($< 0.5meV$) considering the spectral linewidth of the laser. The laser spot size had a diameter

of $\simeq 30\mu m$ and the sample was pumped at an angle of $\simeq 8°$.

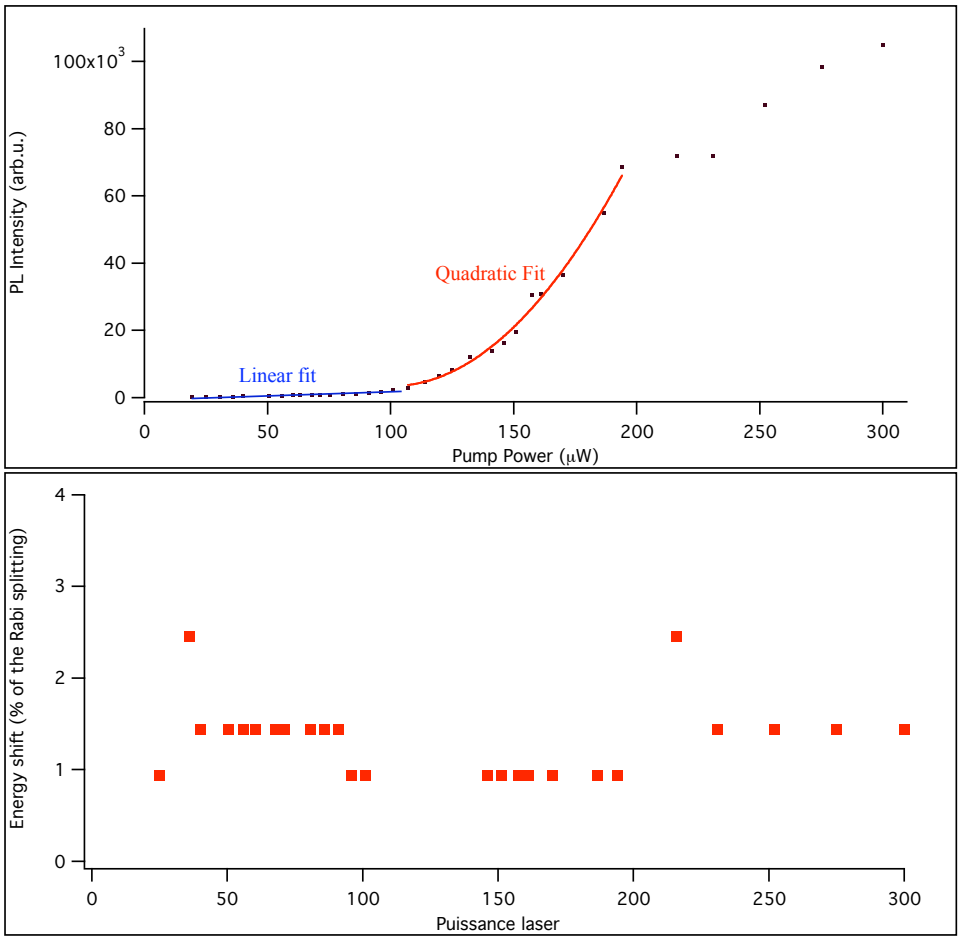

Figure 5.13: (a) PL Intensity of the bottom of the lower polariton dispersion as a function of the pump power. (b) Energy shift, the shift is by less than two linewidths, and keeps the energy far from the exciton line which is at $1.487eV$.

Results and interpretation

As seen on Fig.5.13, at low pump power, a linear behavior of the emission peak is observed, followed by a quadratic regime. After the latter, a linear regime appears, characteristic of the saturation in population of the system.

The quadratic behavior is due to a polariton polariton scattering below the parametric oscillation threshold, namely parametric luminescence, having the $k = 0$ state as the signal state. Fig.5.14 shows the evolution of the LP dispersion for various pump powers. Above the quadratic threshold, the signal state is clearly dominant, but we were not able to observe the idler state.

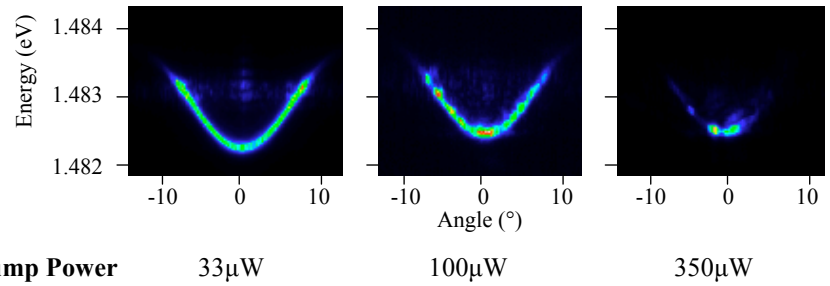

Figure 5.14: Evolution at various pump powers of the PL signal along the LP dispersion.

As it is at high wave vectors, its excitonic component is preponderant, so the emitted intensity is weaker than for the $k = 0$ state. Another factor due to this excitonic component is that it may relax by interaction with phonons and high **k** (non-radiative) excitons [Savona and Piermarocchi, 1997].

Nevertheless this state exists and certainly emits enough to be detected with a more sensitive apparatus as single-photon sensitive photodiodes. Correlation measurements could be made to show that photons emitted by the signal k_s and idler k_i states are intensity-correlated (one photon is emitted in the idler state means that one photon is emitted simultaneously in the signal state) [Karr et al., 2004]. But as no exponential behavior is observed before saturation, we can deduce the absence of stimulation and of parametric oscillation, thus we do not expect any phase relation between signal and idler photons.

Threshold comparison

We saw in section 5.3.1 that the parametric oscillation density threshold depends on the spectral linewidths of the polariton states. In order to try to figure out why we did not observe any parametric scattering in this sample, let us compare the linewidths in various experiments: in the case of our sample (1.), the sample of Stevenson et al. [2000] (2.) and the sample of Kundermann et al. [2003] (3.). Let us assume that $\gamma_0 \simeq \gamma_{k_p} \simeq \gamma_{2k_p}$. The linewidths are:

1. $\simeq 350\mu eV$
2. $\simeq 750\mu eV$ with three quantum wells and a Rabi splitting of $\simeq 6meV$
3. $\simeq 100\mu eV$ with exactly the same structure and Rabi splitting than ours.

As we are not able to determine precisely the proportionality factor of equation 5.2, we can assume that it is of the same order for similar structures,

but for the case (2.), as the number of quantum wells is multiplied by 3, the apparent saturation density is increased by a factor equal to this number of quantum wells, as excitons in the various quantum wells do not interact, while the parametric oscillation threshold scales like the linewidth.

One can see that in case (2.) the threshold is twice higher than ours, but the saturation density 3 times higher, so the threshold in term of excitation power is twice lower. As for the case (3.), the threshold excitation power should be in our case a little more than 3 times higher. These differences are apparently significant enough to let a breaking of the strong-coupling appear before the parametric oscillation threshold, but after the parametric luminescence threshold.

5.3.4 Parametric processes in a $9\mu m$ mesa

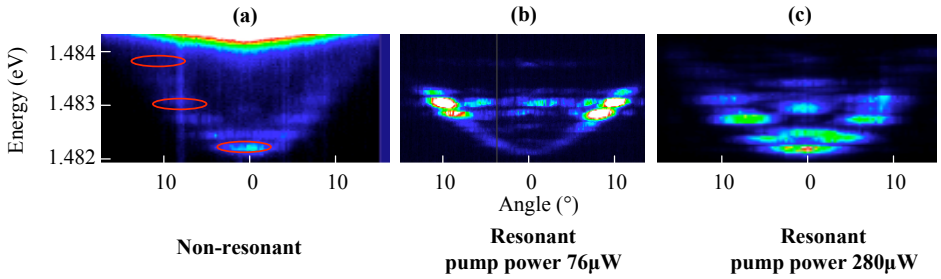

Figure 5.15: (a) Dispersion in photoluminescence under non-resonant excitation of the $9\mu m$-diameter mesa lower polariton at zero detuning, the white signal at high energy is the 2D lower polariton (at the exciton's energy). The pump state and its potential signal below (respectively idler above) are circled in red. (b) Resonant pumping with a spectrally broad laser. (c) Emission at the nonlinear threshold. Mentioned pump powers correspond to the experiment shown on Fig.5.16

We performed the same kind of experiment on 0D polaritons, in a first step we will show the results for a $9\mu m$-diameter mesa, as shown in the precedent chapter, these mesas show a quantized quasi dispersion, the mesa presented in this section has a dispersion as shown on Fig.5.15(a). The ground state is at slightly negative detuning $\delta_{0D} \simeq -0.25meV$.

The excitation conditions are as described for the 2D-polaritons, the energy linewidth of the pump laser allows here again to be independent from the possible shift of the pumped levels, as can be seen on Fig.5.15(b), the excitation angle is $\simeq 10°$, and the central energy of the laser pulse is $1483.3meV$. One can see on the reciprocal space images (taken in PL while pumping non-resonantly) that the confined states have lobes depending on

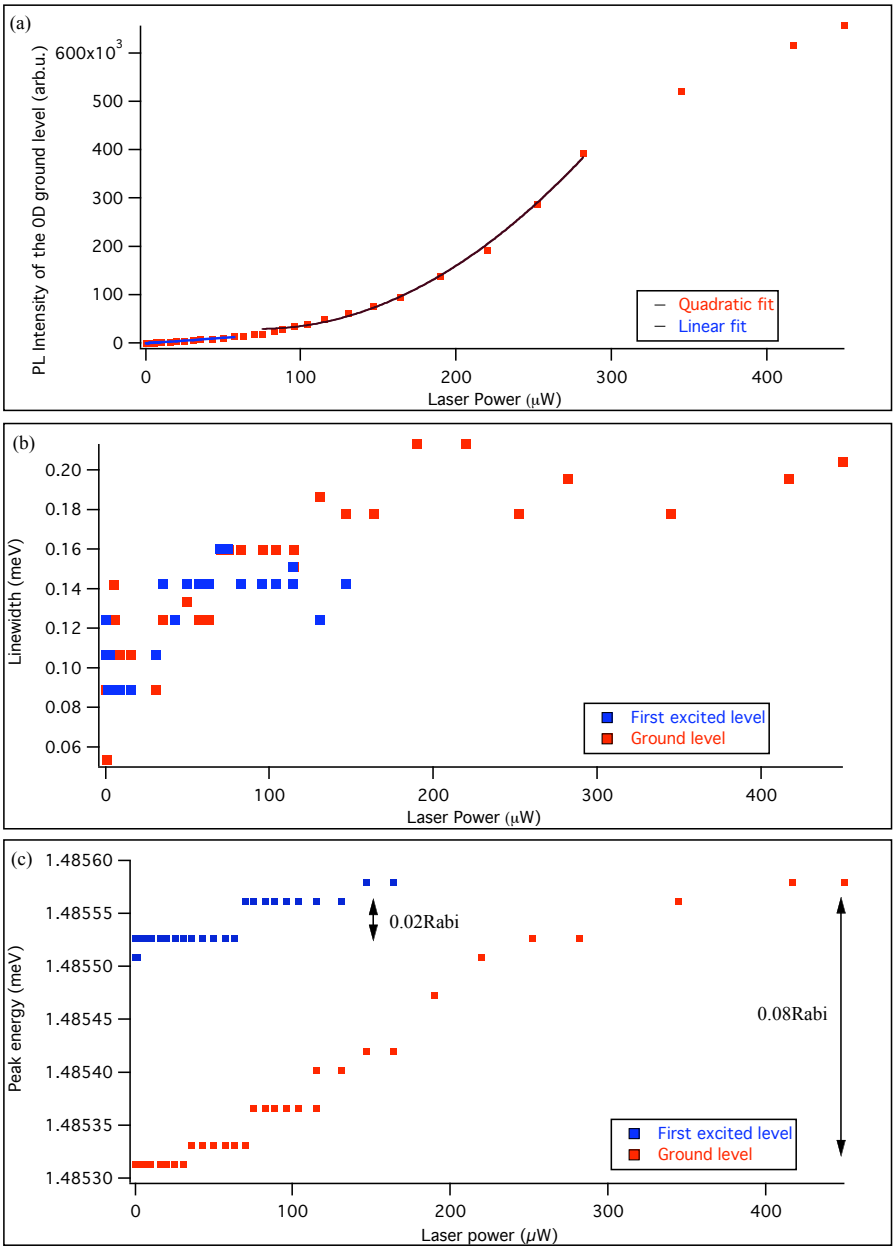

Figure 5.16: (a) PL intensity of the lower polariton ground confined level as a function of the laser power. (b) Linewidth of the lower polariton ground confined level (red squares), and first excited level (blue squares). (c) Energy shift of the lower polariton ground confined level (red squares), and first excited level (blue squares), the ratio of the largest shift over the Rabi splitting is given.

the angle of detection[4], so at the angle which was chosen to populate the system shown on Fig.5.15, corresponds to a lobe. The energy chosen shows a signal-idler couple of states fulfilling the energy conservation with a precision better than the linewidth: $E_{idler} - E_{pump} = 0.87meV$ and $E_{pump} - E_{signal} = 0.90meV$, where the signal state is the LP ground confined state. These values are smaller than the linewidth of the confined photon: $0.90 - 0.87 = 0.03meV < 0.1meV \simeq \gamma_{0D}$, and thus of the confined polariton.

Results

Results obtained are shown on Fig.5.16, as in the 2D case, three regimes are distinguishable: linear, quadratic and linear again. We integrated the whole angular extension of the 0D ground state, the signal shown on Fig.5.16(a) is thus directly proportional to the whole population of this state. A quadratic fit describes well the evolution between 60 and $260\mu W$. We were easily able to trace the evolution of the linewidth and energy of this state on Fig.5.16(b) and (c), there is indeed a small increase of the linewidth due to density effects. There is also for the same reason a slight blueshift of the resonance energy.

The quadratic regime can be attributed to parametric luminescence (polariton polariton scattering), as in the precedent case, the following linear regime can be attributed to a saturation in population, it may also be due to a loss of the strong-coupling regime, but as there is no significant blueshift, it is not possible to conclude with certainty. We will discuss further this issue at the end of this chapter.

5.3.5 Continuous wave pumping of a $9\mu m$ mesa

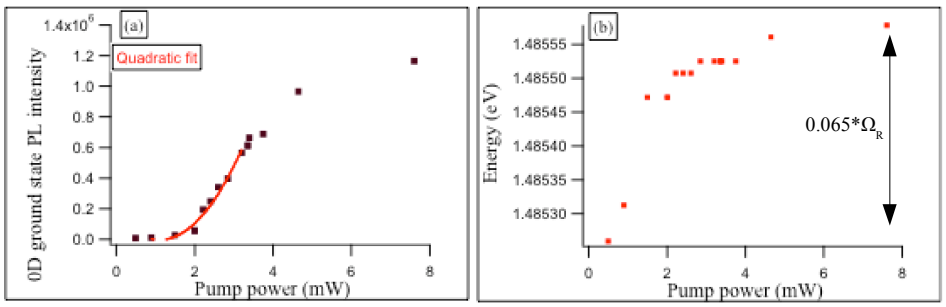

Figure 5.17: PL intensity (a) and energy (b) of the LP ground mode of a $9\mu m$ mesa, as a function of the pump power, under continuous wave resonant pumping.

[4]These lobes correspond to the quantum number m.

For sake of comparison, we performed the same kind of experiment under resonant continuous pumping, tuning the laser's energy at every pump power, in order to keep it resonant with the blueshifted pumped polariton state. As seen on Fig.5.17, we observed similar behaviors than in pulsed pumping, with 3 successive regimes: linear, quadratic and then linear again, and a very small shift of the resonance.

Thresholds

The nonlinear threshold appears at a pump density of $150 W/cm^2$. This threshold value allows us to calculate the number of polaritons created in the pump state through a method inspired from ref. [Senellart et al., 2000]. The first step is to calculate, from the pump density above, which power is reaching the mesa, with its $9\mu m$ in diameter, from a $40\mu m$ spot. The second step is, in reciprocal space, to take into account the fact that we are not in presence of a continuous dispersion curve. As one can see on Fig.5.15, the pumped state (fourth energy level, starting from the lowest) has a certain angular width. We saw in chapter 4 that at a given energy, the degeneracy can not be easily evaluated. We will therefore consider that the quantized character of the energy dependence ensures us that we are populating one state having a ring angular profile. Nevertheless the state is not homogeneously excited on all its angular extension. The laser excites a localized zone within this ring, we calculated this zone to represent around 11.5% of this zone in surface. This yields the following expression:

$$N_{pump} = \frac{P_{laser}\tau_{cav}}{C^2 E} * 11.5/100 \approx 1000 polaritons$$

where N is the number of polaritons in the state, P_{laser} is the laser power impinging on the mesa surface in Watt, τ_{cav} is the cavity photon lifetime, C is the Hopfield coefficient and E is the energy of the state in Joule. With $\tau_{cav} = 10ps \pm 5\%$ and $C^2 = 1/2 \pm 20\%$. One should also to take into account a coupling factor between the external laser field and the cavity internal electromagnetic field, this factor could diminish the effective laser power of one order of magnitude.

The final deduction reads then $50 < N < 1500$ polaritons. Thus

$$N_{polaritons\ in\ the\ pumped\ state} >> 1$$

This number should imply a saturation or nonlinear behaviors, we will see that several interpretations are possible for the pumped state behavior in section 5.3.7.

Excited states behavior

Thanks to the quantized character of the system, we were also able to study the behavior of the first excited state of the 0D lower polariton. During the

fast quadratic increase of the ground state's intensity, it becomes impossible to distinguish the first excited state from the side of the ground state. It is nevertheless clear that both studied state show a blueshift. As the density of polariton per state did in principle not go beyond one (otherwise we would have observed a stimulation effect), the blueshift shows that the confined level are sensitive to the overall density of polariton in the mesa.

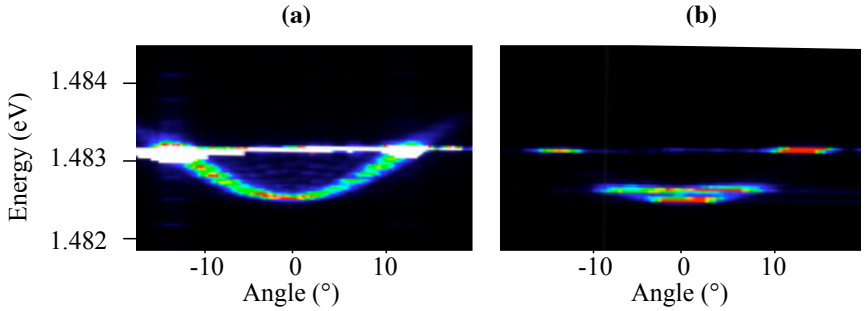

Figure 5.18: Continuous wave resonant pumping of a $9\mu m$ mesa at $1.48645eV$, corresponding to the horizontal line on both figures, but at an angle not contained in the $k-$dimension shown. (a) Linear relaxation regime, the whole lower polariton curve below the pumping energy is visible. (b) Both the ground and first excited states are in a quadratic regime.

This explains the change of regime for excited states of the mesa which we observed, although we could not plot the PL intensity as a function of the pump laser power for these excited states, because they showed high fluctuations and instabilities. It was nevertheless possible to take two interesting images of the dispersion curve, which can be seen on Fig.5.18(a) and (b). Fig.5.18(b) shows a situation where both the ground and first excited states are in a quadratic regime, this is why the first excited state's luminescence can be seen and is not hidden by the ground state's luminescence.

This situation is consistent with the observations reported in section 5.2.3 where, as the system is non-resonantly pumped, the ground LP confined level and the first excited level show several regimes.

5.3.6 Resonant excitation of a $3\mu m$ mesa at zero detuning

Similar studies were performed on the $3\mu m$ mesa studied in chapter 4, its spectrum is shown on Fig.4.5(a). In the case shown here the excitation laser was a continuous wave laser, the excitation was done in reflection. As there are only three 0D confined lower polariton levels, we simply chose to excite the middle one (so the first excited level), with a broad angular aperture of 30°.

The energy difference between the pumped mode (first excited) and the ground mode (respectively the second excited) is $0.79meV$ (respectively

$0.89meV$). The energy matching is fulfilled with a precision approximately twice smaller than the polariton linewidth. We did not do any angular selection in the excitation, as there is a wide $k-$space delocalisation of the energy. The resulting behavior is shown on Fig.5.19, it is qualitatively similar to what was observed for the ground state of the $9\mu m$ mesa studied above.

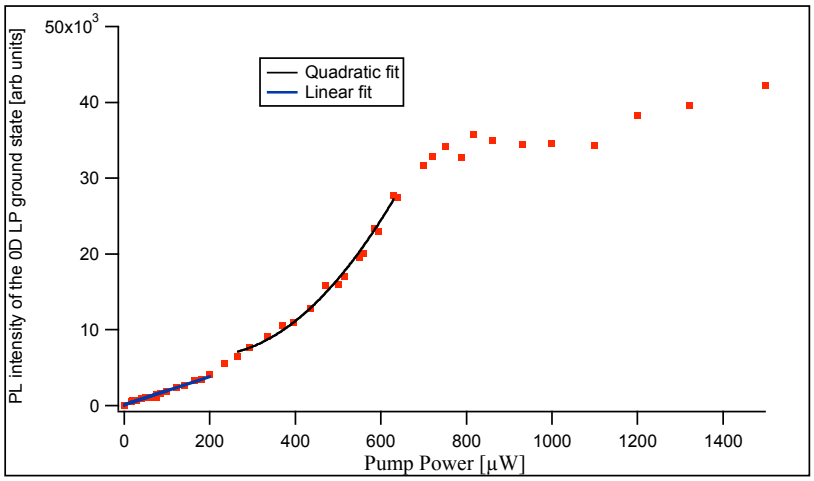

Figure 5.19: PL intensity of the lower polariton ground confined level as a function of the laser power. A quadratic and a linear fit are shown.

5.3.7 Alternative points of view: signs of bistability?

One can see that the behavior of the ground state of the system as a function of the pump power is fairly reproducible in the mesas, as can be seen on Figs. 5.19, 5.17 and 5.16. It consists of a linear behavior followed by a quadratic one, and then linear again. Although we gave an explanation to the various regimes we observed, we did not expect to see a linear regime before any parametric oscillation behavior.

The fundamental reason may be related to the phase and energy-matching conditions required to observe parametric conversion behaviors. We saw that energy-matching conditions were always fairly fulfilled, but in a confined quantized level a small mismatch is unavoidable. One possibility, to try to improve these conditions fulfillment, is to tune temperature, but the strong-coupling regime can not be guarantied any more after $30K$ because of the broadening of the exciton resonance. Rapid power studies at temperatures till $30K$ did not show any qualitatively different behavior. On the other hand, phase-matching conditions consist here in conditions on the conservation of the azimuthal m quantum number. It is however difficult to determine with certainty whether these conditions are fulfilled or not. We saw in chapter 4 that we probably excite a superposition of modes, and can only suppose (and hope!) that the suitable quantum number combination is excited through this superposition.

We tried to adopt another point of view for the description of the collision phenomena observed: we were able to fit the peculiar shapes of the ground state intensity evolution by cubic polynomial expressions, by inverting the two axes of the plotted graphs. Fig.5.20 shows again the evolution of the emitted PL intensity of the ground state for a $9\mu m$ mesa in two cases studied in this chapter, but with another point of view: the pump power is plotted as a function of the emitted PL intensity. A cubic fit was done and fits very well the measurements.

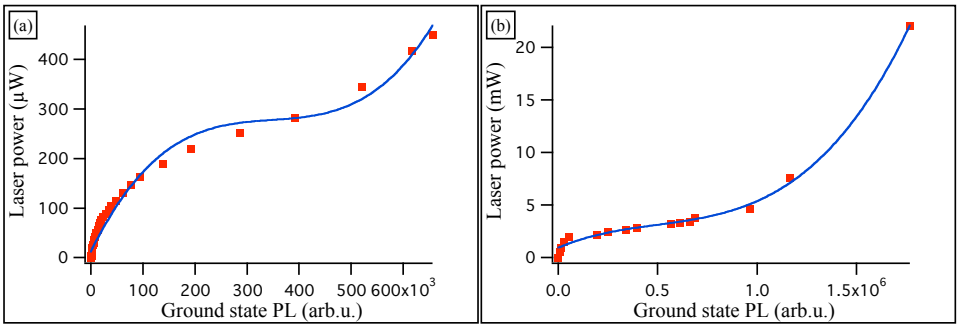

Figure 5.20: Cubic fit of the pump power as a function of the ground state PL intensity for the case of (a)Fig. 5.16 and (b) 5.17. The fits are performed on the whole range of points taken.

This dependence is characteristic of bistable phenomena: for a given value of one of the fit parameters, a cubic dependence can show a hysteresis cycle, characteristic of bistable phenomena. Two different phenomena can be concerned here:

Degenerate scattering

This dependence can be characteristic of a degenerate parametric oscillator, meaning that the polaritons scatter within a single state. The population of the considered state evolves in this case as follows, as demonstrated through a mean-field theory by A. Baas and his colleagues in ref. [Baas et al., 2004], and as detailed in his thesis [Baas, 2003]:

$$n_p(\gamma_p^2 + (\delta_p + \alpha_p n_p)^2) = 2\gamma_m C_0^2 I^{in} \tag{5.3}$$

Where n_p is the mean number of polaritons in the considered state, $\gamma_p = C_0^2\gamma_C + X_0^2\gamma_X$ is the linewidth of the polariton branch, δ_p is the detuning of the laser with respect to the pumped polariton energy, and γ_m is the dissipation coefficient coefficient of the mirror through which the system is being pumped, this coefficient needs to be taken into account as the laser is not necessarily resonant. For certain values of δ_p, equation 5.3 shows a hysteresis characteristic of a bistability behavior which was observed in the references mentioned ([Baas et al., 2004] and [Baas, 2003]) of the emitted PL intensity versus the pump power (*i.e.* the mean number of polaritons n_p).

We tried to perform new series of measurements varying exclusively one parameter: the pump power of a continuous wave laser. This experiment is similar to the one shown in section 5.3.5 but *we did not tune the laser's energy or any other parameter*, trying to fix the parameter δ_p. The result of this experiment is shown on Fig.5.21 in two configurations: on the first graph we performed the usual quadratic and linear fits, on the second graph we draw, as opposed to usual, the pump power as a function of the ground level population, this shows a clear cubic dependence. However, we did not observe any hysteresis or instability behavior. The variation of the various parameters were always smooth. We tried to impose $\delta_p > 0$, a situation which should show hysteresis, but were never able to observe any hysteresis nor to find the corresponding value in the fitting parameters.

This interpretation would mean that polaritons scatter coherently within the pumped state (where energy and phase-matching conditions are obviously fulfilled) yielding a nonlinear dependence of the polariton field with I^{in}. Polaritons then relax linearly through phonons towards the ground state. The evolution of the ground state population is thus representative of the evolution of the pumped state population.

This point of view suggests that we are in presence of a degenerate parametric oscillator in the pumped state. But this phenomenon, for positive

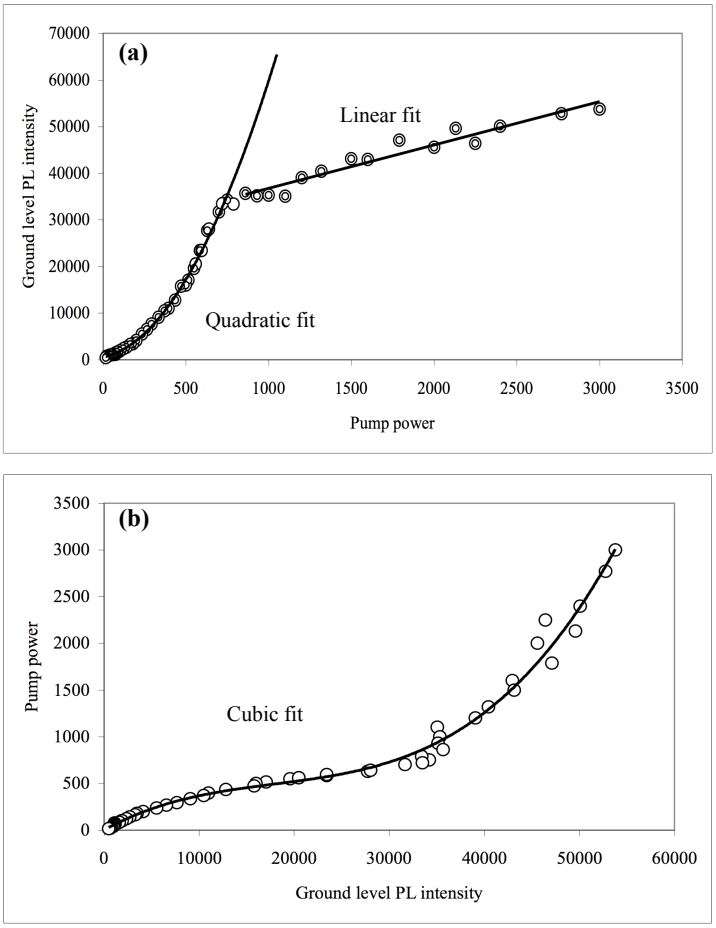

Figure 5.21: Evolution of the ground state PL intensity of a $9\mu m$ mesa, seen in two different ways: on one graph the PL intensity is shown as a function of the pump power, in the other graph it is the pump power which is seen as a function of the PL intensity.

values of δ_p, detuning of the laser energy with respect to the pumped state energy, should show a bistable behavior. However, despite several different values of δ_p tried, we were not able to observe any bistability. Added to that, we did not manage to fit in the same way the data taken for other kinds of mesas, or for the 2D polaritons, neither to take new data which would show the same behavior. We will hence try to adopt again a different point of view.

Bleaching of the strong-coupling regime

Tredicucci et al. [1996] suggests another phenomena yielding a bistable behavior in the dependence of a polariton population with respect to a pump

intensity: the bleaching of the strong coupling regime, while exciting resonantly a polariton state. The developed model uses the experimental parameters of Norris et al. [1995] (an AlGaAs/AlAs cavity with five embedded GaAs quantum wells). This may explain the apparent absence of loss of strong-coupling, despite the high pump powers reached: the system reaches an equilibrium between

- a blueshift of the LP resonance (due to the strong-coupling bleaching) decreasing the coupling efficiency between the laser and the polariton resonance
- a redshift of the resonance back to the LP energy, when the laser is not efficiently coulped anymore, and thus does not create a high population density in the system

These two phenomena of course reach an equilibrium corresponding to the cubic dependence we observed. According to Tredicucci et al., bistability depends on a broadening factor directly related to the linewidth of the exciton resonance. If the latter is too large, no bistability is observed, but simply a cubic behavior. We could therefore not tune this parameter, as we worked on one sample showing a given linewidth.

Future samples with various exciton linewidths may help us to discriminate between the various possible phenomena which one we observed.

5.4 Balance and conclusions

We performed many different studies, sharing all a same objective: the observation of a massive redistribution of the polariton population towards a single state. A phenomenon which would lead us towards condensation in the case of non-resonant pumping, and which would open the way to parametric oscillation and amplification in the case of a resonant pumping. We did not observe any of these phenomena, most probably because the nonlinear thresholds were too high, compared to the strong-to-weak coupling threshold. A solution to overcome this effect would be to increase the number of quantum wells within the cavity, as we will see in chapter 7. This could yield an increase of the strong-to-weak-coupling transition without affecting the nonlinear threshold.

5.4.1 Balance of the observed phenomena

Let us recall and classify the diverse and rich phenomenology

1. Non-resonant excitation:

   Phonons and collisions In any configuration we tried (size of the mesa or detuning), we observed a relaxation towards the ground

state of the system through phonons at low densities and then collisions, characterized by a quadratic dependence of the PL with respect to the pump power.

Loss of the strong-coupling regime During the quadratic regime, we systematically observe a loss of the strong-coupling regime.

VCSEL This loss of strong-coupling is followed by a lasing regime characteristic of VCSEL.

2. Resonant excitation:

Nonlinearities We observed nonlinear behaviors (a quadratic increase of the PL as a function of the pump) of the confined lower polariton, for any size of confinement.

Saturation This nonlinearity is followed by a linear behavior in the case of 3 and $9\mu m$ mesas.

Bistability? We were able to fit the behavior of the pumped state of the 9μ mesa with a cubic fit. This kind of dependence can show hysteresis for certain values of the fitting parameter. This hysteresis is a sign of optical bistability, either through a process of degenerate scattering in the pumped state, either through bleaching of the strong-coupling regime and loss of resonance with the laser. We did not observe this, probably because of the impossibility to play on the suitable fitting parameter.

3. Interactions

Trapping mechanism We nevertheless could improve the understanding of the trapping mechanism: our observations of sections 5.2.3 indeed tend to prove that the 2D and 0D polaritons share the same reservoir.

Effective density We confirmed in section 5.3.5 that the confined levels are sensitive to the overall density of polaritons, although they do not necessarily feel the same effective density, depending on spatial overlaps of the wave functions.

5.4.2 Conclusion

It is the first time that these nonlinear phenomena are observed with confined 0D polaritons in a doubtless strong-coupling regime. In the precedent cases, it was not possible to observe directly the strong-coupling regime: either due to the temperature increase [Bajoni et al., 2007], yielding an increase of the linewidths; or due to the impossibility to measure the upper polariton [Dasbach et al., 2001].

The observations under resonant non-excitation are now well understood: the interplay between zero and two dimensional polaritons is promising for further relaxation studies.

Further studies would need to be done in order to discriminate between the various interpretations we propose. Whatever the right interpretation proves to be, we already have clearly proven the occurence of nonlinear phenomena, and the potentiality to observe bistability phenomena.

This varied phenomenology is promising under resonant excitation both for applied (Fast switching using microcavities [Tredicucci et al., 1996], single photon emitters see [Deveaud-Plédran et al., 2006] and references therein) and fundamental (Study of optical bistabilities, of photon and polariton blockade, of ultralow threshold lasers [Baas et al., 2004, Imamoglu et al., 1996, Verger et al., 2006]) physics.

Part III

Perspectives and discussions

Chapter 6

Applications

We propose in this section some potential applications based on the structure introduced and developed in this thesis, we will discuss their feasibility and use.

Based on this work, two patents were deposited, the first one about a polariton single photon source [Deveaud-Plédran et al., 2006], which theoretical description was developed in a paper by Verger et al. (C. Ciuti, coauthor of this paper, is coauthor of the patent), the second about a polariton twin photon source [Daïf et al., 2006a], based on the idea of parametric scattering in a confined polariton system[1].

We will first describe rapidly the principles of these two patents, as they may be potential starting points to applications based on the structure described in this work. We will then discuss their feasibility and more in general the proximity of applications based on microcavity polaritons, according to the state of the art described all along this work, and in the references we could reach.

6.1 Polariton single photon source

Single photon sources are potentially important devices for quantum communications. Presently, the realization of single photon sources is based on the attenuation of a laser beam, down to the level where the photons may be statistically separated with a good probability. A wide range of improved single photon sources has been proposed, mostly based on the use of the emission of a single quantum dot. The prominent publications in this field being the realization of an electrically driven single photon source [Yuan et al., 2002, Park et al., 2004]. Such sources offer the strong advantage of compactness, with the drawback of poor collection efficiency and a repetition rate limited by the lifetime of the carrier pairs in the dot to about 100

[1] For more details the reader can refer to ref. [Verger et al., 2006] and references therein, and we recall that chapter 5 deals with issue.

MHz.

A device based on 0D polaritons could constitute a very efficient single photon source with a very high repetition rate. The collection efficiency may in principle be made very close to 100% by proper tailoring of the parameters of the device, and the repetition rate may be improved by at least a factor of 100 to reach 10 GHz.

6.1.1 Principle

Given a 0D polariton trap as presented in this work, simple calculations based on the exciton nonlinear interactions show that when two polaritons are present in the trap, the renormalized single-polariton energy is blue shifted by an amount comparable or even larger than its linewidth, provided that the trap size is smaller than a critical value [Imamoglu et al., 1996, Verger et al., 2006]. For typical GaAs-like parameters, a blue shift of the order of $100\mu eV$ is computed for a trap lateral size of the order of one micron [Verger et al., 2006]. Hence, the dynamics of a polariton trap with a size around or below 1 micron becomes strongly nonlinear already at the single polariton level, which explains in simple terms why the light emission out of the polariton traps can be highly non-classical. In fact, the absorption of a nearly resonant laser beam, with a frequency slightly red shifted with respect to the polariton ground mode (or resonant with it) is quantum blocked when the excited number of trapped polaritons exceeds one. This is analog to the photon blockade effect predicted for optical cavities containing atoms [Imamoglu et al., 1996]. The experimental set-up necessary to produce such signal is sketched on Fig.6.1. In order to demonstrate the single photon nature of the emitted signal, one should add a second-order correlation measurement set-up at the detection.

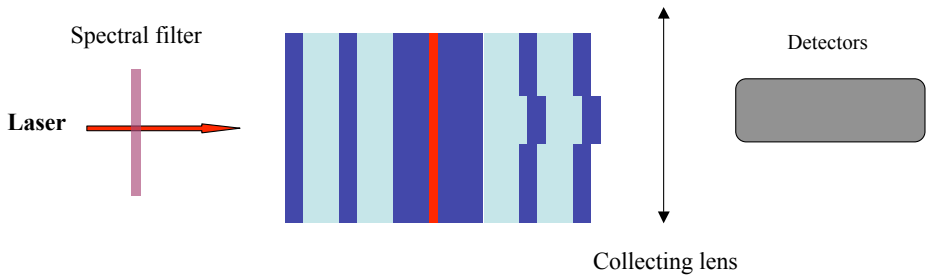

Figure 6.1: Principle of the experimental set-up to be used to create single-photons on-demand.

6.1.2 Potential advantages

If the pump intensity is low enough, only one polariton can be excited in the polariton trap. The polariton will then escape the trap within the radiative time (around 10 ps) before another polariton can be re-injected inside the trap. Excitation by a pulsed laser with a spectral width comparable or smaller than the polariton linewidth will lead to the emission of single-photon pulses on demand out of the polariton traps. The repetition period, being limited only by the pulse duration, will be of the order of a few tens of picoseconds, i.e. a repetition rate more than 2 orders of magnitude higher than in electronic quantum dot single-photon emitters. Moreover, unlike self-assembled electronic quantum dots, the spatial position of polariton traps can be fully controlled by the lithography (see chapter 2), paving the way to the realization of integrated arrays of single-photon emitters whose excitation and detection can be efficiently obtained through the use of optical fibers.

6.2 Twin photon source in the near infrared

6.2.1 Existing devices and principle

A twin photon source presents two optical outputs in which the photons are strongly correlated. If one photon is emitted through one of the two outputs, there is necessarily one corresponding photon at the other output. This type of source is very interesting from a fundamental point of view, as it is based on one of the main concepts of quantum mechanics: entanglement. From an applied point of view, it is for example often used in quantum cryptography experiments or in quantum information protocols.

The twin sources usually used are optical parametric oscillators (OPO), which present very strong quantum correlations between the photons of the two outputs. They use parametric scattering to produce the quantum correlated emission.

A similar device was developed using parametric oscillation with a very low pump intensity threshold, in a similar but original structure, though not based on strong coupling: a triple cavity with embedded quantum wells [Diederichs and Tignon, 2005]. The peculiar shape of the dispersion of the triple cavity allows to observe the pump, signal and idler states with similar intensities [Diederichs et al., 2006].

6.2.2 Feasibility with 0D polaritons: use of polariton parametric scattering

The demonstration of polariton parametric oscillation in semiconductors has been followed by many proposals for the measurement of quantum correlations between signal and idler modes. But they all come up against the same

problem, which is that signal and idler polariton modes have very different photonic components. This yields signal and idler radiative emissions that are strongly detuned in intensity. In our case the signal and idler modes will have similar photonic components, with a precision better than a few percents, the corresponding emissions thus will have almost the same intensity. A polariton trap can present a lot of discrete levels, therefore offering in the same sample several sets of three levels for the parametric oscillation. Once the set chosen, the energy splitting between the three levels can be tuned in the same sample, simply by changing the position of the excitation spot on the sample in order to modify the exciton-cavity detuning.

The semiconductor device would present several advantages compared to an OPO: The structure is monolithic, the cavity doesn't need to be aligned and the cavity thickness doesn't need to be electronically controlled.

6.2.3 Advantages of 0D polaritons

It is possible to realize this in a semiconductor microcavity in strong coupling regime similar to the sample presented in this work. These zero dimensional polaritons can show several accessible levels, which positions depend on the lateral size and depth of the trap. As we saw in chapter 2, a suitable calibration allows to conceive a trap with precise depth and width. We studied in chapters 3 and 4, the relation between the dimensions of the traps and the number and spectral profile (in real and reciprocal spaces) of the confined states. We are now able to design a sample where three levels are positioned in such a way that one is equally spectrally separated from the two others. This level will be the pump mode, and the two others the signal and idler modes, for the parametric oscillation.

The experiment can be done in the continuous wave regime, producing in this case quantum correlated beams, which entanglement can be evidenced by noise measurements [Karr et al., 2004] on the beam. This configuration could be useful for protocols of quantum information with continuous variables. It can also work in pulsed regime and produce few signal-idler pairs per pulse. As the polariton modes have the same photonic component, the signal and idler emission have the same intensity and can be both attenuated in the same way without losing the correlation in order to have single pairs.

Two different configurations have to be considered, depending on the polarization of the pump. For a circularly polarized pump, the parametric effect, that conserves the spin, will produce signal and idler pairs polarized as the pump. This yields entanglement in intensity. For a linearly polarized pump, signal and idler pairs will be totally unpolarized and the entanglement will be in polarization. It can be detected as represented on Fig.6.2[2].

[2]Courtesy of Augustin Baas.

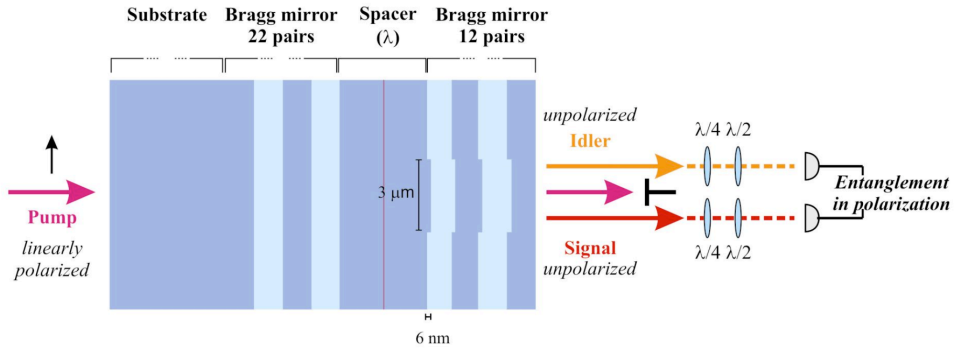

Figure 6.2: Principle of the twin photon source.

This idea of using confined polaritons having similar photonic components is the basis of ref. [Bajoni et al., 2007] we mentioned in chapter 5.3.

6.3 Feasibility

At the moment, given the experimental conditions under which the presented structures show the suitable properties, it is not realistic to think about industrial applications for the two ideas developed above. Nevertheless, the realization of these devices at low operating temperatures is feasible in the near future. As we will see in the next chapter, it depends strongly on the reliability of the samples' source (so the MBE). As one understands intuitively, a reliable source of samples is necessary in order to fabricate original structures. This aspect is being worked on by François Morier-Genoud, Gaël Nardin, and Taofiq Paraïso.

These devices could be used for various kinds of research, as a reliable single photon or correlated photon source. The latter is indeed needed for quantum communication and cryptography experiments, as well as a reliable correlated photon source[3].

This potential opening is a concrete application for these proposals, as it is for the structure developed by Diederichs et al. [2006]. We would tend to propose that, as the mentioned researches are so far performed in an overwhelming majority by public laboratories, the application can not be called industrial. This kind of knowledge is being published in open scientific journals, and these proposals could also be published, in a near future, as an ensemble of useful proposals for experimentalists.

[3]The interested reader can have a look at the work performed in the group of applied optics (GAP) of the University of Geneva, cf. http://www.unige.ch/gap/welcome.html

6.3.1 Global warming!

Are industrial applications based on polaritons, and further on polariton BEC, realistic? Several steps are now further needed for thinking about industrial applications: the ease of high-quality sample production, and the on-demand production of room temperature strong-coupling under electrical injection, followed by room-temperature BEC.

The strong-coupling at room temperature seems to be now established in nitride based materials [Christmann et al., 2006], although the ratio Ω/γ (which is an indicator of the coupling strength) needs to be improved. Several groups are working on strong-coupling under electrical injection. A very recent paper [Hofmann et al., 2007] reports the observation of a suitable excitonic emission in an InGaAs quantum well, that should allow strong-coupling to be observed under electrical injection for the first time.

Finally BEC was observed, but within a sample which is in principle reproducible, as the parameters of its growth were carefully chosen, but which at the moment no group is able to reproduce.

The convergence of these various parameters (quality, room-remperature, electrical injection, ease...) is necessary in order to think about further applications. So industrial considerations are not surrealistic, it is simply a bit early.

Chapter 7

Experimental perspectives

Now that we have discussed long-term perspectives, let us finish this work by discussing short term perspectives that our successors are already leading or that could be the near future.

We will first have a look at what could be done on the present sample, in order to further understand relaxation mechanisms towards the trapped states. We will then see how we could fabricate a new sample, through different techniques. We will then see what interesting experiments could be done with condensed phases, obtained either through spontaneous condensation or through parametric scattering. Indeed we designed a new mask, with new trap shapes, which could allow a wide variety of experiments in the condensed regime, but also with a non-condensed fluid of polaritons.

7.1 Perspectives on this sample

We present in this work the achievement of a polariton trapping structure, on which we performed a large number of time-integrated studies. Several axes can be taken for the future work on this first achieved sample. The first and most original one, compared to what was done so far, is to add a time-resolution to the set-up[1], another interesting axis would be to try to complete the imaging experiments presented in chapter 4, and finally to understand definitely the nonlinear behaviors observed in chapter 5, section 5.3.

[1]Taofiq Paraïso and Gaël Nardin (who are taking over with the confined polaritons project) and Sébastien Beaumont (who did a diploma work –master's- with us), are performing, among others, time-resolved experiments.

7.1.1 Time-resolved studies

Spectrally and time-resolved studies

First time-resolved images were already taken with spectral filtering. We will not enter into the details of the set-up and of the streak-camera principle, the most important for us is to know what kind of images were taken: the streak-camera is placed after the spectrometer, takes from the latter a spectrally dispersed image of a real space line (E, x) and, disperses energy in time at a given position, usually chosen to be the center of a mesa. One can see the principle[2] applied to a $9\mu m$ mesa on Fig.7.1.

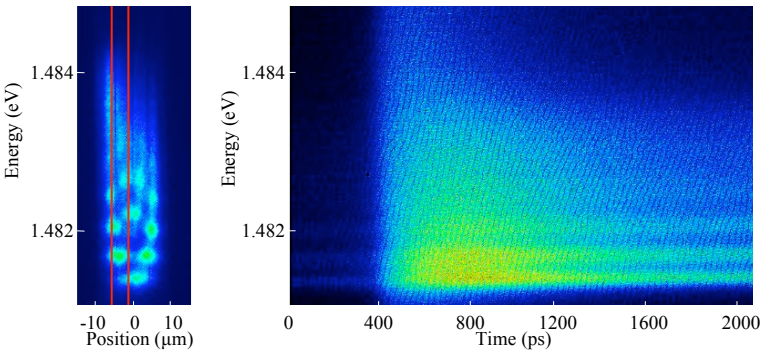

Figure 7.1: Principle of the streak camera applied to a 0D polariton signal: time dispersion of one band at a given position of the (E, x) space.

The preliminary results tend to confirm the interaction between 2D and 0D polaritons, through different relaxation times. They also clearly show several relaxation times depending on the relaxation mean: through polariton scattering or phonons.

Next step: spectrally and spatially resolved time-resolved studies

In order to deepen the study, it will be interesting to see, at a given energy, the behavior along a whole spatial line. Figure 7.2 shows an example of a line which could be selected and then dispersed in time. One could select successively lines at relevant energies, including the 2D lower polariton energy, and reconstruct a 3D image (E, x, t).

Some work about the propagation of polaritons was performed by Sermage et al. [2001], they demonstrated that polaritons propagate in the wedge's direction, and that this propagation depends on the detuning. We will thus be able to excite selectively the 2D states at a given distance from the mesa, and observe the trapping.

[2] I thank Sébastien Beaumont for the figures, see appendix C.1 for details on his diploma work about these issues.

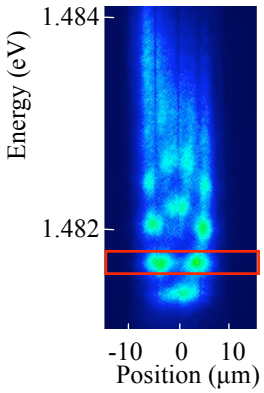

Figure 7.2: Selection of a line at a given energy.

7.1.2 Complete imaging of the confined modes

Following the observations presented in the last part of chapter 4, one could perform complementary images in order to check the interpretations proposed. We already mentioned the possibility of turning the incidence angle of the laser on a given solid angle, in order to check the combination of states resonantly excited.

One can also imagine performing a whole set of images, exciting resonantly successively each energy level, in order to reconstruct the whole confined modes' profile.

Finally, an interesting experiment will be to compare images taken in the low density linear regime, to images taken in the nonlinear regime, in order to see the behavior of the modes' profile in the real and reciprocal spaces.

7.1.3 Further nonlinear studies

We saw that the various confined states show blueshifts of their peak energy, and feel the overall density of polaritons (or excitations) created. We however can not quantify the influence of this effect for each state.

Thus, when experiments are performed under resonant excitation, it is likely that the excited state shows a more important shift than the confined LP ground state. This can be checked by following the shift of the excited state's energy, while measuring the transmitted laser signal along the increase of its power. It could give clues about the strong-coupling loss.

7.2 The next generation of samples

In order to favor relaxation towards the ground state of the mesas, and a lowering of the parametric thresholds, we intend to build new samples

with new structures. We will se in this section some proposals, and then various possibilities ideas to improve fabrication method, radical changes with respect to what we presented in chapter 2.

7.2.1 A new sample structure

In order to lower the thresholds and improve the strong-coupling in the sample, several possibilities exist: increasing the number of quantum wells, or improving the linewidths.

The number of quantum wells Let me cite Maxime in his Ph.D. thesis [Richard, 2004], with whom I agree on this point[3]:

> The scientific community agrees on the fact that the difficulty to obtain a polariton condensate in GaAs microcavities, holds on the too weak saturation density of the excitons. The stimulation threshold is indeed too much in the vicinity of this saturation density. There is however still hope to obtain a stimulation regime under non-resonant excitation with GaAs microcavities: [...]through the increase of the wells' number in order to lower this density [...]

We are thus working on multiple well structures. In order for them to be efficient, the wells must be placed at an antinode of the electromagnetic field so that they couple with the cavity mode.

Improving the linewidths Another important track is to work on the linewidths, indeed we saw in chapter 5.3 that nonlinear parametric thresholds depend on the polariton linewidth, the latter depending on the exciton and cavity photon linewidths. In case of a non-resonant excitation, there is no theoretical description of the dependence of the thresholds on the linewidths, but one can intuitively imagine that the lower the losses are, the lower the thresholds will be.

We performed and are still performing many kinds of tests on these two parameters, an overview of these tests is given in students' works mentioned in appendix C.2.

[3]The original citation reads: La communauté scientifique s'accorde aujourd'hui à reconnaître que la difficulté à obtenir un condensat de polariton dans les microcavités GaAs, réside dans la trop faible densité de saturation de l'exciton dans ce matériau. Le seuil de déclenchement des effets de stimulation se trouve en effet trop proche de la densité de saturation. Il reste cependant quelques espoirs d'obtenir le régime de stimulation en excitation non-résonante avec les microcavités GaAs : outre la possibilité de multiplier le nombre de puits afin de faire baisser la densité de saturation apparente, une solution consiste à doper les puits quantiques avec des porteurs libres afin de fournir aux polaritons un canal de relaxation vers l'état fondamental par collision polariton-électron (ou trou).

7.2.2 Improving fabrication methods

We proposed at the end of chapter 2 several improvements to the method we chose to fabricate our sample. Let us now see completely new methods which could be used for the various steps of the fabrication, and their potential advantages, with respect to the present one.

Regrowth after GaAs evaporation

It is possible to consider performing a regrowth after the etching of the mesas above the semi-cavity, without having cleaned the surface[4], through GaAs evaporation. Two layers must be grown above the GaAs spacer: one layer of AlAs and above it one layer of GaAs. As gallium arsenide evaporates at a lower temperature than aluminium arsenide, it is possible to heat the sample, inside the MBE growth chamber, and to evaporate the upper GaAs layer without influencing the AlAs layer. The sample's surface would be then composed entirely of highly smooth AlAs. And as we saw a small number of AlAs monolayers influences in a negligible way the cavity mode.

Wafer bonding

Another possibility is to try to completely avoid regrowth. For this one can think about wafer bonding. This technique consists in the bonding of two wafers of similar lattice parameters. A simple heating of the surfaces in contact will favor the creation of chemical bonds between the surface atoms. This needs of course atomically clean surfaces. Some tests are being performed, according to the sate of the art for GaAs based materials, the latter can be found for example in [Faure, 2006].

7.3 New trap shapes: from simple confinement to condensate interference

7.3.1 A new mask

The work presented here shows that trapping of polaritons in the 0D structure is effective in the simple circular wells, thus no trick is needed to accompany the polaritons towards the bottom of the trap. Given this ease of trapping and the orders of magnitudes of sizes needed (widths of some microns), we designed a new mask where a various range of phenomena could be observed. We will give a rapid overview of the traps shapes designed and of the planned study.

[4]One important point to take into account is that we do not have access anymore to an MBE showing *in situ* hydrogen cleaning, so this point has anyway to be overcome.

Simple structures

As we confirmed the possibility of trapping on the micron range, we designed circular (resp. squared) traps with a wider range of sizes: diameters (resp. sides) ranging from $0.5\mu m$ to $5\mu m$ by steps of 0.5. The smallest sizes should allow us, for a suitable energy depth of the trap, to observe polariton quantum blockade [Verger et al., 2006]. We also designed between 10 and $50\mu m$ diameter mesas, in order to observe the whole transition from a discrete distribution of states to a 2D continuum.

Coupled structures

We then designed coupled traps: mesas of diameter small enough and with separating barriers allowing tunneling effect to occur. As the coupling between two mesas is increased with a larger length of the sides facing each other, we designed squared shapes added to the usual circles. In order to favor even more the possibility of coupling, we designed rectangles of dimensions $L_x * L_y$ with $L_x >> L_y$ so that one dimension yields quantization while the other lets a continuous density of states. This allows on the one hand to increase the distance over which coupling can occur, as one can see on Fig.7.3, and to increase the number of states involved.

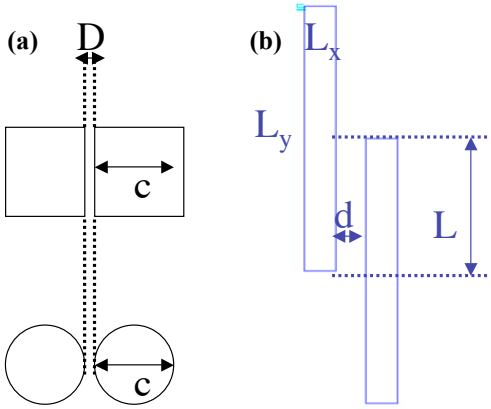

Figure 7.3: Shapes for tunneling effect. tunnel dimensions are in these ranges: $0.3\mu m < (d, D) < 1\mu m$. Confining dimensions: $0.5\mu m < c,\ L_x < 20\mu m$. Interaction dimension: $L = 1 - 5\mu m$.

Using the model of Leyronas and Combescot [2001] -rapidly explained in the first chapter (section 1.5)- and a simple evanescent wave model (one can refer for example to the book of Cohen-Tannoudji et al.), one can obtain some orders of magnitudes for trap and barrier sizes, given on Fig.7.3.

In case of the observation of a condensed phase in the coupled traps, it is possible to imagine observing Josephson effect, as was proposed for Bose-Einstein Condensates [Giovanazzi et al., 2000].

Various structures

One can imagine to create several condensates and to make them interact or even to make them scatter. We designed various kinds of shapes to be ready for any experimental funny idea... one will find a sample of these shapes on figure 7.4.

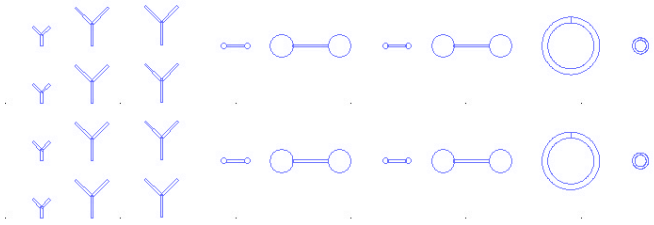

Figure 7.4: Different structures for various phenomena: interference, propagation...

7.3.2 Multiple etchings: stairway to... ?

To perform even a wider range of shapes one can imagine having various trap depth (or mesa height!). This could allow for example a control of the reservoir: one could excite in a large trap on a weakly confined level, showing a controlled surface or angular distribution, in order to observe the population relaxation in a small trap. For this, it is possible to design a suitable series of etchstops which will allow to perform the etching process twice. The only difference between these two successive etching processes is the mask used to design the shapes of the mesas to be produced by the etching: the second mask should contain the first one. Figure 7.5 shows the three main steps of such a process, which could theoretically be repeated several times.

7.3.3 Electron-beam lithography

In order to be able to design small structures, it may be necessary to have a very good lithography resolution, we saw in the conclusion of chapter 2 that this may be reached by electron beam lithography.

This technique does not require a prefabricated mask as optical lithography, the shapes to be drawn are introduced as a program included in the apparatus, this may facilitate the multiple etching through a precise location of the shapes drawn on the surface of the sample with respect to its borders.

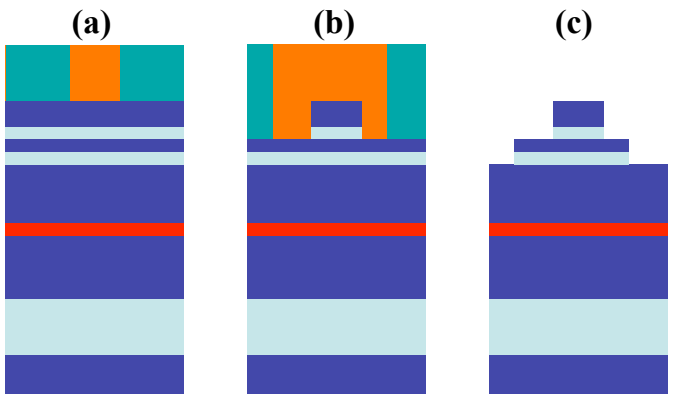

Figure 7.5: (a) A semi-cavity sample with a multiple etchstop structure above the spacer. (b) After a first chemical etching: a mesa recovered by exposed photoresist. (c) After a second chemical etching: a stairway.

7.4 And now... just do it?

Tests are being performed in order to fabricate a multiwell sample with confined states. We now have a know-how of all the techniques mentioned above, and enough tools to be confident about the techniques we still did not try. The element which proved to be the key for success in this project is a reliable sample source. François Morier-Genous is heroically working on this, and from his success and fruitful collaboration with Gaël and Tao will the ultimate sample come out!

Chapter 8

Conclusion

Let us take a look at the main aspects of this work. Its first result was the successful development of a new kind of sample, where 2D polaritons are trapped along their two free spatial dimensions, yielding 0D polaritons. We achieved successful control in each step of the fabrication process. In particular, we developed an original method of alternating between growth, characterization and simulation that proved to be very efficient and useful. It can also be applied to other means of fabrication.

We characterized these mesa structures which prove to show a cohabitation of 0D and 2D polaritons, an unprecedented situation. Nonlinear behaviors were observed by studying the response of the ground confined polariton state, under non-resonant and resonant excitation, with increasing power.

Under non-resonant excitation, we observed several regimes successively. We first measured a quadratic increase of the emission characteristic of Coulomb scattering between the excitonic part of the polaritons. We were then able to observe the transition from strong to weak coupling and then to the lasing regime, building thus an original kind of vertical cavity surface emitting laser (VCSEL).

We performed similar studies in which a given confined lower polariton state was excited at resonance. We observed again several nonlinear behaviors as a function of pump power, without any apparent loss of strong-coupling. That may be understood as parametric effects due to Coulomb interaction, or indications of bistable behaviors in the system: we developed both interpretations, without being able to discriminate unambiguously between the two. Both of them would indicate however a new kind of nonlinearity in such 0D systems.

These studies also indicated that 0D and 2D polaritons share the same reservoir, although their wave functions do not spatially extend over the same zones.

Direct imaging with different sets of spectral, spatial and momentum

resolution allowed the observation of the wave functions of confined and extended polaritons. It also permitted the observation of wave function behavior in the regimes observed. This imaging proved to be a useful tool to help understand the observed phenomena

Present work is focused on a further understanding of the open questions, in particular the nature of the observed nonlinearities. Time-resolved studies are on the way and may help choose between nonlinearities due to strong-coupling loss or to parametric effects.

The fabrication of a new sample is also under way. We tested new multiple quantum well structures while performing the work presented in this thesis, and these tests are still going on. Their aim is to favor a diminution of nonlinear thresholds, along with a rise in the threshold for the loss of strong-coupling regime, in order to allow nonlinear phenomena, whether under resonant (yielding condensation) or non resonant excitation (yielding parametric oscillations).

Along with the testing of new sample structures, we conceived and built a new mask with coupled structures patterns. Its use for the fabrication of new samples may allow the observation of parametric oscillations between confined states of twin mesas, coupled through a tunneling effect. The creation of a condensed phase in a coupled structure, whether through non-resonant pumping (yielding BEC) or resonant pumping may allow the observation of various phenomena, such as Josephson oscillations.

This work is a first step in a long-term project, which may proceed in several directions. Unfortunately we could not fulfill the aims which we assigned ourselves: we did neither observe Bose-Einstein condensation (BEC) of polaritons, nor any clear evidence of parametric oscillations. However, research takes unexpected paths and a number of new open and interesting issues are raised here, in particular through the beautiful wave function images we were able to generate, and through the nonlinear studies.

The observation of nonlinear behaviors showed that the confined polaritons are sensitive to the overall density of created polaritons. This gives hope concerning the feasibility of devices in the field of single or correlated photon emission, for research and development applications. It also opens the way to the observation of parametric oscillations between confined states of a mesa.

As one can see, we were able to produce a wide range of phenomena, from the most fundamental to the applied, in the structures that we presented. These studies, coupled with the multidimensional and high quality imaging developed in this work, should lead to fascinating observations.

Epilogue: Between applied and basic research

The reading of chapters 4 and 5 of this work shows that several studies, showing original measurements and promising results, still have open interpretations. A striking example is the issue of the interpretation of the resonant nonlinear studies, we proposed in section 5.3.7 some interpretations of the observed phenomena which compete with the interpretation chosen along the presentation of the experimental results, without being able till now to discriminate.

Several questions arise from this observation. The first question is why: is there a reason for which we did not perform further studies in order to understand scattering mechanisms? If yes, is it possible to decide whether it was justified or not? In general –and to decide whether these decisions were justified- one needs to define the kind of research performed. It is expectable for applied research not to be lead as basic research. In order to answer these questions, we will try to clarify first what were the objectives assigned to the present work, and then, given these objectives (or the absence of objectives!) to classify it.

Objectives of this research...

The LOEQ, as several laboratories working on the optical properties of semiconductors –and in particular on excitons and polaritons- has been involved in the quest for solid Bose-Einstein condensation (BEC) for many years. The project of trapping polaritons was started in this frame, with the clear objective to observe BEC of polaritons through their trapping.

It is interesting to mention at this point, that since the works of Moskalenko and Blatt in 1962 [Moskalenko, 1962, Blatt et al., 1962] who developed the theory of BEC of excitons, all the excitons' community is convinced that BEC of excitons or one of their derivatives (confined excitons, indirect excitons, polaritons) is just a matter of time. Ironically, it is a matter of time in its many meanings, as the lifetime of excitons and then polaritons was one of the theoretical obstacles to condensation, along with many others (density, temperature...).

We will not mention all the works which tried to observe this condensation, it is sufficient to mention that they were many. Lately a series of works was performed in a system of indirect excitons, which yielded many interesting publications [Butov et al., 2002, Lai et al., 2004].

A paper giving the definitive ensemble of proofs was published last year jointly by my neighbors, friends and collaborators in the LOEQ, together with the University of Grenoble, partly supported by theoreticians [Kasprzak et al., 2006]. This paper shows without any ambiguity, that the polariton phase observed shows all key elements of a condensed phase, under certain density and temperature conditions. We saw these conditions in chapter 1.4.2 at the beginning of the manuscript.

...and their influence on the daily work

The general direction of research in the labs in EPFL is given by the Professors, who systematically lead a lab. It is also the case in the LOEQ, where this work took place. As all labs, these directions being given, a huge freedom is let in the daily activities, and these directions need to be adopted by the researchers (Ph. D. students, grower and post-docs in our case) in order to be effective. This was the case: a real effort directed towards the observation of BEC of polaritons was made, and finally reached its goal, although in an unexpected way.

While studying the optical properties of the sample presented in this work, we always had in mind that we aimed at observing a BEC-type behavior. This often yielded a first negative conclusion for a series of experiments, followed later by the discussion of the details of the results, sometimes after the passing to the next series. When it became clear that we would not observe any condensation in the sample, attention was focused on the building of a new sample, so far unfortunately unsuccessfully. Optical studies could really go on only when external help (through diploma students first, and now new Ph.D. students) arrived.

We can therefore wonder if we missed any important phenomenon, while being focused on reaching this goal. It is of course difficult to say *a posteriori*, especially because the study of solid states materials has always been polluted by the unavoidable disorder, and the difficulty to distinguish original disorder from known disorder! And it may be considered coherent with the aims assigned to our research to let aside secondary results.

The various kinds of research: the eternal difficulty of classification

In order to propose a classification of the various kinds of existing researches, without entering in too deep philosophical considerations, we will quote Pierre Joliot, a French researcher in Bioenergetics. He proposes in his book

La recherche passionnément [Joliot, 2001], a classification of the various kinds of research.

The original citation is in French[1], it can be translated as follows[2]:

> The goal of *basic research*, in all areas of science without exception, is above all the advancement of knowledge. Such research [...] is only possible in an intellectually free environment. [...] The goal of *end research*, on the other hand, is to meet the specific needs of society in areas where the available conceptual basis is still insufficient. It is therefore a type of hybrid research. This offers the advancement of knowledge while at the same time remaining focused on well-defined goals. One example is cancer research [...]. End research, because it is sometimes over ambitious or premature, has often led to failures that are particularly costly to society. Finally, I define *applied research* as being of technological nature, whose objective is to transfer knowledge acquired in either basic or end research to concrete applications. Generally speaking, this short-term research is based on previously established concepts. [...]

And ours? Notion of orientated research

Taking the definition of Joliot, let us try to define what we are doing. As we said we do not search completely freely, having precise and pre-established aims in mind, on the other hand we are not working in close collaboration with the industrial world, so we should be doing end research. This concept

[1]The whole French citations is as follows: L'objectif de la *recherche fondamentale* est avant tout le progrès de la connaissance et cela dans tous les secteurs de la science sans exclusives. Une telle recherche, dont la vocation est essentiellement cognitive, ne peut être pratiquée efficacement que dans un climat de liberté intellectuelle. Cette liberté concerne aussi bien les sujets de recherche que leur mode d'approche. L'objectif de la *recherche finalisée* est au contraire de répondre à des besoins précis, exprimés par la société dans des domaines où les bases conceptuelles disponibles sont encore insuffisantes. Il s'agit donc d'une forme de recherche hybride. Elle se propose à la fois de faire progresser la connaissance tout en restant ciblée sur des objectifs bien définis. On peut citer comme exemple les recherches sur le cancer ou, dans l'actualité, les recherches sur le prion, responsable de la maladie de la "vache folle". Les processus par lesquels une protéine, en l'absence de tout matériel génétique, peut présenter un caractère infectieux pose à la biologie des problèmes entièrement nouveaux sur le plan conceptuel. La recherche finalisée a souvent conduit, à travers des programmes ambitieux mais prématurés, à des échecs particulièrement coûteux pour la société. Je définirai enfin la *recherche appliquée* comme une recherche de caractère technologique, se fixant pour objectif le transfert de connaissances acquises dans le cadre d'une recherche fondamentale ou finalisée vers des applications concrètes. Il s'agit donc généralement de recherches à court terme qui s'appuient sur des bases conceptuelles déjà établies. Dans la mesure du possible, de telles recherches doivent être menées en relation étroite avec le monde industriel, agroalimentaire ou médical susceptible de tirer parti des progrès technologiques réalisés.

[2]Translation by Carol Bonvin. Mille mercis !

is nevertheless only partially satisfactory, as we are not really answering a society demand... or one should restrict to the physicists society. So I would propose that we are performing orientated basic research. This research is probably growing in a situation where the number of research laboratories and scientific publications is continuously and nonlinearly increasing, and where each lab needs to try to build an identity and to situate itself.

For a starting researcher, it is necessary to understand this in order to be able to get a realistic idea of his work. Indeed, on one hand, the latter is a simple link (*chaînon*) in the path towards a given goal, which did not begin at his arrival, and will not finish at his departure. On the other hand the content of this link can change dramatically the content of the next link and finally the possible reaching (or discovery of unreachability!) of the final goal. Being aware of these facts, one should at some point be able to figure out whether the assigned goal is reachable, or not, in order to constructively lead research forward.

Part IV

Appendices

Appendix A

Theoretical description

In order to support the measured data, Pierre Lugan, Davide Sarchi and Vincenzo Savona developed a theoretical model of trapped polaritons published in refs. [Kaitouni et al., 2006, Lugan et al., 2006]. We will try to sum it up in this appendix, presenting the useful tools to support our experiments. This section is inspired from the two references cited, we did not contribute to the calculation, other than by cordial and sometimes intense discussions!

For a shallow mesa of lateral extension larger than the optical wavelength, we can safely assume that the electromagnetic modes at in-plane position $\boldsymbol{\rho}$ are locally equivalent to those of a planar microcavity: $E(\mathbf{r}) = E(\boldsymbol{\rho})\exp(ik_z(\boldsymbol{\rho})z)$, where $k_z(\boldsymbol{\rho})$ is piecewise constant. For simplicity, here we assume a scalar electric field. Neglecting border effects at the mesa contour, Maxwell equations give

$$\nabla_\rho^2 E(\boldsymbol{\rho}) + \left(\frac{\omega^2}{c^2}\epsilon_0 - k_z^2(\boldsymbol{\rho})\right) E(\boldsymbol{\rho}) = 0\,, \tag{A.1}$$

where ϵ_0 is the background dielectric constant of the MC spacer layer. Outside the mesa, the MC resonance is $k_z = 2\pi/\lambda_c$. Inside the mesa we can relate the offset Δk_z to the energy offset $\Delta\omega_c$, as $\Delta k_z = \sqrt{\epsilon_0}\Delta\omega_c/c$. Eq. (A.1) is then solved in cylindrical coordinates, assuming a circular mesa of diameter D. The eigenmodes are therefore expressed as $E(\boldsymbol{\rho}) = U_{nm}(\rho)\exp(im\phi)$, where $n = 0, 1, \ldots$ and $m = -n, \ldots, n$ are the radial and angular mode numbers respectively. The corresponding energy-momentum spectral function are plotted in Fig.4.8 for a mesa of diameter $D = 8.6\mu m$, as an example. A discrete energy spectrum appears, whose modes show a flat extended signature in momentum space, reflecting their spatial confinement. For energies above the 9 meV barrier, we find a continuum of states whose energy-momentum signature practically coincides with that of a planar MC. This result already suggests that the structure is able to confine photons in the three spatial directions.

We similarly express the exciton center-of-mass wave function in terms of Bessel functions. These are the modes of a free particle, as the exciton motion is not affected by the mesa structure. By introducing Bose operators $\hat{A}_{nm}$ and $\hat{B}_{nm}$ for photon and exciton modes respectively, the linear exciton-photon Hamiltonian can be finally expressed in second quantization as

$$\begin{aligned} H &= \sum_m \left[\sum_n \hbar\omega_{nm}^{(ph)} \hat{A}_{nm}^\dagger \hat{A}_{nm} + \sum_n \hbar\omega_{nm}^{(exc)} \hat{B}_{nm}^\dagger \hat{B}_{nm} \right. \\ &+ \left. \left(\sum_{nn'} \frac{\hbar\Omega_{nn'}^{(m)}}{2} \hat{A}_{nm}^\dagger \hat{B}_{n'm} + \text{h.c.} \right) \right] , \end{aligned} \tag{A.2}$$

where $\omega_{mn}^{(ph)}$ and $\omega_{mn}^{(exc)}$ are the eigenenergies of the photon and of the (free) exciton modes. As required by symmetry, the angular number m is conserved in the coupling. The energies $\hbar\Omega_{nn'}^{(m)}$ are expressed in terms of the Rabi splitting of the planar cavity $\hbar\Omega_R$ and of exciton-photon overlap integrals. Here, the vacuum-field Rabi splitting of the planar MC is assumed as an input parameter.

For a planar geometry, momentum conservation implies a one-to-one coupling between exciton and photon modes. Here, on the contrary, no selection rule on the radial quantum number n exists. For the numerical solution we therefore choose to retain only a finite number of cavity modes N_c and exciton modes N_x for each value of m. The polariton operators obtained from the diagonalization of (A.2) are expressed as $\hat{P}_{nm} = \sum_{n'} (X_{nm}^{n'} \hat{B}_{n'm} + W_{nm}^{n'} \hat{A}_{n'm})$. Each polariton mode exhibits an angular emission pattern according to its photon component in momentum space, defined as $I_{nm}(\mathbf{k}) = |\langle \mathbf{k}|\hat{P}_{nm}^\dagger|0\rangle|^2$, that is easily computed from the model. By assuming for each mode a lorentzian energy broadening, we can finally compute energy-momentum spectral function. In the discrete part of the spectrum, polariton modes present a flat, broad energy-momentum signature, which corresponds to the Fourier transform of spatially confined states. The continuous part of the spectrum, on the other hand, simply corresponds to the dispersion of free two-dimensional polaritons. These are the scattering states above the finite energy barriers of the potential well formed by the mesa. Correspondingly, the energy-momentum dispersion is well defined, with a negligible broadening in k-space. For the present detuning, the radiative spectrum of the lower extended polariton is weak, as these are almost fully exciton-like with vanishing photon fraction.

The angle-resolved PL spectra in Figs. 4.8 (a)-(c) show, as a general trend, a narrowing of the angular pattern at fixed energy and a decrease of the energy spacing as the mesa diameter increases. This trend is observed for any value of the exciton-cavity detuning. Spatial confinement explains in a natural way these observations. Indeed, confinement induces a discrete energy spectrum and localization of the wave functions in real space, which

in turn produces flat extended features in reciprocal space. Moreover, these spectra provide clear evidence for the coexistence of confined and extended polariton states in our patterned mesas.

The model described allows to simulate the shape of the measured spectra. For these simulations, circular mesas were assumed. The values of the diameter D and the detuning δ used in the simulations were fitted to the experimental data. For the 3, 9 and 19 μm mesas we obtained, respectively, D = 3.46, 8.6, and 20.0 μm, and δ = 5.9, 6.8, and 7.1meV. For the remaining parameters, the nominal values of the sample were used. Figs. 4.8 (d)-(f) display the simulated polariton spectral density for the three different mesas. The relative spectral intensities in the measured PL are a direct mark of the population of each state, whereas population densities are not taken into account in the simulation which give only the density of states. This implies that it is not relevant to compare experimental and simulated intensities. A slight discrepancy in the energies of the smallest mesa is probably due to its not perfectly circular shape. In general however, the model faithfully reproduces both the energy position and angular extension of the various spectral features.

We point out that the discrete modes in Fig.4.8(b) and (e), follow a pattern that mimicks the energy-momentum dispersion of 2-D polaritons. For diameters larger than 20 μm, the simulation results in a spectrum practically identical to that of 2D polaritons in a MC of thickness $\lambda_c + \Delta L$.

For the interest of the reader, we give hereafter a figure (Fig.A.1) published in [Kaitouni et al., 2006], which shows for several confined (n, m) states the exciton content of the polariton, for a zone containing a mesa. One will notice that the exciton component of the 2D continuum is smaller above the mesa, but is nevertheless not vanishing, this tends to confirm the assumption that, on real space images where no 2D signal is observed above the mesa, there is an efficient relaxation towards the confined states.

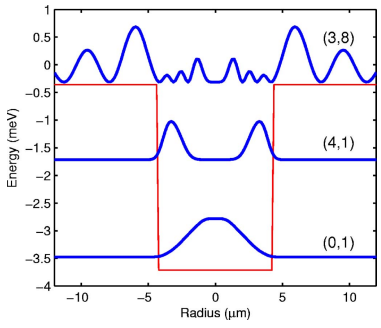

Figure A.1: Simulated squared wave functions of the exciton component as a function of radius, for three selected lower polariton states. Polar numbers (m, n) are indicated. Thin curve: lower polariton confinement potential

Appendix B

Clean room/Salle blanche

We sum up here the main points developed during the work in the clean room, with photolithography. These points are not original but of particular relevance for this work. One part is written in French, due my lack of vocabulary in the clean-room domain.

B.1 Parameters used for photolithography

As developed in chapter 2, the mesas' patterns are reproduced on the surface of the sample through photolithography. This technique requires a quartz mask where the pattern is drawn with a metallic material (in our case chrome).

Two masks are presented in this work, the first and oldest one is described in chapter 2 section 2.1.5. It is the one which was used for the sample studied in this thesis. The second one presented in chapter 7 section 7.3.1, was drawn during the testing of new samples (which did not yield any working sample so far).

We consequently present two series of parameters which were used in the clean room. The first one corresponds to the first mask, where isolated shapes with sizes ranging from 3 to 19μm were drawn. It is mainly presented for the interest of the reader, as in the future it is only the second mask which will probably be used.

The second series are the result of the numerous tests[1] performed in order to reproduce with the highest fidelity possible, the large variety of shapes present on the second mask. With sizes ranging from 0.5 to 50μm, and a new difficulty: shapes *separated* by 0.4 to 1μm.

I will directly list the parameters used for the various steps described in chapter 2 section 2.2.2.

[1] The interested Ph.D. or diploma student will find the detail of these tests in the green book (cahier vert) *Salle blanche & caract échantillons*, July 2005.

Spin-coating 1st mask: Acceleration 2, during 40sec, at 5000rpm. Drying 5min at 90°

2nd mask: Acceleration 4, during 40sec, at 8000rpm. Drying 5min under air (in the chemical hood) and 90° at 90°.

UV exposition in the mask aligner 1st mask: 2sec

2nd mask: 1sec, hard contact

Development 1st mask: 1min 28sec

2nd mask: $\approx 4min$

B.2 Récapitulatif des points critiques en salle blanche

Pour suivre, se référer au chapitre 2, partie 2.2 : le détail des étapes de la croissance (*Growth of a microcavity with embedded mesas*) de l'échantillon 1485.

Les figures de type interférences qui peuvent apparaître à la fin du processus de déposition du resist (soit la partie 2.2.2 sont plutôt dues au sous-développement (en solution, point 3 de la photolitho) qu'à une surexposition aux UV (point 2 de la photolitho).

Pour être sûr d'être en champ-proche lors de l'exposition aux UV (nécessaire pour faire l'image réelle du masque sur la surface de l'échantillon, sinon on va se heurter à des effets type interférences diffraction qui vont complètement modifier la forme des plots)

- Resist fin, donc lors du spin-coating -étape 1 de la photolitho- augmenter accélération et rpm (rotations par minute)
- Resist sec, sinon ça fait des bourrelets. Donc laisser sécher à l'aire PUIS au chaud (cf les paramètres ci-dessus pour du quantitatif)
- Utiliser hard-contact à l'aligneur de masque (Maski aligner, où se fait l'exposition aux UV), bien plaquer l'échantillon contre le masque (attention c'est fragile).

Nettoyage du masque Nettoyer le masque entièrement avant chaque utilisation. Cf cahier de modes d'emplois pour la méthode. Attention à:

- Attention la résine peut laisser des tracts, donc même si on a l'impression de ne pas avoir exposé le masque autrment qu'en le emttant au contact de l'échantillon, faire le méga nettoyage à chque utilisation.
- Nettoyer avec des gants en **Nytrile**. La vynil ou le latex laissent des tracts à cause de l'utilisation de l'acétone.

Photoresist (Résine photosensible)

- Attention il peut très facilement être poussiéreux si le flacon est vieux ou mal rangé. S'il y a trop de saloperies sur l'échantillon après plusieurs essais de spin-coating et malgré des nettoyages à répétition, les saloperies viennent certainement du photoresist.
- Donc: ne pas utiliser le fond du flacon. Eventuellement si pas d'autre source disponible, utiliser une seringue avec filtre. On peut aussi faire deux spin-coating de suite (en remettant du resist) , ça peut aplanir la surface.

B.3 Diffraction limit in the case of photolithography

We propose here a very simple calculation in order to have an idea of the minimal size of the pattern which can be drawn on the sample's surface, with a photolithography technique, described in chapter 2 section 2.2.2. Let us mention first that the photoresist thickness of $4\mu m$ described in the latter section was measured with the first series of parameters. With the second series of parameters we evaluate from the absence of diffraction pattern this thickness to be $\approx 0.5\mu m$ (this absence indicates that we are in a Fresnel configuration, see next section).

The diffraction limited angle of resolution of light incident is given by $\theta = 1.22\frac{\lambda}{D}$ in radians, where θ is the angle shown on Fig.B.1, D is the diameter of the diffracting pattern on the mask.

Through the relation $\tan\theta = \Delta/l$, where l is the photoresist thickness, this yields a minimal size on the sample's surface of $\Delta = l\ \tan 1.22\frac{\lambda}{D}$. Given the photoresist refraction index of $n = 1.7$ at $\approx 800nm$[2].

If $D = 0.4\mu m$, $l = 0.5\mu m$ and $\lambda/n = 0.4\mu/1.7$ then on obtains a good result of $\Delta \simeq 0.43\mu m$.

Fresnel number

As we mentioned in section 2.2.2 of chapter 2, the Fresnel number F determines if the system studied is in a situation of near-field (Fresnel diffraction, $F \geq 1$) or far-field (Fraunhoffer $F << 1$) diffraction. Let us calculate this number again in the case of small shapes with sizes down to $0.5\mu m$.

This number is given by $F = a^2/(\lambda R)$ where a is a characteristic length of the diffracting object, R is the distance from the object to the screen (here it is the resist thickness), and λ is the light's wavelength ($\approx 400nm$). We need to be in a situation of near-field diffraction in order to reproduced the

[2]As given by Shipley's MICROPOSIT® S1800® SERIES PHOTO RESISTS data sheet.

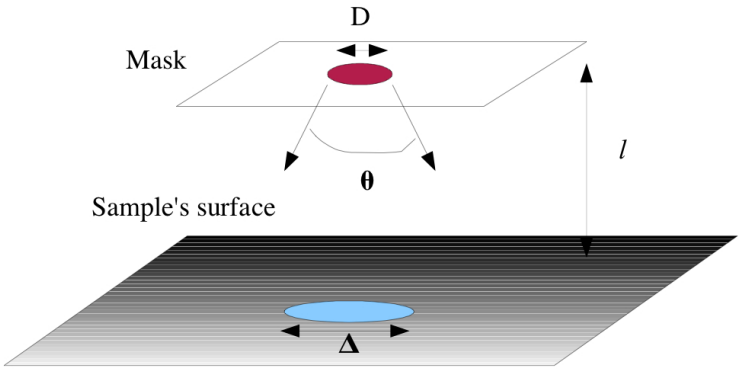

Figure B.1: Diffraction process. D is the shape's diameter on the mask, θ is the diffraction limited angular resolution, l is the resist thickness, Δ is the deposited shape's diameter on the sample's surface.

shapes designed and not to observe interference patterns, so if $a \simeq 0.5\mu m$, $R \leq 0.5\mu m$ is needed.

Appendix C

Various works

Here is a short overview of the students works related to the subject of this thesis, and which I supervised or co-supervised. Some of them will hopefully be soon available on the lab's website : loeq.epfl.ch

C.1 Diploma works on 0D polaritons

Spectroscopie dans l'espace réciproque de boîtes quantiques à polaritons

Pierre Lugan, Feb 2005

This work deals with the building of the reciprocal space imaging set-up.

Interactions entre polaritons de différentes dimensionalités

Jean-Philippe Brantut, Feb 2006

Linear and non-linear optics of 0D polaritons

Gaël Nardin, Feb. 2006

These two works describe non-linear studies under non-resonant excitation, mainly of $3\mu m$ mesas, and also of $9\mu m$ mesas.

They performed preliminary studies through real-space imaging of two kinds: imaging of the confined modes with a spectral filter, and study of the confined modes emission as a function of the distance between a $2\mu m$ diameter excitation spot and the mesa.

The three above mentioned works' results are mostly included in this thesis.

Imagerie résolue en temps des polaritons 0D dans une microcavité semicondutrice

Sébastien Beaumont, Feb. 2007

This work describes the building of the setup for time-resolved studies, and gives preliminary results.

Its results are mentioned in the perspectives chapter.

C.2 Quantum well and microcavity samples characterization

Shorter works have focused on the characterization of new samples, mainly quantum well samples. They tried to show a relationship between the exciton linewidth, its luminescence intensity and the MBE growth parameters. They also studied multiple InGaAs wells structure (each well being similar to the one described in this thesis), showing that below 5nm of barrier a coupling occurs and shifts the peak towards low energies.

- Caractérisation par luminescence de boîtes quantiques à polaritons dans des microcavités semiconductrices, Jean-Philippe Brantut, Juin 2005.
- Microcavités et puits quantiques: caractéristion d'échantillons, Sébastien Beaumont, Juin 2006.
- Expériences de photoluminescence sur des boîtes quantiques et de réfléctiivité sur des microcavités, Christophe Hurni, Juin 2006.

These works were performed in close collaboration with F. Morier-Genoud.

Bibliography

S. Adachi. *Properties of Gallium Arsenide*. INSPEC, London, 1990.

A. Baas. *Amplification paramétrique et réduction de bruit quantique dans les microcavités semi-conductrices.* Université Pierre et Marie Curie, Paris VI, 2003.

A. Baas, J. Ph. Karr, H. Eleuch, and E. Giacobino. Optical bistability in semiconductor microcavities. *Physical Review A (Atomic, Molecular, and Optical Physics)*, 69(2):023809, 2004. URL `http://link.aps.org/abstract/PRA/v69/e023809`.

A. Baas, O. El Daïf, M. Richard, J.-P. Brantut, G. Nardin, R. Idrissi Kaitouni, T. Guillet, V. Savona, J. L. Staehli, F. Morier-Genoud, and B. Deveaud. Zero dimensional exciton-polaritons. *physica status solidi (b)*, 243(10):2311–2316, 2006a. URL `http://www3.interscience.wiley.com/cgi-bin/abstract/112700934/ABSTRACT`.

A. Baas, J.-Ph. Karr, M. Romanelli, A. Bramati, and E. Giacobino. Quantum degeneracy of microcavity polaritons. *Physical Review Letters*, 96 (17):176401, 2006b. URL `http://link.aps.org/abstract/PRL/v96/e176401`.

Antonio Badolato, Kevin Hennessy, Mete Atature, Jan Dreiser, Evelyn Hu, Pierre M. Petroff, and Atac Imamoglu. Deterministic Coupling of Single Quantum Dots to Single Nanocavity Modes. *Science*, 308 (5725):1158–1161, 2005. doi: 10.1126/science.1109815. URL `http://www.sciencemag.org/cgi/content/abstract/308/5725/1158`.

D. Bajoni, E. Peter, P. Senellart, J. L. Smirr, I. Sagnes, A. Lemaitre, and J. Bloch. Polariton parametric luminescence in a single micropillar. *Applied Physics Letters*, 90(5):051107, 2007. URL `http://link.aip.org/link/?APL/90/051107/1`.

D. Bimberg, M. Grundmann, and N. N. Ledentsov. *Quantum dot heterostructures*. Wiley, 1999.

John M. Blatt, K. W. Böer, and Werner Brandt. Bose-einstein condensation of excitons. *Phys. Rev.*, 126(5):1691–1692, Jun 1962. doi: 10.1103/PhysRev.126.1691.

J. Bloch, F. Boeuf, J. M. Gérard, B. Legrand, J. Y. Marzin, R. Planel, V. Thierry-Mieg, and E. Costard. Strong and weak coupling regime in pillar semiconductor microcavities. *Physica E*, 2:915–919, 1998.

Satyendra Nath Bose. Plancks gesetz und lichtquantenhypothese. *Zeitschrift für Physik*, 26:178–181, 1924.

C. Bosio, J. L. Staehli, M. Guzzi, G. Burri, and R. A. Logan. Direct-energy-gap dependence on al concentration in al_xga_{1-x}as. *Phys. Rev. B*, 38(5): 3263–3268, Aug 1988. doi: 10.1103/PhysRevB.38.3263.

V. B. Braginsky, M. L. Gorodetsky, and V. S. Ilchenko. Quality-factor and nonlinear optical properties of optical whispering-gallery modes. *Physics Letters A*, 137(7-8):393–397, May 1989.

L. V. Butov, A. C. Gossard, and D. S. Chemla. Macroscopically ordered state in an exciton system. *Nature*, 418:751–754, 2002.

R. Butté, G. Delalleau, A. I. Tartakovskii, M. S. Skolnick, V. N. Astratov, J. J. Baumberg, G. Malpuech, A. Di Carlo, A. V. Kavokin, and J. S. Roberts. Transition from strong to weak coupling and the onset of lasing in semiconductor microcavities. *Phys. Rev. B*, 65(20):205310, Apr 2002. doi: 10.1103/PhysRevB.65.205310.

G. Christmann, R. Butte, E. Feltin, J.-F. Carlin, and N. Grandjean. Impact of inhomogeneous excitonic broadening on the strong exciton-photon coupling in quantum well nitride microcavities. *Physical Review B (Condensed Matter and Materials Physics)*, 73(15):153305, 2006. URL `http://link.aps.org/abstract/PRB/v73/e153305`.

C. Ciuti, P. Schwendimann, B. Deveaud, and A. Quattropani. Theory of the angle-resonant polariton amplifier. *Physical Review B (Condensed Matter and Materials Physics)*, 62(8):R4825–R4828, Aug 2000. doi: 10.1103/PhysRevB.62.R4825.

C. Ciuti, P. Schwendimann, and A. Quattropani. Theory of polariton parametric interactions in semiconductor microcavities. *Semiconductor Science and Technology*, 18(10):S279–S293, 2003. URL `http://stacks.iop.org/0268-1242/18/S279`.

Cristiano Ciuti, Paolo Schwendimann, and Antonio Quattropani. Parametric luminescence of microcavity polaritons. *Phys. Rev. B*, 63(4):041303, Jan 2001. doi: 10.1103/PhysRevB.63.041303.

Claude Cohen-Tannoudji, Bernard Diu, and Franck Laloë. *Mécanique quantique*. Hermann, 2000.

O. El Daïf, A. Baas, B. Deveaud-Plédran, and F. Morier-Genoud. Near infrared twin photon source. *Patent: (EP 06 001 889.2, filed 30.01.2006).*, 2006a.

O. El Daïf, A. Baas, T. Guillet, J.-P. Brantut, R. Idrissi Kaitouni, J. L. Staehli, F. Morier-Genoud, and B. Deveaud. Polariton quantum boxes in semiconductor microcavities. *Applied Physics Letters*, 88(6):061105, 2006b. URL `http://link.aip.org/link/?APL/88/061105/1`.

G. Dasbach, M. Schwab, M. Bayer, and A. Forchel. Parametric polariton scattering in microresonators with three-dimensional optical confinement. *Physical Review B (Condensed Matter and Materials Physics)*, 64(20): 201309, Oct 2001. doi: 10.1103/PhysRevB.64.201309.

G. Dasbach, C. Diederichs, J. Tignon, C. Ciuti, Ph. Roussignol, C. Delalande, M. Bayer, and A. Forchel. Polarization inversion via parametric scattering in quasi-one-dimensional microcavities. *Physical Review B (Condensed Matter and Materials Physics)*, 71(16):161308, 2005. URL `http://link.aps.org/abstract/PRB/v71/e161308`.

B. Deveaud, L. Kappei, J. Berney, F. Morier-Genoud, M.T. Portella-Oberli, J. Szczytko, and C. Piermarocchi. Excitonic effects in the luminescence of quantum wells. *Chemical Physics*, 318:104–117, Aug 2005.

B. Deveaud-Plédran, F. Morier-Genoud, and C. Ciuti. Micro-cavity for optical telecommunication device, comprises two bragg reflectors separated by at least one semiconductor layer. *Patent: (EP 05 011 604.5, filed 30.05.2005 awarded 6.12.2006). US2007007507-A1*, 2006.

C. Diederichs and J. Tignon. Design for a triply resonant vertical-emitting micro-optical parametric oscillator. *Applied Physics Letters*, 87(25): 251107, 2005. URL `http://link.aip.org/link/?APL/87/251107/1`.

C. Diederichs, J. Tignon, G. Dasbach, C. Ciuti, A. Lemaître, J. Bloch, Ph. Roussignol, and C. Delalande. Parametric oscillation in vertical triple microcavities. *Nature*, 440:904–907, Apr 2006. doi: 10.1038/nature04602.

A. Einstein. Quantentheorie des einatomigen idealen gases. *Sitzungsber. Kgl. Preuss. Akad. Wiss.*, 1924.

Bruce Faure. Review of compound materials bonding and layer transfer for optoelectronic applications. *ECS Transactions*, 3(6):293–304, 2006. URL `http://link.aip.org/link/abstract/ECSTF8/v3/i6/p293/s1`.

J. M. Gerard, D. Barrier, J. Y. Marzin, R. Kuszelewicz, L. Manin, E. Costard, V. Thierry-Mieg, and T. Rivera. Quantum boxes as active probes for photonic microstructures: The pillar microcavity case. *Applied Physics Letters*, 69(4):449–451, 1996. URL `http://link.aip.org/link/?APL/69/449/1`.

S. Giovanazzi, A. Smerzi, and S. Fantoni. Josephson effects in dilute bose-einstein condensates. *Phys. Rev. Lett.*, 84(20):4521–4524, May 2000. doi: 10.1103/PhysRevLett.84.4521.

M. Grassi Alessi, F. Fragano, A. Patanè, M. Capizzi, E. Runge, and R. Zimmermann. Competition between radiative decay and energy relaxation of carriers in disordered $in_xga_{1-x}as/gaas$ quantum wells. *Phys. Rev. B*, 61 (16):10985–10993, Apr 2000. doi: 10.1103/PhysRevB.61.10985.

T. Gutbrod, M. Bayer, A. Forchel, J. P. Reithmaier, T. L. Reinecke, S. Rudin, and P. A. Knipp. Weak and strong coupling of photons and excitons in photonic dots. *Physical Review B (Condensed Matter and Materials Physics)*, 57(16):9950–9956, Apr 1998. doi: 10.1103/PhysRevB.57.9950.

H. Haug and S. Koch. *Quantum theory of the optical and electronic properties of semiconductors*. World Scientific, Singapore, 1990.

J. Hegarty, M. D. Sturge, C. Weisbuch, A. C. Gossard, and W. Wiegmann. Resonant rayleigh scattering from an inhomogeneously broadened transition: A new probe of the homogeneous linewidth. *Physical Review Letters*, 49(13):930–932, Sep 1982. doi: 10.1103/PhysRevLett.49.930.

Kevin Hennessy, Antonio Badolato, M. Winger, D. Gerace, Mete Atatüre, S. Gulde, S. Fält, Evelyn L. Hu, and Atac Imamoglu. Quantum nature of a strongly coupled single quantum dot-cavity system. *Nature*, 445: 896–899, 2007. doi: 10.1038/nature05586.

H. F. Hess, E. Betzig, T. D. Harris, L. N. Pfeiffer, and K. W. West. Near-Field Spectroscopy of the Quantum Constituents of a Luminescent System. *Science*, 264(5166):1740–1745, 1994. doi: 10.1126/science.264.5166.1740. URL `http://www.sciencemag.org/cgi/content/abstract/264/5166/1740`.

H. Hofmann, H. Scherer, S. Deubert, M. Kamp, and A. Forchel. Spectral and spatial single mode emission from a photonic crystal distributed feedback laser. *Applied Physics Letters*, 90(12):121135, 2007. URL `http://link.aip.org/link/?APL/90/121135/1`.

J. J. Hopfield. Theory of the contribution of excitons to the complex dielectic constant of crystals. *Physical Review*, 112(5):1555–1567, 1945-1946.

R. Houdré, C. Weisbuch, R. P. Stanley, U. Oesterle, P. Pellandini, and M. Ilegems. Measurement of cavity-polariton dispersion curve from angle-resolved photoluminescence experiments. *Physical Review Letters*, 73(15): 2043–2046, Oct 1994. doi: 10.1103/PhysRevLett.73.2043.

R. Houdré, C. Weisbuch, R. P. Stanley, U. Oesterle, and M. Ilegems. Coherence effects in light scattering of two-dimensional photonic disordered systems: Elastic scattering of cavity polaritons. *Physical Review B (Condensed Matter and Materials Physics)*, 61(20):R13333–R13336, May 2000. doi: 10.1103/PhysRevB.61.R13333.

Marc Ilegems. *The technology and physics of Molecular Beam Epitaxy*, pages 83–138. Plenum, 1985.

A. Imamoglu, H. Schmidt, G. Woods, and M. Deutsch. Strongly interacting photons in a nonlinear cavity. *Physical Review Letters*, 79(8):1467, 1996.

Ioffe. This page sums up optical propoerties of gaas based on the compilation of several publications. 199X. URL `http://www.ioffe.rssi.ru/SVA/NSM/Semicond/GaAs/optic.html`.

J.D.Joannopoulos, R.D.Mealde, and J.N.Winn. *Photonic Crystals*. Princeton University Press, 1995.

Pierre Joliot. *La recherche passionnément*. Editions Odile Jacob, 2001.

R. Idrissi Kaitouni, O. El Daïf, A. Baas, M. Richard, T. Paraiso, P. Lugan, T. Guillet, F. Morier-Genoud, J. D. Ganière, J. L. Staehli, V. Savona, and B. Deveaud. Engineering the spatial confinement of exciton polaritons in semiconductors. *Physical Review B (Condensed Matter and Materials Physics)*, 74(15):155311, 2006. URL `http://link.aps.org/abstract/PRB/v74/e155311`.

J. Ph. Karr, A. Baas, R. Houdre, and E. Giacobino. Squeezing in semiconductor microcavities in the strong-coupling regime. *Physical Review A (Atomic, Molecular, and Optical Physics)*, 69(3):031802, 2004. URL `http://link.aps.org/abstract/PRA/v69/e031802`.

Jean-Philippe Karr. *Effets non-linéaires et quantiques dans les microcavités semi-conductrices*. Ph.D. thesis, Université Paris VI et Ecole normale supérieure, 2001.

J. Kasprzak, M. Richard, S. Kundermann, A. Baas, P. Jeambrun, J. M. J. Keeling, F. M. Marchetti, M. H. Szymanska, R. André, J. L. Staehli, V. Savona, P. B. Littlewood, B. Deveaud, and Le Si Dang. Bose-einstein condensation of exciton polaritons. *Nature*, 443:409–414, Sep 2006. doi: 10.1038/nature05131.

A. Kavokin, G. Malpuech, and F. P. Laussy. Polariton laser and polariton superfluidity in microcavities. *Physics Letters A*, 306:187–199, Jan 2003.

C. F. Klingshirn. *Semiconductor Optics*. Springer, 1995.

S. Kundermann, M. Saba, C. Ciuti, T. Guillet, U. Oesterle, J. L. Staehli, and B. Deveaud. Coherent control of polariton parametric scattering in semiconductor microcavities. *Physical Review Letters*, 91(10):107402, 2003. URL `http://link.aps.org/abstract/PRL/v91/e107402`.

Stefan Kundermann. *Coherence properties of microcavity polaritons: from parametric scattering to Bose-Einstein condensation*. Ph.D. Thesis, EPFL, Lausanne, 2006.

C. W. Lai, J. Zoch, A. C. Gossard, and D. S. Chemla. Phase Diagram of Degenerate Exciton Systems. *Science*, 303(5657):503–506, 2004. doi: 10.1126/science.1092691. URL `http://www.sciencemag.org/cgi/content/abstract/303/5657/503`.

Ph. Lalanne, J. P. Hugonin, and J. M. Gérard. Electromagnetic study of the quality factor of pillar microcavities in the small diameter limit. *Applied Physics Letters*, 84(23):4726, 2004. URL `http://dx.doi.org/10.1063/1.1759375`.

Wolfgang Langbein. Spontaneous parametric scattering of microcavity polaritons in momentum space. *Physical Review B (Condensed Matter and Materials Physics)*, 70(20):205301, 2004. URL `http://link.aps.org/abstract/PRB/v70/e205301`.

J. J. LePore. An improved technique for selective etching of gaas and $ga_{1-x}al_xas$. *Journal of Applied Physics*, 51(12):6441, 1980.

N. LeThomas, U. Woggon, O. Schops, M.V. Artemyev, M. Kazes, and U. Banin. Cavity qed with semiconductor nanocrystals. *Nano Letters*, 6(3):557–561, 2006. ISSN 1530-6984. URL `http://pubs3.acs.org/acs/journals/doilookup?in_doi=10.1021/nl060003v`.

X. Leyronas and M. Combescot. Quantum wells, wires and dots with finite barrier: analytical expressions for the bound states. *solid state communications*, 119:631–635, 2001.

R. A. Logan and F. K. Reinhart. Optical waveguides in gaas-algaas epitaxial layers. *Journal of Applied Physics*, 44(9):4172, 1973.

H. Lohmeyer, K. Sebald, C. Kruse, R. Kroger, J. Gutowski, D. Hommel, J. Wiersig, N. Baer, and F. Jahnke. Confined optical modes in monolithic ii-vi pillar microcavities. *Applied Physics Letters*, 88(5):051101, 2006. URL `http://link.aip.org/link/?APL/88/051101/1`.

D. Lu, J. Ahn, S. Freisem, D. Gazula, and D. G. Deppe. Lens-shaped all-epitaxial quantum dot microcavity. *Applied Physics Letters*, 87(16): 163105, 2005. URL `http://link.aip.org/link/?APL/87/163105/1`.

Pierre Lugan, Davide Sarchi, and Vincenzo Savona. Theory of trapped polaritons in patterned microcavities. *physica status solidi (c)*, 3(7):2428–2431, Jul 2006. URL `http://www3.interscience.wiley.com/cgi-bin/abstract/112691345/ABSTRACT`.

Gustav Mie. Beiträge zur optik trüber medien, speziell kolloidaler metallösungen. *Annalen der Physik*, 25(3):377–445, 1908.

S. A. Moskalenko. Reversible optico-hydrodynamic phenomena in a nonideal exciton gas (published in russian). *Fiz. Tverd. Tela*, 4:276, 1962.

Andreas Muller, Chih-Kang Shih, Jaemin Ahn, Dingyuan Lu, Deepa Gazula, and Dennis G. Deppe. High q (33 000) all-epitaxial microcavity for quantum dot vertical-cavity surface-emitting lasers and quantum light sources. *Applied Physics Letters*, 88(3):031107, 2006. URL `http://link.aip.org/link/?APL/88/031107/1`.

R. E. Nahory, M. A. Pollack, Jr. W. D. Johnston, and R. L. Barns. Band gap versus composition and demonstration of vegard's law for $in_{1-x}ga_xas_yp_{1-y}$ lattice matched to inp. *Applied Physics Letters*, 33(7): 659–661, 1978. URL `http://link.aip.org/link/?APL/33/659/1`.

T. B. Norris, J.-K. Rhee, C.-Y. Sung, Y. Arakawa, M. Nishioka, and C. Weisbuch. Time-resolved vacuum rabi oscillations in a semiconductor quantum microcavity. *Phys. Rev. B*, 50(19):14663–14666, Nov 1994. doi: 10.1103/PhysRevB.50.14663.

T. B. Norris, J. K. Rhee, D. S. Citrin, M. Nishioka, and Y. Arakawa. Coherent and incoherent dynamics of excitons in semiconductor microcavities. *Nuovo cimento D*, 17(11-12):1295–1303, Nov.-Dec. 1995.

M. Obert, J. Renner, A. Forchel, G. Bacher, R. André, and D. Le Si Dang. Nonlinear emission in ii–vi pillar microcavities: Strong versus weak coupling. *Applied Physics Letters*, 84(9):1435–1437, March 2004. doi: 10.1063/1.1651646.

D. W. Palmer. Energy-gap values for ingaas. *www.semiconductors.co.uk*, 2001.

Giovanna Panzarini and Lucio Claudio Andreani. Quantum theory of exciton polaritons in cylindrical semiconductor microcavities. *Phys. Rev. B*, 60(24):16799–16806, Dec 1999. doi: 10.1103/PhysRevB.60.16799.

H.G. Park, S. H. Kim, S. H. Kwon, Y. G. Ju, J. K. Yang, J. H. Baek, S. B. Kim, and Y. H. Lee. Electrically driven single-cell photonic crystal laser. *Science*, 305(5689):1444–1447, Sep 2004.

Stanley Pau, Gunnar Björk, Joseph Jacobson, Hui Cao, and Yoshihisa Yamamoto. Microcavity exciton-polariton splitting in the linear regime. *Phys. Rev. B*, 51(20):14437–14447, May 1995. doi: 10.1103/PhysRevB.51.14437.

E. Peter, P. Senellart, D. Martrou, A. Lemaitre, J. Hours, J. M. Gerard, and J. Bloch. Exciton-photon strong-coupling regime for a single quantum dot embedded in a microcavity. *Physical Review Letters*, 95(6):067401, 2005. URL `http://link.aps.org/abstract/PRL/v95/e067401`.

E. J. Petit and F. Houzay. Optimal surface cleaning of gaas (001) with atomic hydrogen. *Journal of Vacuum Science and Technology B: Microelectronics and Nanometer Structures*, 12(2):547–550, 1994. URL `http://link.aip.org/link/?JVB/12/547/1`.

D. Porras, C. Ciuti, J. J. Baumberg, and C. Tejedor. Polariton dynamics and bose-einstein condensation in semiconductor microcavities. *Physical Review B (Condensed Matter and Materials Physics)*, 66(8):085304, Aug 2002. doi: 10.1103/PhysRevB.66.085304.

E. M. Purcell. Spontaneous emission probabilities at radio frequencies. *Physical Review*, 69:681, 1946.

Baron Lord Rayleigh, John William Strutt. On the light from the sky, its polarization and colour. *Philosophical magazine*, 41(107, 274):87–103, 1871.

J. P. Reithmaier, G. Se ogonk, A. Löffler, C. Hofmann, S. Kuhn, S. Reitzenstein, L. V. Keldysh, V. D. Kulakovskii, T. L. Reinecke, , and A. Forchel. Strong coupling in a single quantum dot–semiconductor microcavity system. *Nature*, 432:197–200, Nov 2004.

M. Richard. *Quasi-condensation de polaritons sous excitation incohérente dans les microcavités II-VI à base de CdTe*. Université de Grenoble, 2004.

M. Richard, J. Kasprzak, R. André, R. Romestain, Le Si Dang, G. Malpuech, and A. Kavokin. Experimental evidence for nonequilibrium bose condensation of exciton polaritons. *Physical Review B (Condensed Matter and Materials Physics)*, 72:201301(R), Nov 2005.

M. Saba, F. Quochi, C. Ciuti, U. Oesterle, J. L. Staehli, B. Deveaud, G. Bongiovanni, and A. Mura. Crossover from exciton to biexciton polaritons in semiconductor microcavities. *Physical Review Letters*, 85(2):385–388, Jul 2000. doi: 10.1103/PhysRevLett.85.385.

M. Saba, C. Ciuti, J. Bloch, V. Thierry-Mieg, R. André, Le Si Dang, S. Kundermann, A. Mura, G. Bongiovanni, J. L. Staehli, and B. Deveaud. High-temperature ultrafast polariton parametric amplification in semiconductor microcavities. *Nature*, 414:731, Dec 2001.

Bahaa E. A. Saleh and Malvin Carl Teich. *Fundamentals of photonics*. Wiley-Intersience, 1991.

D. Sanvitto, A. Daraei, A. Tahraoui, M. Hopkinson, P. W. Fry, D. M. Whittaker, and M. S. Skolnick. Observation of ultrahigh quality factor in a semiconductor microcavity. *Applied Physics Letters*, 86(19):191109, 2005. URL `http://link.aip.org/link/?APL/86/191109/1`.

D. Sarchi and V. Savona. Collective excitation kinetics in the condensation of polaritons. *physica status solidi (b)*, 243(10):2317–2321, Aug 2006. ISSN 0370-1972.

V. Savona and C. Piermarocchi. Microcavity polaritons: Homogeneous and inhomogeneous broadening in the strong coupling regime. *physica status solidi (a)*, 164(1):45–51, 1997. doi: 10.1002/1521-396X(199711)164:1⟨45::AID-PSSA45⟩3.0.CO;2-7.

V. Savona, C. Piermarocchi, A. Quattropani, P. Schwendimann, and F. Tassone. Optical properties of microcavity polaritons. *Phase Transitions*, 68: 169–279, 1999.

Vincenzo Savona. Effect of interface disorder on quantum well excitons and microcavity polaritons. *arXiv.org*, pages cond–mat/0702179, Feb 2007. URL `http://arxiv.org/abs/cond-mat/0702179`.

P. G. Savvidis, J. J. Baumberg, R. M. Stevenson, M. S. Skolnick, D. M. Whittaker, and J. S. Roberts. Angle-resonant stimulated polariton amplifier. *Physical Review Letters*, 84(7):1547–1550, Feb 2000. doi: 10.1103/PhysRevLett.84.1547.

P. Senellart, J. Bloch, B. Sermage, and J. Y. Marzin. Microcavity polariton depopulation as evidence for stimulated scattering. *Physical Review B (Condensed Matter and Materials Physics)*, 62(24):R16263–R16266, Dec 2000. doi: 10.1103/PhysRevB.62.R16263.

B. Sermage, G. Malpuech, A. V. Kavokin, and V. Thierry-Mieg. Polariton acceleration in a microcavity wedge. *Phys. Rev. B*, 64(8):081303, Aug 2001. doi: 10.1103/PhysRevB.64.081303.

Anthony E. Siegman, M. W. Sasnett, and Jr. T. F. Johnston. Choice of clip levels for beam width measurements using knife-edge techniques. *Journal of Quantum Electronics*, 27(4):1098–1104, Apr 1991.

RP. Stanley, R. Houdré, U. Oesterle, M. Gailhanou, and M. Ilegems. Ultra-high finesse microcavity with distributed bragg reflectors. *Applied Physics Letters*, 65(15):1883–1885, Oct 1994. doi: 10.1063/1.112877.

R. M. Stevenson, V. N. Astratov, M. S. Skolnick, D. M. Whittaker, M. Emam-Ismail, A. I. Tartakovskii, P. G. Savvidis, J. J. Baumberg, and J. S. Roberts. Continuous wave observation of massive polariton redistribution by stimulated scattering in semiconductor microcavities. *Physical Review Letters*, 85(17):3680–3683, Oct 2000. doi: 10.1103/PhysRevLett.85.3680.

M. D. Sturge. Optical absorption of gallium arsenide between 0.6 and 2.75 ev. *Physical Review*, 127(3):768–773, Aug 1962. doi: 10.1103/PhysRev.127.768.

F. Tassone, C. Piermarocchi, V. Savona, A. Quattropani, and P. Schwendimann. Bottleneck effects in the relaxation and photoluminescence of microcavity polaritons. *Physical Review B (Condensed Matter and Materials Physics)*, 56(12):7554–7563, Sep 1997. doi: 10.1103/PhysRevB.56.7554.

Alessandro Tredicucci, Yong Chen, Vittorio Pellegrini, Marco Börger, and Franco Bassani. Optical bistability of semiconductor microcavities in the strong-coupling regime. *Phys. Rev. A*, 54(4):3493–3498, Oct 1996. doi: 10.1103/PhysRevA.54.3493.

Victor Twersky. Rayleigh scattering. *Applied Optics*, 3(10):1150–1162, Oct. 1964.

Lambert K. van Vugt, Sven Rühle, and Daniël Vanmaekelbergh. Phase-correlated nondirectional laser emission from the end facets of a zno nanowire. *Nano letters*, 6(12):2707–2711, November 2006. URL `http://pubs.acs.org/cgi-bin/abstract.cgi/nalefd/2006/6/i12/abs/nl0616227.html`.

A. Verger, C. Ciuti, and I. Carusotto. Polariton quantum blockade in a photonic dot. *Phys. Rev. B*, 73(19):193306, May 2006. doi: 10.1103/PhysRevB.73.193306.

C. Weisbuch, M. Nishioka, A. Ishikawa, and Y. Arakawa. Observation of the coupled exciton-photon mode splitting in a semiconductor quantum microcavity. *Physical Review Letters*, 69(23):3314–3317, Dec 1992. doi: 10.1103/PhysRevLett.69.3314.

T. Yoshie, A. Scherer, J. Hendrickson, G. Khitrova, H. M. Gibbs, G. Rupper, C. Ell, O. B. Shchekin, and D. G. Deppe. Vacuum rabi splitting with a single quantum dot in a photonic crystal nanocavity. *Nature*, 432:200–203, Nov 2004.

Z.L. Yuan, B. E. Kardynal, R. M. Stevenson, A. J. Shields, C. J. Lobo, K. Cooper, N. S. Beattie, D. A. Ritchie, and M. Pepper. Electrically driven single-photon source. *Science*, 295(5552):102–105, Jan 2002.

Roland Zimmermann. Theory of resonant rayleigh scattering of excitons in semiconductor quantum wells. *Il Nuovo Cimento D*, 17(11-12):1801–1805, November 1995. doi: 10.1007/BF02457284. URL `http://springerlink.com/content/x37w1u311810201p/`.

Academic Curriculum Vitae

Ounsi EL DAÏF
Rue de Lausanne 61,
CH-1020 Renens,
Switzerland

Born September the 28th, 1979
French
+41 76 433 32 07
ounsi.eldaif@epfl.ch

Professional experience

Since May 2003 Ph. D. student at the Institut de photonique et d'électronique quantiques (IPEQ) of the Ecole polytechnique fédérale de Lausanne (EPFL - Swiss Federal Institute of Technology, Lausanne).

- Full time researcher in semiconductor optics.
- Coordination of a project involving several research fields.

Since Ocotber 2003 EPFL Physics section, assistant teacher

- Thesis advisor for three Masters students during 5-month internships.
- Teaching assistant in physics (awarded).

2001 - 2002 Research intern in Optics at the Physics Institute of Humbolt University, Berlin (NanoOptik Lab) during 6 months, and at the Physics Department of the American University of Beirut (on Electron Paramagnetic Resonance techniques) during 2 months.

1999-2000 Journalist cofounder and co-editor of *L'Avenir, EuroPresseMagazine*, a Mediterranean bilingual (French and Arabic) cultural magazine based in Lyon and distributed in Lyon, Paris and Marseilles.

1997 - 2002 Private and group instructor in maths, physics and chemistry at levels up to 2nd University year and professional trainees.

Academic qualifications

Since 2003 Ph.D. in physics at EPFL, thesis director : Prof Benoît Deveaud-Plédran, Institute of Quantum Electronics and Photonics (IPEQ).

2002 - 2003 Magistère Interuniversitaire de Physique at the Ecole normale supérieure (ENS) in Paris. **Bachelor's** Degree in physics (July 2001), **Master's** Degree in physics (December 2001), and 2nd year of the Magistère (September 2002, with honors).

1997 - 2000 Preparatory classes for the French scientific schools (Grandes Ecoles) in Lyon (Intensive courses of maths, physics and chemistry).

1996 - 1997 High school at the Lycée international in Lyon. **Baccalauréat**, science major, with honors.

Participation to conferences

July 2006 International Conference on Physics of Semicondutors (ICPS, Vienna).

Talk : Quantum confinement of microcavity polaritons.

February 2006 Swiss physical society meeting, Lausanne

Talk : Engineering the dimensionality of polaritons in semiconductor microcavities.

September 2005 International Conference on Optics of Excitons in Confined Systems (OECS 9) and International Conference on Spontaneous Coherence in Excitonic Systems (ICSCE 2), Southampton

Talk (during the joint session) and Poster (ICSCE 2) : Polariton quantum boxes in semiconductor microcavities.

June 2005 Photon Mediated Phenomena Network Team Workshop, in Autrans (France, organized by the University of Grenoble).

Invited talk : Polariton QDs in semiconductor microcavities.

Publications

- *Coherence properties of polaritons in semiconductor microcavities*
  Kundermann S, Guillet T, Saba M, Ciuti C, El Daif O, Staehli JL, Deveaud B
  in Physica Status Solidi A-Applications and Materials Science **201** (3): 381-388 Feb 2004

- *Polariton quantum boxes in semiconductor microcavities*
  El Daif O, Baas A, Guillet T, Brantut JP, Kaitouni RI, Staehli JL, Morier-Genoud F, Deveaud B
  in Applied Physics Letters **88** (6):061105 FEB 6 2006

- *Engineering the spatial confinement of exciton polaritons in semiconductors*
  Kaitouni RI, El Daif O, Baas A, Richard M, Paraiso T, Lugan P, Guillet T, Morier-Genoud F, Ganiere JD, Staehli JL, Savona V, Deveaud B
  PHYSICAL REVIEW B **74** (15): Art. No. 155311 OCT 2006

- *Zero dimensional exciton-polaritons*
  Baas A, El Daif O, Richard M, Brantut JP, Nardin G, Kaitouni RI, Guillet T, Savona V, Staehli JL, Morier-Genoud F, Deveaud B
  PHYSICA STATUS SOLIDI B-BASIC SOLID STATE PHYSICS **243** (10): AUG 2006

- To be submitted: *Nonlinear emission of trapped microcavity polaritons*

- *0D microcavity polaritons. Trapping light-matter quasiparticles*
  Ph.D. thesis: the present work will be published on the EPFL library website at this address: http://library.epfl.ch/theses/?nr=3815

Patent

Near infrared twin photon source
O. El Daïf, A. Baas, B. Deveaud-Plédran and F. Morier-Genoud
Patent: (EP 06 001 889.2, filed 30.01.2006).

Patent partly based on this work

Micro-cavity for optical telecommunication device, comprises two bragg reflectors separated by at least one semiconductor layer
B. Deveaud-Plédran, F. Morier-Genoud, and C. Ciuti
Patent: (EP 05 011 604.5, filed 30.05.2005 awarded 6.12.2006). US2007007507-A1, 2006.

Scientific acknowledgments

This work is my contribution to the study of light-matter interaction, it does nevertheless of course not belong to me, and in particular would not have been possible without the work of many of my colleagues and friends. I had the chance to work with extremely competent people, chronologically I would like to mention Thierry Guillet, who patiently translated the physics language for me in the first months of my stay in Lausanne. He has at the same time a wide view on physics and science and a very pragmatic view on the necessary tools to understand it. François Morier-Genoud started with Thierry this project, and is still now working on it in the lab. He is an incredible cristallo-genitor, interested in the optical properties of the samples he grows, enough to have a very good understanding and participate in any discussion, but he is able to keep away from too many details, because he knows that he, on his side, has many details to keep in mind. The successful collaboration between Thierry and him, and then him and me, was the real clue to the birth of the mesas. After Thierry left, Augustin Baas joined the polariton group in the LOEQ, and we worked together for the three following years. We spent many long sunny days in the lab's darkness, and we discovered together, on a sunny day (where we would have preferred to say hi to the Lac Léman !) that our samples showed 0D confinement of the polaritons. Again with him I found someone with a wide and wise view on physics, and in particular a theoretical and fundamental point of view which impressed me a lot. In the last two years of my stay, Maxime Richard joined the group for a post-doc, and enlightened us with his photographer's magic. He was again a very competent physicist joining us, but also a super experimentalist, who solved for us many imaging problems, was precious.

I would like to thank Benoît Deveaud for being my thesis director. He allowed me to work in his lab and trusted me through letting a huge freedom in research and in the daily work, I am really grateful to him for this and also for what makes a lab's life beautiful: the incredible joyful atmosphere! Along with being a visionary and a manager, Benoit is a great physicist, all these ingredients together make the success he had so far and I wish him even more.

Along with them many people contributed to this work, I would like to thank the Master's students who made internships with me and whose works were largely used in this writing: Pierre Lugan, Jean-Philippe Brantut, Gaël Nardin, who is now starting a Ph.D. on this subject, and Sébastien Beaumont. It was nice to work with all of them.

Taofiq Paraïso joined me one year ago to take over the subject, and we were joined 6 months ago by Gaël. I would like to thank them for the new life they bring to this subject, it is really encouraging to see that the work does not stop, and that it is taken by motivated and competent guys. I really wish them good luck, and hope they won't hesitate to call me, wherever I

will be, to ask me why their exciton line has not the right energy ... or to discuss some deep questions about research!

The incredible office we are working (and living!) in, with its fridge sofa and bikes, had its own scientific and non-scientific life. Cristiano Ciuti stayed in it for a couple of months, and this was enough for him to write a program we are still now using, his contribution was thus punctual but essential. I would like also to thank Stefan Kundermann, who was working on polaritons, for the many discussions we had, and his successor Konstantinos Lagoudakis, who is impressively taking the very complex experiment left by Stefan. We stayed together with Andrea Feltrin having desks one in front of the other for three years, I must thank him for his patience: he always took the time to answer to my very basic (but existential) questions. I should also mention Reda Idrissi Kaitouni, who stayed for a while in the office, we tried to work together on the sample I develop in this work, it was not always easy, despite real efforts from both of us, it nevertheless finished by producing beautiful images, and taught me a lot about research in general.

I would like also to thank the institute, starting by Jean-Louis Staehli, who helped me in many respects, and who read some pages of this work, and all the people who made and make the scientific and non-scientific life of the institute nice and enlightening : Samuel, Ferran, Nicolas, Pascale, Jean, Pablo *et al.*.... And to wish good luck to the newcomers: Verena, Roland, Jelena... they all seem to have started pretty well! We really have a wonderful secrétariat, I would like to thank Claire-Lyse, Suada and the colleagues.

I was formed to research through many internships, I would thus like to thank successively the American University of Beirut, and Profs. Samih Isber and Malek Tabbal, who welcomed me first. Then I went to Berlin, where I worked with Stephan Götzinger, Prof. Benson, and shared the office with Valéry Zwiller, now also Prof. in the Netherlands. He answered many questions even late at night and is the one who introduced me to the EPFL in Lausanne. In Lausanne I also started by an internship with the group of Romuald Houdré, whom I thank for the work he allowed me to perform.

I would like to thank the physics department of the Ecole normal supérieure in Paris and in particular Jean-Michel Raimond and Pierre-François Cohadon. And further in the past I would like to thank Marc Vincent, who made me like physics in my first years of study in La Martinière in Lyon.

This manuscript

I would like to particularly thank Augustin and Maxime who spent many hours on this manuscript ! Thanks also to François, Gaël, Taofiq, Konstantinos and Jean-Louis who also took part in the corrections and reading. To Carol Bonvin who helped me with the French-to-English translation, Awos

Al-Salman helped me with the English-to-Arabic, and to incredible Krystel who took time to reread the Arabic (and discuss its content !).

Reconnaissance

Au-delà de la physique, mon séjour à Lausanne m'a plus largement permis de me former intellectuellement, je veux ici mentionner - sans forcément les nommer - celles et ceux qui m'ont permis d'avancer, de réaliser que nous vivons dans une société complexe mais compréhensible, et qu'il existe des valeurs simples comme la solidarité ou la justice sociale sur lesquelles s'appuyer. J'ai eu la chance de voir ici en Suisse une société riche en diversité, colorée de l'intérieur et de l'extérieur. Je ne vais pas m'amuser à citer tout le monde, je m'excuse bien évidemment auprès de celles ou ceux que j'aurais oublié-e-s.

De manière générale je voudrais remercier l'association attac suisse, qui dans toute sa diversité, m'a offert une formation intellectuelle unique et large, trop d'actives et d'actifs sont passé-e-s pendant ces 4 années pour pouvoir citer qui que ce soit, je ne peux que les saluer toutes et tous, du groupe multis à la campagne AGCS, en passant par les différentes coordinations, du local au global. J'ai aussi participé à la genèse d'un groupe au Liban, ça a été très formateur, et j'y ai rencontré des personnes extraordinaires. Dans tous les cas de solides amitiés se sont formées et j'espère bien que nous allons continuer là aussi très longtemps à cheminer côte à côte... Toutes ces rencontres m'ont y compris permis de poser progressivement un regard différent de critique constructive sur la recherche.

Pour le plaisir de les citer ici je voudrais remercier les ami-e-s de la librairie Basta!, et plus loin de la librairie Avicenne (Beit Mouawieh, ma 2e famille parisienne), les copains et copines d'Ingénieurs du Monde (EPFL) et du Groupe regard critique (UNIL), qui apportent un peu de sel à la vie intellectuelle du campus. De l'Espace autogéré, de la coordination des Marches européennes contre la précarité, du comité d'organisation du Forum social méditéranéen de Barcelone, des coalitions antiguerre qui ont entre autres organisé les manifs de l'été 2006.

J'ai eu la chance de trouver de très bons amis dans mes collègues de boulot et de bureau cités plus haut, nous avons partagé des pause nutella mémorables, des matchs de foot et de volley, des pizzas au bureau, mais aussi des pizzas chez Imam, voilà qui me permet de faire un clin d'oeil au restaurant Anatolie (à Renens), tenu par le meilleur cuisinier de Lausanne et environs, qui aura contribué à la bonne marche de l'EPFL ces dernières années, vu le nombre de visites que nous lui avons rendues ! J'ai aussi eu la chance de rencontrer tout un tas de gens bien, que ce soit dans les couloirs de l'EPFL, dans les rues de Lausanne où je déambulais sans connaître personne

les premiers mois de mon séjour, ou dans les méandres du militantisme suisse, je les salue toutes et tous. Parmi eux la communauté libanaise de l'EPFL, avec qui nous avons partagé beaucoup de moments de rires mais aussi quelques moments de larmes qui nous ont soudés. J'ai eu la chance d'y rencontrer un noyau d'ami-e-s avec qui j'ai en plus partagé des conversations sur mille sujets différents (merci Pascale, qui m'a permis de rouler les r dans les couloirs du labo).

Beaucoup de gens drôles, graves, intelligents, internationalistes ou nationalistes, de gauche ou pas du tout, anarchistes un peu ou beaucoup, parfois communistes aussi, étudiants chomeurs chercheurs (d'emploi ? d'avenir ?) actives actifs etc... m'ont offert un peu de leur temps et de leur énergie, qu'ils et elles en soient remercié-e-s, je leur envois d'ici un salut fraternel.

Florence a fait bien plus que m'offrir de son temps, elle m'a supporté, soutenu, a eclairé les méandres de mes jours et nuits ces 3 dernières années. Je crois que je l'ai beaucoup fait rire de mon ignorance, et elle continue de m'impressionner chaque jour. Je ne saurai sans doute pas la remercier à la hauteur de ce qu'elle m'a apporté, disons que ces quelques lignes sont un début.. J'en profite pour saluer et remercier les valaisan-ne-s, et en particulier 5 jeunes de Veyras-sur-Sierre (dite Veyras-city) : ses 4 superbes enfants, Thaïs, Tristan, Baptiste et Noé, ainsi qu'Issam, qui m'ont beaucoup fait rire et ont pas mal mis d'ambiance dans un certain bureau de l'EPFL, peut-être des futurs physiciens parmi eux.

Je voudrais remercier les ami-e-s (nouveaux et anciens) de Lyon et de Paris, de m'avoir accueilli pour des week-ends salvateurs. Encore une fois beaucoup de monde que je ne vais pas citer mais à qui je pense. J'ai la chance d'avoir deux amis d'enfance à Lyon, Luc et Fethi, ils suivent des trajectoires très différentes de la mienne, mais ils font leur bout de chemin et je les admire pour leur persévérance et compétences, et les remercie de répondre presque tout le temps au téléphone quand je leur dis "j'arrive". Je salue aussi ceux qui sont plus loin, que je ne vois que de temps en temps, mais qui sont pourtant bien là.

Et enfin je vais terminer par ma famille, je veux saluer et remercier mes parents, Elisabeth et Rachid, qui m'ont appris à lire, à parler, à vivre. J'ai beaucoup de chance de les avoir et suis très fier d'eux, je ne le leur dis certainement pas assez.

Je salue mes grands-mères Madi et Yasmine, qui ont grandement (même si très différemment) participé à mon éducation, ma tante Labibé toujours présente, je pense à ceux qui sont partis, et je salue tout le monde, tantes, oncles, cousins, cousines, neveux, nièces et filleul... Elie et Antonio sont les frères que je n'ai pas eus, je les remercie pour leur présence et les éclats de rire, et leur souhaite tout le beau qu'ils méritent. Maha, Rita, Maëlle, cousins, cousines... Ma famille est grande et belle, je ne peux pas citer tout le monde, je ne peux qu'envoyer des pensées, des saluts, et des remerciements!